Identification of the Activator Binding Residues in the Second Cysteine-Rich Regulatory Domain of Protein Kinase C Theta (PKCθ)

A Dissertation Submitted to

The Department of Pharmacological and Pharmaceutical Sciences

College of Pharmacy

University of Houston

In Partial Fulfillment of

The Requirements for the Degree

of

Doctor of Philosophy

By

Ghazi Muhammad Sayedur Rahman

May 2012

“For my parents,

brothers and my

loving wife and their

dreams”

ACKNOWLEDGEMENTS

I would like to thank my Ph.D. advisor Dr. Joydip Das for his inspiration, patience and guidance throughout the time of my dissertation. I had been through difficult times during the course of my graduate studies, which sometimes made me vulnerable, but Dr. Das has never stopped encouraging me to do the right things at right moment. He made me who I am today. As a graduate advisor he has always been methodical and perfectionist. I remember during writing the manuscript on my dissertation work, we talked a lot on what to write, how to write, what figures and tables to be incorporated and how should it be. He has been totally thorough on writing styles, on fine details of every piece of figures and illustrations and tables. He made me to change in the figures and illustrations and putting the right words in places over and over again until he finds the piece of work is absolutely perfect. Dr. Das is an excellent researcher and his passion for science is undoubtedly beyond comparison. He always told me to make one step at a time and guided me through the whole time towards the final goal.

When I first came to Dr. Das lab, he just joined in the department and was in a process to establish the lab. Having Pharmacy background, I knew less about molecular biology, protein biochemistry and medicinal chemistry. We used to spend lots of time before we procured different lab items, instruments, chemicals and reagents. Those days were full of thrill, almost every day we had some training for some new piece of instruments, on their installation, operation, maintenance etc. I am lucky being the first graduate student in the lab, Dr. Das spent hours to clarify the theoretical part of different techniques that I used in my work. Later that year Dr. Satyabrata Pany joined as post-doc in the lab. He has been a wonderful colleague and a good friend all along. He helped me to learn different techniques in molecular biology and became a constant support. I knew Pany has always been there to extend his hand of co-operation in any circumstances.

When I came to Houston, I first met two of my good friends Quaisar Ali and Abdul Bari Muhammad. It was cold December night they waited at the IAH to pick me and my wife up. Abdul Bari and his wife Rifat Sabuhi left their bedroom for us for three days before we moved to our apartment. The very first day Abdul Bari took me to UH main campus; it was a cold rainy day, January 05, 2007. Throughout the whole time until Quaisar Ali graduated and left UH to take the position of post-doc in Auburn University, he was always within reach for any help.

I belonged originally to Fall 2006 batch but due to visa problem I came in Spring 2007. All my Fall 2006 batch mates welcomed me when I came first to the class of "Experimental Design and Analysis". My first TA assignment was to assist first year Pharm. D. students to learn the compounding in PCCA. I didn't know anything about the transportation in Houston, senior third year Pharmaceutics graduate student Elimika Pfuma (now works in FDA) arranged for me the ride to PCCA.

I found Odelia Bongmba and Anirudha Chillar were almost at the same age, we quickly became good friends. Anirudha was probably the most colorful student with all the freaky ideas in the department I have ever found. I thank you two for being always very supportive and appreciative.

The day I came in PPS, I first met Dr. Tahir Hussain. He told me that he took the initiative to support my application for admission in the graduate program. I thank you Dr. Hussain. Because of you I am here today.

As a pharmaceutics graduate student, I attended all my core courses in the TMC building. My first year was practically packed with courses and amidst I attended two rotations in Dr. Ming Hu and Dr. Diana Chow's lab. I am thankful to them.

As a new graduate student, I first met Dianne Salazar among the office staffs. She helped me to enroll for the Spring 2007 courses and to complete all the necessary paper works. She has been always ready with a smile in her face to help me out for any official difficulties. Mona Williams in TMC building was the most pro-active among the staffs. She didn't give me chance to say good bye before she recently left her job in PPS.

Mona I am grateful to you for all your support in those critical days.

I attended “Scientific Writing” course in the main campus, where I interacted with Dr. Mustafa F. Lokhandwala, Dr. Carlos Pedemonte, Dr. Yuen-Sum Lau and Dr. Douglas Eikenburg. I am grateful to all for their valuable inputs to write the Dissertation proposal. Dr. Eikenburg is a wonderful instructor. He provided me the vision to go deep into a problem and to ask the right question on the very issue. I am thankful to Dr. Ke He Ruan for providing me the computational facilities for molecular modeling and docking. Dr. Louis Williams introduced me to MALTO, the regional medicinal chemistry conference in miniature for the southern states. Because of his inspiration I gave my first podium presentation in MALTO. Sometimes I am wondering how Dr. Brian J. Knoll as the director of DOGE manages all the issues of the graduate students. Dr. Knoll, please accept my heart full of thanks. “Think outside the box” was the motto I learned from Dr. Richard Bond. He was always easy going with the graduate students on topic or off topic.

Dr. Karim Alkhadi has always been an inspiration to me. He showed me how to analyze a situation logically and to respond rationally. Dr. Alkhadi, please accept my thanks. I would like to thank Dr. Samina Salim, Dr. Mohammad Asghar and Dr. Anees Banday for their support and inspiration during the difficult moments I had been through.

I like to thank Dr. B. V. V Prasad for providing me the advice and technical support for determining the protein structure. I am in debt to Dr. Peter M. Blumberg for the support of estimating the binding affinity of the common activators to the isolated PKCθ C1B mutants.

I am especially thankful to my loving wife Rumana for her support (I mean every possible way) during the whole time of the Ph.D. My special gratitude goes to my mother and father for their never ending love and inspiration. My two young loving brothers, Badal and Tito, you two have made my world happier. I thank you for your love and affection. My late father in law and grandma from my mother side would have been very happy to hear the news of my graduation. My thanks go to all my relatives, well wishers, and former colleagues who believed I would get the job done in time.

Identification of the Activator Binding Residues in the Second Cysteine-Rich Regulatory Domain of Protein Kinase C Theta (PKCθ)

A Dissertation Submitted to

The Department of Pharmacological and Pharmaceutical Sciences

College of Pharmacy

University of Houston

In Partial Fulfillment of

The Requirements for the Degree

of

Doctor of Philosophy

By

Ghazi Muhammad Sayedur Rahman

May 2012

ABSTRACT

Protein kinase C theta (PKCθ) is a serine threonine kinase, which is predominantly expressed in the T-cells and is selectively translocated in the immunological synapse upon activation. Active PKCθ initiates the downstream activation of the immunological responses against the intruders. Selective PKCθ inhibition may manage autoimmune disorders. PKCθ belongs to novel class of PKCs. Diacylglycerol (DAG) and phorbol esters are the common activators, which bind to the C1 domains of the novel and conventional PKCs. Design of PKCθ selective inhibitors targeting its activator binding C1 domain, requires the knowledge of C1 domain structure and the activator binding residues. PKCθ C1 domain consists of twin cysteine-rich subdomains, C1A and C1B, of which C1B plays a major role in the activation followed by the membrane anchoring PKCθ. To this end we determined the crystal structure of PKCθC1B subdomain at 1.63 Å, which showed a similar overall structure to that of PKCδC1B, except that the orientation of the Trp-253 residue is towards the membrane and the width of the activator pocket opening is narrower. The homologous Trp-252 in PKCδC1B is oriented away from the membrane with wider activator pocket opening. Using this structure, five possible activator binding residues were identified though the overlaying of the crystal structure, and alignment of the sequences of PKCθC1B and PKCδC1B, followed by molecular docking of a library

of DAG and phorbol ester analogs into PKCθC1B as receptor. To determine the role of these residues, Y239A, T243A, W253G, L255G and Q258G mutants in isolated PKCθ C1B domain were designed, expressed and purified from *E. coli* and their binding affinity (K_d or K_i) for phorbol 12, 13-dibutyrate (PDBu) and *Sn*-1,2-dioctanoylglycerol (DOG) were measured by radioactive PDBu binding assay. All the mutants showed significantly reduced binding affinity for both PDBu and DOG. Among all the mutants, Q258G showed highest reductions in activator binding affinity than the wild type. The extent of reductions in the binding affinity for θC1B mutants of Y239A, W253A and L255G were different however was much lesser than the homologous mutations in δC1B. All the five mutants of full length PKCθ were expressed in HEK293 cells and showed reduced phorbol 12-myristate 13-acetate (TPA) and DOG induced membrane translocation compared to wild type. These results provide insights into the PKCθ C1B activator binding domain, which will aid in future design of PKCθ selective inhibitors.

CONTENTS

Page #

Abstract ---------- xi

List of abbreviations ---------- xviii

List of materials and reagents ---------- xx

List of tables ---------- xxii

List of figures ---------- xxiii

1. INTRODUCTION ---------- 2

1.1. GENERAL STATEMENT ---------- 3

1.1.1. Protein kinase C (PKC) ---------- 3

1.1.2. PKC function and the disease states ---------- 4

1.2. LITERATURE REVIEW ON PKC AND C1 DOMAIN ---------- 5

1.2.1. Types of PKC ---------- 5

1.2.2. Activators of PKC ---------- 6

1.2.3. Mechanism of PKC activation ---------- 9

1.2.4. Domain organization in PKC and their functions ---------- 11

1.2.5. PKC C1 domains ---------- 13

1.2.6. Typical and atypical PKC C1 domains ---------- 18

1.2.7. Typical non-PKC C1 domains ---------- 20

1.2.8. Atypical non-PKC C1 domains ---------- 22

1.2.9. C1 domain and their functions ---------- 24

1.2.10. Structural features of known C1 domains ---------- 26

1.2.11. Binding affinity of the activators in typical PKC C1domains ---------- 28

1.2.12. PKCδC1B complexed with phorbol-13-O acetate ---------- 31

1.2.13. Challenges in development of PKC specific molecules ------ 33

1.3. PROTEIN KINASE C THETA (PKCθ) ---------- 34

1.3.1. Characteristics of PKCθ ---------- 34

1.3.2. Mechanism of PKCθ mediated activation of immune response ---------- 34

1.3.3. Compensatory mechanism of TNFα mediated activation of immune response ---------- 35

1.3.4. Involvement of PKCθ in different T-cells ---------- 39

1.3.5. PKCθ knockout animals and autoimmune diseases ---------- 40

1.4. PKCθ INHIBITOR ---------- 41

1.4.1. Rationale of targeting PKCθ ---------- 41

1.4.2. Challenges in targeting PKCθ ---------- 43

1.4.3. Activator binding in novel PKC C1 domains ---------- 44

1.4.4. Unique activator binding nature of PKCθ C1B subdomain - 45

1.4.5. Basis of targeting the PKCθ C1B subdomain ---------- 46

2. STATEMENT OF THE PROBLEMS ---------- 48

CENTRAL HYPOTHESIS ---------- 49

AIMS ---------- 50

WORKING HYPOTHESIS ---------- 51

3. METHODS ---------- 53

3.1. Expression vector construction ---------- 53

3.2. Generation of PKCθC1B and PKCθ mutants ---------- 53

3.3. Competent cells ---------- 54

3.4. Transformation of BL21 Gold DE3 competent cells ---------- 54

3.5. Preparation of stock culture and large scale bacterial culture ---------- 55

3.6. Protein expression and purification ---------- 56

3.7. Characterization of the proteins ---------- 57

3.7.1. SDS PAGE ---------- 58

3.7.2. MALDI TOF mass spectral analysis ---------- 58

3.7.3 Fluorescence study of Sapintoxin-D (SAPD) binding ------- 59

3.7.4. Fluorescence quenching study of activator binding to PKCθC1B and its mutants ---------- 59

3.8 Cell culture ---------- 60

3.8.1. Western blot analysis ---------- 60

3.9. Crystallization, data collection and refinement ---------- 61

3.10. Molecular docking ---------- 62

3.11. [^{3}H]PDBu binding assay ---------- 62

3.12. Membrane translocation of PKCθ ---------- 64

3.13. Statistical analysis ---------- 65

4. RESULTS ---------- 67

4.1. Protein expression and purification ---------- 67

4.2. Protein characterization ---------- 67

4.2.1. Gel permeation chromatography ---------- 67

4.2.2. SDS PAGE ---------- 68

4.2.3. MALDI TOF mass spectroscopy ---------- 68

4.2.4. Fluorescence study of SAPD binding ---------- 68

4.3. Expression and characterization of PKCθ and its C1B subdomain mutants in HEK293 cells ---------- 74

4.4. Crystal structure of PKCθC1B ---------- 75

4.4.1. Intramolecular cation-π and π stack interaction 92

4.5. Molecular docking ---------- 96

4.6. Phorbol esters and diacylglycerol binding of PKCθC1B and its mutants ---------- 102

4.7. Effect of the phospholipid composition on [^{3}H]PDBu binding ------- 107

4.8. Effect of mutation in the C1B domain on membrane translocation -- 111

5 DISCUSSION ---------- 115

6. CONCLUSION ---------- 129

7. FUTURE DIRECTION ---------- 132

8. REFERENCES ---------- 135

LIST OF ABBREVIATIONS

PKCθ	Protein kinase C theta
DAG	*Sn*-1, 2-diacyl glycerol
PE	Phorbol esters
DOG	*Sn*-1, 2-dioctanoylglycerol
PDBu	Phorbol 12, 13-Dibutyrate
PMA	Phorbol 12-Myristate 13-Acetate
TCR	T cell receptor
APC	Antigen presenting cells
MHC	Major Histocompatibilty complex
PLCγ1	Phospholipase C gamma 1
IP_3	Iinositol-1, 4, 5-triphosphate
PIP_2	Phospatydilinositol 4, 5-bisphosphate
NFκ-B	Nuclear factor kappa-B
NFAT	Nuclear factor of activated T cells
AP1	Activator protein 1
IL-2	Interleukin 2
IFNγ	Interferon-γ
TNFα	Tumor necrosis factor-α

TGFβ	Transforming growth factor-β
Treg	Regulatory T cells
CTL	Cytotoxic T-cells
SAPD	Sapintoxin-D
GST	Glutathion-S-transferase
GFP	Green fluorescent protein

LIST OF MATERIALS AND REAGENTS

E. coli BL21 Gold DE3 competent cells were from Stratagene (Santa Clara, CA); super optimal culture (SOC) media, luria broth (LB) media and terrific broth (TB) media were from Invitrogen (Carlsbad, CA); glycerol, IPTG, zinc sulphate, ampicillin, lysozyme, triton X-100, polyetheneimine, sodium chloride, γ-Globulins (G5009), tween 20 and methanol were from Sigma-Aldrich, Inc. (St. Louis, MO); thrombin, glutathion sepharose 4B, and superdex 75 prepacked column were from GE Healthcare Biosciences (Little Chalfont, United Kingdom); phosphate buffered saline was from VWR International, (Radnor, PA, USA); tris and DTT were from Promega (Fitchburg, WI); phorbol-12-myristate-13-acetate (PMA) and phorbol 12, 13-dibutyrate (PDBu) were from LC Laboratories (Woburn, MA); *sn*-1, 2-dioctanoyl glycerol (DOG), L-alpha-phosphatidylserine (PS) and L-alpha-phosphatidylcholine (PC) were from Avanti Polar Lipids, Inc. (Alabaster, Al); ammonium sulphate, polyethylene glycol 6000 and bovine serum albumin were from EMD Chemicals, Inc. (Gibbstown, NJ); sapintoxin-D was from Alexis Biochemicals (Farmingdale, NY). [20-^{3}H]Phorbol 12, 13-dibutyrate was custom synthesized from Perkin-Elmer Life Sciences, Inc. (Boston, MA). DMEM high glucose, fetal bovine serum and antibiotic-antimycotic used for the cell culture were from Gibco (Carlsbad, CA). Anti-GFP rabbit antibody and rabbit IgG HRP linked used for the Western blot analysis was purchased from Cell Signaling (Danvers, MA), and

supersignal west femto maximum sensitivity substrate used for chemi-luminescence was obtained from Thermo Scientific (Waltham, MA).

LIST OF TABLES

Page #

Table 1: Sequence alignment of all PKC C1 domains ---------- 15

Table 2: Sequence comparison of the atypical PKC C1 domains ---------- 19

Table 3: Sequence comparison of the typical non-PKC C1 domains ---------- 21

Table 4: Atypical Non-PKC C1 domains ---------- 23

Table 5: Known C1 domain structures ---------- 25

Table 6: Comparison of activator binding sites in all known C1 domains ---------- 27

Table 7A: Binding affinity of common C1 activators with purified PKC C1 domains ---------- 29

Table 7B: Binding affinity of common C1 activators with purified non-PKC C1 domains ---------- 30

Table 8: Yield of pure PKC C1 proteins ---------- 67

Table 9: PKCθC1B crystal data processing and refinement statistics ---------- 79

Table 10A: List of DAG analogs docked in PKCθC1B ---------- 89

Table 10B: List of phorbol ester analogs docked in PKCθC1B ---------- 90

Table 11: Binding affinity of PDBu and DOG to PKCθC1A, C1B and its mutants 103

Table 12: Sequence alignment of known C1 domains structure ---------- 123

Table 13: Comparison of the PDBu binding affinity for θC1B and δC1B ---------- 125

LIST OF FIGURES

Page #

Figure 1: PKC activators ---------- 8

Figure 2: Activation of PKCs through Gq-protein mediated signaling by GPCRs - 10

Figure 3: Schematic representation of three classes of PKCs ---------- 12

Figure 4: Crystal structure of PKCδC1B bound with Phorbol-13-O-acetate -------- 32

Figure 5A: Mechanism of T-cell activation and differentiation ---------- 36

Figure 5B: Mechanism of PKCθ mediated immune response ---------- 37

Figure 5C: Compensatory mechanism of TNFα mediated immune response ------- 38

Figure 6: A single symmetrical elution peak indicates the purity and proper folding of A) PKCθC1A, B) PKCθC1B, and C) PKCθC1B L255G ---------- 70

Figure 7: 15% SDS PAGE gel analysis of the GST cleaved PKCθC1B and all its isolated C1B mutants ---------- 71

Figure 8: A sharp single peak of A) pure PKCθC1A at m/z 7.4, and B) pure PKCθC1B at m/z 7.3 in MALDI TOF mass spectra ---------- 72

Figure 9: Blue shift of SAPD emission maxima with A) PKCθC1A, and B) PKCθC1B ---------- 73

Figure 10: Western blot image of whole HEK293 cell lysate expressing full length PKCθ and its C1B mutants ---------- 74

Figure 11: A) Diamond shaped crystal of PKCθC1B, B) PKCθC1B crystal retains blue color of Izit dye and C) Sodium acetate crystal ---------- 76

Figure 12: X-ray diffraction image of PKCθC1B (1.60Å) ---------- 77

Figure 13: A) Electron density map of the PKCθC1B, In the inset the electron density map of single tryptophan, B) Ribbon structure of PKCθC1B

superimposed on the contour surface. ---------- 78

Figure 14A: Ramachandran plot of the residues in PKCθC1B crystal structure ---- 80

Figure 14B: Ramachandran plot of the general, glycine, pre-pro and proline residues in PKCθC1B ---------- 81

Figure 15: Overlay of the crystal structure of PKCδC1B and PKCθC1B ---------- 85

Figure 16: Electron density map of, A) first zinc coordinating site, and B) second zinc coordinating site in PKCθC1B ---------- 86

Figure 17: Overlaying structure of PKCθC1B (NMR), PKCθC1B (X-ray), and PKCδC1B shows the relative orientation of their corresponding tryptophan ------- 87

Figure 18: Extra N-terminal and C-terminal residues in PKCθC1B ---------- 88

Figure19: Overlay of the crystal structure of PKCδC1B complexed with Phorbol 13-O-acetate and PKCθC1B ---------- 91

Figure 20: Cation-π interaction between acetylcholine and its receptor ---------- 93

Figure 21: pH dependant cation-π interaction in M2 proton channel in influenza-A virus ---------- 94

Figure 22: π stacking interaction between "Tacrine" and the acetylcholinesterase 96

Figure 23A: DAG analogs docked in PKCθC1B crystal structure ---------- 100

Figure 23B: Phorbol ester analogs docked in PKCθC1B crystal structure ---------- 101

Figure 24: Determination of K_d of PDBu to, A) PKCθC1B, and B) PKCθC1B L255G ---------- 104

Figure 25: Determination of K_i of DOG to, A) PKCθC1B wild type, and B) PKCθC1B L255G ---------- 105

Figure 26: Dependence on phospholipid composition of [3H]PDBu binding to wild type PKCθC1B domains and the C1B mutants ---------- 110

Figure 27: Plot of activator induced % membrane translocation of PKCθ an its C1B mutants and western blot images of the cytosol & membrane fractions from

HEK293 cells treated with, A) 50 nM TPA, and B) 250 nM DOG for 2 hrs ------ 113

Figure 28: Relative orientation of Trp-252 in PKCδC1B and Trp-253 in PKCθC1B ---------- 121

Figure 29: Activator binding pocket topology of PKCθC1B and PKCδC1B ------- 122

Figure 30: Relative orientation of the tryptophan in different C1 domains -------- 123

Figure 31: Possible water mediated hydrogen bond formation with Arg-272 of PKCθC1B ---------- 124

CHAPTER 1

1. INTRODUCTION

According to World Health Organization, arthritis, asthma and other autoimmune diseases are the major life threatening ailments. Collectively autoimmune diseases are among the most prevalent diseases in the U.S., affecting between 14.7-23.5 million people [1]. In 2006, prevalence of asthma in African Americans was 20.1% higher than in Caucasians [2]. In 2005, approximately 300 million people worldwide suffer from asthma with a death toll of 250,000 annually [3]. Every year there are about 500,000 hospitalizations for asthmatic conditions [4]. Students miss 13 million school days per year due to asthma [4]. Asthma was responsible for 3,384 deaths in the United States in 2005 [5]. Approximately 34.1 million Americans have been diagnosed with asthma during their lifetime [6]. An estimated 46 million adults in the U.S. reported being told by the doctor that they have some form of arthritis, rheumatoid arthritis, gout, [7]. About five millions of Americans have fibromyalgia, roughly one in every 50 Americans (2% of the populations). Fibromyalgia is the second most common musculoskeletal disease after arthritic conditions (American College of Rheumatology, 2004). The Lupus Foundation of America estimated around 1.5 million Americans, and nearly five million people worldwide have some form of lupus. According to recent studies of the World Psoriasis Day consortium, nearly 7.5 million Americans (2.2% of the population) have been

suffering from psoriasis. 125 million people worldwide (2-3% of the world population) have some form of psoriasis.

All these immunity related patho-physiological conditions has one thing in common, overactive immune system is responsible for their progression. Yet there is no medication that can eliminate the root cause of these autoimmune diseases. All current therapy can only relief the symptomatic manifestations of the disease conditions. This warrants the development of new molecules, which can cause the remission of the diseases in the sub-cellular level. Selective Protein kinase C theta (PKCθ) inhibition can manage the autoimmune conditions. Therefore development of selective PKCθ inhibitor can be a new therapeutic choice.

1.1. GENERAL STATEMENT

1.1.1. Protein kinase C (PKC)

Protein kinase C (PKC) comprises a super family of protein kinase enzymes, which are involved in the phosphorylation of other proteins. PKCs are serine threonine specific kinases. They selectively phosphorylate the hydroxyl groups of serine and threonine amino acid residues of the target proteins. PKC enzymes are activated by signals such as increase in the concentration of diacylglycerol (DAG) or calcium ions (Ca^{2+}). PKCs are important role player in several signal transduction pathways.

There are total eleven subtypes present in the PKC super family in humans [8]. All PKCs are divided under three subfamilies, based on their second messenger requirements. The subfamilies are conventional, novel, and atypical [9]. Conventional PKCs are α, β_I, β_{II}, and γ. They require Ca^{2+}, DAG, and an anionic phospholipid such as phosphatidylserine for activation. Novel PKC subfamily consists of the δ, ε, η, and θ subtypes. Novel PKCs are independent of Ca^{2+} for activation but they require DAG. Conventional and novel PKCs are activated through the same signal transduction pathway. On the other hand atypical PKCs include ζ, ι and λ subtypes, which require neither Ca^{2+} nor diacylglycerol for their activation. All PKC has N-terminal regulatory region and a C-terminal catalytic region joined together by a hinge region (Figure 3). The catalytic region is highly conserved among different subtypes. The second messenger requirements for the different subtypes differ as a result of the variation in the organization of the N-terminal regulatory domains. N-terminal regulatory domains are similar within but different among the subfamilies.

1.1.2. PKC function and the disease states

Protein kinase C (PKC) is critically involved with many signaling pathways [10]. PKCs have been known for long time for their roles on the cellular level in regulating metabolic pathways, smooth muscle contraction, cellular proliferation and growth, differentiation, membrane conductance, exocytosis, synaptic plasticity, long-term potentiation, gene expression, and the down-regulation of receptors [11]. On the organ

level, expression of PKC subtypes and their roles in different organ specific functions are largely variable. The level of PKCs expression are highest in the brain, which made it possible to first purify PKC in large quantities from brain tissue homogenate [12]. PKCs are well known for their involvement in memory and learning, visual and immune responses [8, 13]. However, PKC first came under limelight for its role in binding with the tumor promoting phorbol esters to initiate the tumor progression [14, 15]. PKC signaling upon activation by endogenous activator diacylglycerol (DAG) is generally rapid but transient [16], but phorbol ester binding to the activator binding domains in PKCs results in chronic activation of PKCs [14]. Activation of protein kinase C by tumor promoter phorbol ester may phosphorylate potent activators of transcription factors leading to increased expression of oncogenes, promoting cancer progression [17]. Therefore insight into the molecular mechanisms of the activation of PKCs, by both endogenous DAG and exogenous plant origin phorbol esters, are critical for the understanding of PKC signal transduction pathways and to the design the discrete PKC subtype specific modulators.

1.2. LITERATURE REVIEW ON PKC AND C1 DOMAIN

1.2.1. Types of PKC

The PKCs comprise a super family consisting of total eleven subtypes, which have been categorized under three subfamilies, conventional, novel, and atypical.

Conventional and novel PKC C1 domains bind to the common activators like DAG or phorbol esters, whereas the single copy of the C1 domain is present in atypical PKCs (ζ and ι/λ), which are insensitive to the activators like DAG and phorbol esters (Figure 1) [9, 18, 19]. Conventional (α, βI, βII and γ) and the novel (δ, ε, θ and η) PKCs, each has four domains. N-terminal regulatory region has C1 and C2 domains whereas highly homologous C-terminal kinase region consists of C3 and C4 (Figure 3) [9]. Both conventional and novel PKCs has N-terminal regulatory region consisting of tandem repeat highly conserved cysteine-rich, DAG/ phorbol ester responsive zinc-finger subdomains known as C1A and C1B. Novel PKCs require endogenous DAG but conventional PKCs additionally require Ca^{2+} for its activation. DAG is a lipid second messenger which selectively interacts with proteins containing a C1 domain and induces their translocation to discrete sub-cellular compartments such as cell membrane, Golgi, nuclear membrane etc.

1.2.2. Activators of PKC

1, 2-diacyl-*sn*-glycerol (DAG) is endogenous lipid second messenger, which is generated in the cell membrane in response to numerous extracellular stimuli such as growth factors, hormones, neurotransmitters, and a variety of other agonists those bind to the cell surface receptors such as G-protein coupled receptors (GPCRs). There are multiple pathways in the body through which DAG can be derived in the cells. Among the different pathways, hydrolysis of phosphatidylinositol-4, 5-biphosphate (PIP2) by

specific enzyme PLCγ1 into DAG and inositol-3, 4, 5-triphosphate (IP3) has been extensively studied and considered to be the major pathway for the physiological production of DAG. DAG remains in the plasma membrane and serves as an activator for classical and novel protein kinase C (PKC) isozymes. For the experimental purpose often DOG, a short chain hydrophilic analog of DAG is commonly used (Figure 1) [20, 21].

Phorbol esters are diterpenoids, a type of natural products, originally isolated from the plant *Croton tiglium* in sixties; mimic the effects of DAG on PKC [22]. Phorbol esters are tumor promoters [23] and have been widely used as pharmacological tools to study DAG signaling. The basic structure of phorbol esters consists of four carbon rings. Substitutions in positions 12 and 13 form a DAG-like structure. The most commonly used phorbol ester is called TPA (Tetradecanoyl Phorbol Acetate) (Figure 1).

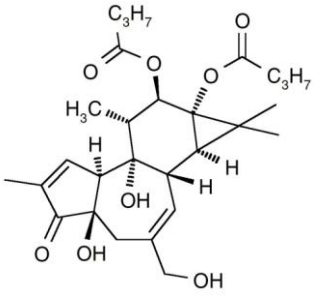

PDBu (Phorbol 12,13-Dibutyrate)

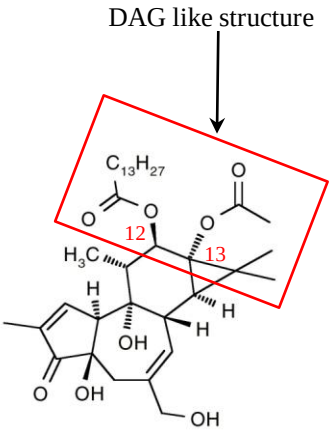

TPA (Phorbol 12-Myristate 13-Acetate)

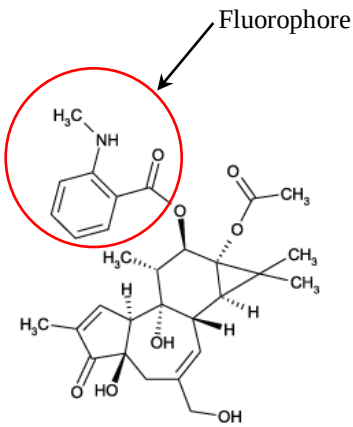

SAPD (Sapintoxin-D) fluorescent phorbol ester

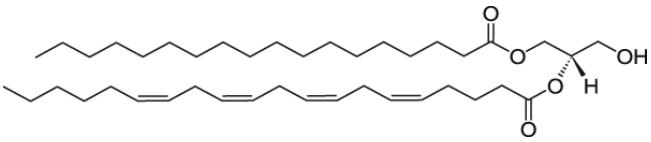

Endogenous DAG (1-stearoyl-2-arachidonoyl-*Sn*-glycerol)

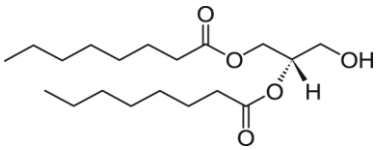

DOG (*Sn*-1,2-dioctanoyl glycerol)

Figure 1: PKC activators

1.2.3. Mechanism of PKC activation

G-protein coupled receptors (GPCRs) sense a variety of extracellular signals from the surrounding environment and help transduce them across the plasma membrane, activate inside signal transduction pathways and, finally leading to cellular responses [24]. One of the common signal transduction pathways involve GPCRs activating the PKCs. Agonist bound GPCRs interact and activate Gq-proteins including some muscarinic acetylcholine receptors, many peptide receptors, and the 5-HT2 serotonin receptors. GTP bound Gq proteins activate phospholipase C γ1 (PLCγ1) to hydrolyze the membrane lipid Phospatydilinositol 4, 5-bisphosphate (PIP2), producing inositol 1, 4, 5-trisphosphate (IP3) and *Sn*-1, 2-diacyl glycerol DAG [24]. IP3 diffuses into the endoplasmic reticulum (ER), where it interacts with calcium channel to open it, releasing calcium from inside the ER into the cytosol. Calcium modulates many cellular processes, partly by binding to regulatory proteins such as calmodulin and calcineurin. Conventional and novel PKCs are activated by the interaction of DAG and calcium leading to the phosphorylation of many different protein targets alters their cellular activity [24] (Figure 2).

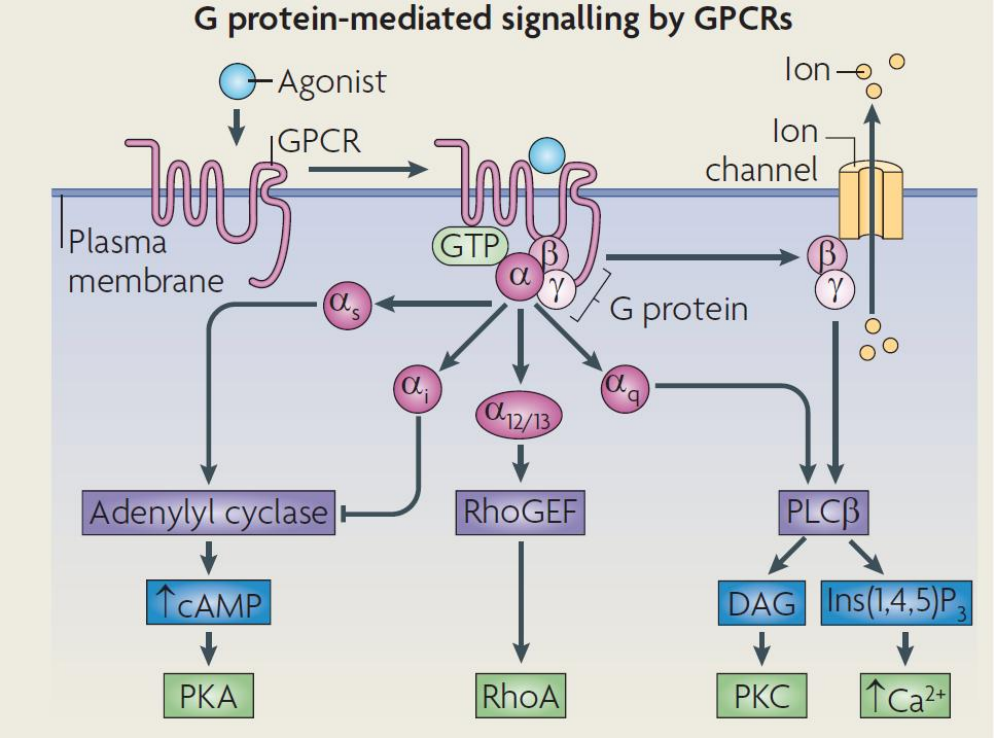

(Adapted from *Nat Rev Mol Cell Biol. 2009 Dec; 10(12):819-30.*)

Figure 2: Activation of PKCs through Gq-protein mediated signaling by GPCRs.

1.2.4. Domain organization in PKC and their functions

In the conventional PKCs (cPKC: α, βI, βII and γ) a pseudosubstrate domain is present on the N-terminal followed by the tandem repeat DAG and phorbol ester sensitive C1 subdomains namely C1A and C1B. Conventional PKCs contain a Ca^{2+} dependant C2 domain after the C1 subdomains. On the C-terminal the kinase region consists of highly homologous ATP binding C3 domain and substrate binding C4 domain (Figure 3). In novel PKCs (nPKC: θ, δ and ε), a non-Ca^{2+} dependant C2 domain is present after N-terminal pseudosubstrate domain followed by the tandem repeat DAG and phorbol ester sensitive C1 sub-domains, C1A and C1B. On the C-terminal the kinase region consists of highly homologous ATP binding C3 domain and substrate binding C4 domain. In Atypical PKCs (aPKC: ζ, ι, and λ), the PB1 domain is present on the N-terminal followed by the pseudosubstrate domain. A single non-DAG binding C1 like domain is present right after the pseudosubstrate domain. Despite the differences in their regulatory domains, all PKCs have highly homologous kinase region on the C-terminal connected through a hinge region to the regulatory domains.

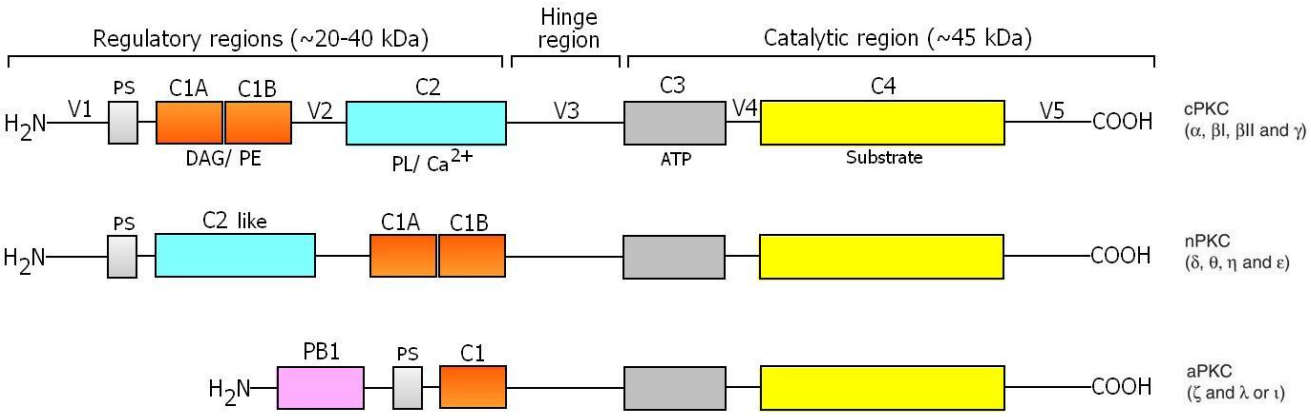

Figure 3: Schematic representation of three classes of PKCs. Conventional and novel PKCs possess four highly conserved regions (C1, C2, C3 and C4) and five variable regions (V1, V2, V3, V4 andV5). The N-terminal regulatory region consists of the pseudosubstrate domain (PS) and a C2 domain, which binds to the phospholipid (PL) cofactors, Ca^{2+} and peptides/ proteins that regulate the activity and localization of conventional and novel PKCs. Phorbol esters and the second messenger diacylglycerol (DAG) bind to the cysteine-rich motif C1A and/ or C1B. The C-terminal catalytic region contains the ATP binding C3 domain and substrate binding C4 domain. Atypical PKCs possess three highly conserved regions (C1, C3 and C4) and five variable regions (V1, V2, V3, V4 and V5). The N-terminal regulatory region consists of the pseudosubstrate domain (PS) and the PB1 (Phox and Bem1) domain containing the OPCA motif mediating protein–protein interactions. Atypical PKCs possess a single phorbol ester/ DAG insensitive C1 domain.

1.2.5. PKC C1 domain

All PKC C1 domains consist of 50 or 51 (for C1A of PKCε and η) amino acid residues and has a common structural motif of $HX_{12}CX_2CXnCX_2CX_4HX_2CX_7C$, where C and H are cysteine and histidine respectively, X represents other residues and *n* is either 13 or (14 for C1A of PKCε and η) [25]. Across all PKC C1 domains (C1A, C1B and non-DAG binding atypical C1 domain) the residues in consensus position 1, 3, 14, 17, 23, 27, 28, 31, 34, 39, 42 and 50 are identical (residues with gray background)(Table-1). For C1A of PKCε and η the last seven consensus positions are 28, 29, 32, 35, 40, 43 and 51 respectively due to one extra amino acid (Table 1).

Among the identical residues six cysteines at consensus position 14, 17, 31, 34, 42 and 50 and two histidines at consensus positions 1 and 39 (for C1A of PKCε and η, cysteines at position 32, 35, 43 and 51 and histidine at position 40 respectively) constitute two zinc coordinating sites [26]. Cysteines at consensus position 31, 34 and 50 and histidine at position 1 coordinates the first zinc finger whereas cysteines at consensus position 14, 17 and 42 and histidine at position 39 constitutes the second zinc finger [26]. Site directed mutation of residues at 1, 14, 17, 31, 34 and 42 in PKCδC1B clearly showed the disruption of the C1 structure due to lack of zinc co-ordinations to retain the functionality, which completely abolished the affinity for the phorbol esters [25]. But mutation of His-39 and Cys-50 still retains the affinity for phorbol ester at significant

proportion [27]. C1A of PKCα, β, ε and η contains on extra cysteines in consensus position 35 and 36 respectively (Table 1).

Table 1: Sequence alignment of all PKC C1 domains (conventional, novel and atypical)

	1 3 14 23 31 34 39 42 50
PKCαC1A	HKFIARFFKQPTFCSHCTDFIWGFGK-QGFQCQVCCFVVHKRCHEFVTFSC
PKCβC1A	HKFTARFFKQPTFCSHCTDFIWGFGK-QGFQCQVCCFVVHKRCHEFVTFSC
PKCγC1A	HKFTARFFKQPTFCSHCTDFIWGIGK-QGLQCQVCSFVVHRRCHEFVTFEC
PKCδC1A	HEFIATFFGQPTFCSVCKDFVWGLNK-QGYKCRQCNAAIHKKCIDKIIGRC
PKCθC1A	HEFTATFFPQPTFCSVCHEFVWGLNK-QGYQCRQCNAAIHKKCIDKVIAKC
PKCεC1A	HKFMATYLRQPTYCSHCRDFIWGVIGKQGYQCQVCTCVVHKRCHELIITKC
PKCηC1A	HKFMATYLRQPTYCSHCREFIWGVFGKQGYQCQVCTCVVHKRCHHLIVTAC
PKCαC1B	HKFKIHTYGSPTFCDHCGSLLYGLIH-QGMKCDTCDMNVHKQCVINVPSLC
PKCβC1B	HKFKIHTYSSPTFCDHCGSLLYGLIH-QGMKCDTCMMNVHKRCVMNVPSLC
PKCγC1B	HKFRLHSYSSPTFCDHCGSLLYGLVH-QGMKCSCCEMNVHRRCVRSVPSLC
PKCδC1B	HRFKVHNYMSPTFCDHCGSLLWGLVK-QGLKCEDCGMNVHHKCREKVANLC
PKCθC1B	HRFKVYNYKSPTFCEHCGTLLWGLAR-QGLKCDACGMNVHHRCQTKVANLC
PKCεC1B	HKFGIHNYKVPTFCDHCGSLLWGLLR-QGLQCKVCKMNVHRRCETNVAPNC
PKCηC1B	HKFSIHNYKVPTFCDHCGSLLWGIMR-QGLQCKICKMNVHIRCQANVAPNC
PKCζC1	HLFQAKRFNRRAYCGQCSERIWGLAR-QGYRCINCKLLVHKRCHGLVPLTC
PKCλC1	HTFQAKRFNRRAHCAICTDRIWGLGR-QGYKCINCKLLVHKKCHKLVSIEC
PKCιC1	HTFQAKRFNRRAHCAICTDRIWGLGR-QGYKCINCKLLVHKKCHKLVTIEC

Additionally all C1 domain has one phenyl alanine, two glycines and one glutamine at consensus positions 3, 23, 28 and 27 respectively (for C1A of PKCε and η 3, 23, 29 and 28 respectively) (Table 1). Phe-3, Gly-23, Gly-28 and Gln-27 play crucial role in binding with activators for conventional and novel PKC C1 domains as evident in mutational study. Mutation of phenyl alanine at position 3 and glutamine at position 27 in PKCδC1B with glycine completely abolished the binding of [^{3}H]PDBu but still retain the affinity for bryostatin1, however an introduction of a tryptophan into Gln-27 can abolish the affinity for both [^{3}H]PDBu and bryostatin-1 [25]. Interestingly it was found that mutation of Phe-3 with either an aromatic or aliphatic hydrophobic residue still retains the phorbol ester binding [25]. A replacement of Pro-11 with glycine significantly reduced the affinity of PKCδC1B for [^{3}H]PDBu [25].

All conventional and novel PKC C1A consists of the additional conserved residues including consensus Ala-5, Gln-10, Ser-15, Phe-20 and Trp-22, whereas all the conventional and novel PKC C1B consists of other conserved residues include consensus Tyr-8, His-16, Gly-18, Met-36, Asn-37, Val-38 and Val-46 (Table 1). All conventional PKC C1B domains have a consensus Tyr-22 whereas the novel PKC C1B has tryptophan in that position. Novel PKC C1B domains translocate to the membrane with higher affinity due to presence of Trp-22, conversely the conventional PKC C1B domains with Tyr-22 require coordinated binding of C1 and calcium regulated C2 domain for the membrane translocation [28]. Also tyrosine at this consensus position causes the

cytosolic localization of conventional PKCs when inactive. On the contrary tryptophan localizes novel PKCs in the Golgi due to increased level of DAG present in that region [28].

Sequence alignment of all DAG-binding conventional and novel PKC C1 domains with known PKCδC1B crystal structure complexed with Phorbol-13-O-acetate [29] revealed an interesting activator binding motif $X_8X_9X_{10}P_{11}T_{12}F_{13}$ (residues 8-13), $X_{20}X_{21}X_{22}G_{23}X_{24}$ (residues 20-24) and Q27 (Q28 for C1A of PKCε and η). X_8 is an aromatic hydrophobic residue either phenyl alanine/ tyrosine but a hydrophobic aliphatic residue can still the retain the functionality (leucine in C1A of PKCε and η), X_9 stands for no consensus residue but a mix match of residues ranging from electropositive lysine and arginine, structurally rigid neutral proline, polar uncharged serine, hydrophobic methionine or even a glycine found in this position. X_{10} is a polar uncharged glutamine/ serine or a hydrophobic valine. In the second region of activator binding motif X_{20} is an aromatic (phenyl alanine) or aliphatic (leucine) hydrophobic residue, X_{21} is a 5-6 carbon containing hydrophobic residue such as valine/ leucine/ isoleucine, X_{22} is an aromatic hydrophobic amino acid either tryptophan or tyrosine, X_{24} is a aromatic/ aliphatic hydrophobic residue such as phenyl alanine/ leucine/ isoleucine or a valine (Table 1).

Among all C1 domains (including atypical C1), 14 amino acids out of 50 are common with overall 28% sequence similarity (except PKCε1A and PKCηC1A, both has one extra residue, 27.45%). Among Conventional PKC C1A domains 44 out of 50

residues is common yielding 88% sequence similarity whereas among C1B the % similarity is 76% (38 out of 50 residues are identical). Overall among all conventional PKC C1 domains, there is 38% sequence similarity (19 residues out of 50 residues are identical). For novel PKC C1A domains 21 out of 50 residues are common yielding 42% sequence similarity whereas among C1B there is 56% sequence similarity (28 out of 50 residues are identical). Overall among all conventional PKC C1 domains, there is 30% sequence similarity (15 residues out of 50 are identical). Among the atypical C1 domains the % sequence similarity is very high 72 % (36 residues out of 50 are identical).

1.2.6. Typical and atypical PKC C1 domains

C1 domains in PKCs can be classified into typical and atypical. Typical C1 domains bind to the common activators like DAG or phorbol esters, whereas the single copy of C1 domains present in atypical PKCs are insensitive to the activators. Conventional (α, βI, βII and γ) and the novel (δ, ε, θ and η) PKCs consist of tandem repeat C1 domains known as C1A and C1B.

In comparison to the DAG/ phorbol ester-sensitive C1 domains, the rim of the binding cleft of the atypical PKC C1 domains possesses five positively charged arginine residues at C1 consensus positions 7, 10, 11, 20 and 26 respectively (Table 2).

Table 2: Sequence comparison of the atypical PKC C1 domains

	1 7 10 20 26
PKCθ C1A	HEFTATFFPQPTFCSVCHEFVWGLNKQGYQCRQCNAAIHKKCIDKVIAKC
PKCδ C1B	HRFKVHNYMSPTFCDHCGSLLWGLVKQGLKCEDCGMNVHHKCREKVANLC
PKCζ C1	HLFQAK**R**FN**RR**AYCGQCSE**R**IWGLA**R**QGYRCINCKLLVHKRCHGLVPLTC
PKCλ C1	HTFQAK**R**FN**RR**AHCAICTD**R**IWGLG**R**QGYKCINCKLLVHKKCHKLVSIEC
PKCι C1	HTFQAK**R**FN**RR**AHCAICTD**R**IWGLG**R**QGYKCINCKLLVHKKCHKLVTIEC

Mutation into arginines of the first four corresponding residues in the PKCδC1B domain completely abolished its high binding affinity for PDBu *in vitro* and with only marginal remaining activity for TPA *in vivo* [30]. Study also demonstrated both *in vitro* and *in vivo* that the loss of affinity to activators was cumulative with the sequential introduction of the arginine residues along the rim of activator binding cavity. Computer modeling revealed that these arginine residues reduced access of ligands to the binding cleft due to the change of the electrostatic potential of the C1 domain surface towards positive, though the basic structure of the binding cleft was still maintained. Finally, mutation of the four arginine residues of the atypical PKC C1 domains into the corresponding residues in the PKCδC1B domain made them DAG/ phorbol ester responsive [30].

1.2.7. Typical non-PKC C1 domains

Though C1 domain is present also as part of other non-PKC proteins but not all are capable of binding to Phorbol ester/ DAG. Typical Non-PKC C1 domains, after their sequence alignment with conventional and novel PKC C1 domains reveal that they yet retain the conserved activator binding motifs (Pro-11, Leu-21, Trp-22, Gly-23, Gln-27 and Gly-28). However in some cases the residues in the conserved activator binding motifs have been replaced by similar type but different residues, which still retain the functionality (example in DAG kinase C1B, phenyl alanine at consensus position 8 has been replaced by aliphatic hydrophobic leucine) (Table 3).

Table 3: Sequence comparison of the typical non-PKC C1 domains

	1 11 21 23 27
PKCαC1A	HKFIARFFKQPTFCSHCTDFIWGFGK-QGFQCQVCCFVVHKRCHEFVTFSC
PKCδC1A	HEFIATFFGQPTFCSVCKDFVWGLNK-QGYKCRQCNAAIHKKCIDKIIGRC
PKCδC1B	HRFKVHNYMSPTFCDHCGSLLWGLVK-QGLKCEDCGMNVHHKCREKVANLC
PKD C1A	HALFVHSYRAPAFCDHCGEMLWGLVR-QGLKCEGCGLNYHKRCAFKIPNNC
β2 chimaerin	HNFKVHTFRGPHWCEYCANFMWGLIA-QGVRCSDCGLNVHKQCSKHVPNDC
PKD C1B	HTFVIHSYTRPTVCQYCKKLLKGLFR-QGLQCKDCRFNCHKRCAPKVPNNC
Munc-13-1	HNFEVWTATTPTYCYECEGLLWGIAR-QGMRCTECGVKCHEKCQDLLNADC
DAG kinase C1B	HQWLEGNLPVSAKCTVCDKTCGSVLRLQDWRCLWCKAMVHTSCKESLLTKC
Consensus	H F F PT C C LWG K QG C C VHKRC P C

1.2.8. Atypical non-PKC C1 domains

The lack of [^{3}H]PDBu binding in PKCζ was primarily thought to be due to absence of Pro-11 but subsequent introduction of a proline in the consensus position 11 of the PKCζ C1 through mutation did not improve the [^{3}H]PDBu binding, indicating the need of some more essential motifs [31]. The sequence analysis of the non-DAG binding C1 domains not always gives any straight forward answer for their DAG non-responsiveness. But in many of the cases the crucial residues for activator binding in consensus position (Pro-11, Gly-23, Gln-27) or the hydrophobic residues required for the membrane insertion (residues in consensus position 20, 22, 24) were missing [31]. The structure of RAF1 C1 and KSR C1 despite of their similarity with typical C1 domains, explains why they do not bind to phorbol ester or DAG. Both of them consist of 2 beta sheets and an alpha helix but the major residues (deletion of four residues at consensus position 22-25) in the activator binding region are missing. Also the Gln-27 has been replaced by asparagine (RAF1 C1) and Phenyl alanine (KSR C1) respectively, which abolished the activator binding affinity (Table 4) [31].

Table 4: Atypical Non-PKC C1 domains

	1 11 21 23 25 27
Ras GRP2	HNFQESNSLRPVACRHCKALILGIYKQGLKCRACGVNCHKQCKDRLSVEC
PKC ι	HTFQAKRFNRRAHCAICTDRIWGLGRQGYKCINCKLLVHKKCHKLVTIEC
VAV1 C1	HDFQMFSFEETTSCKACQMLLRGTFYQGYRCHRCRASAHKECLGRVPP-C
DGKα C1A	HMWRPKRFPRPVYCNLCESSI-GLGKQGLSCNLCKYTVHDQCAMKALP-C
RAF1 C1	HNFARKTFLKLAFCDICQKFL----LNGFRCQTCGYKFHEHCSTKVPTMC
KSR C1	HRFSTKSWLSQV-CNVCQKSM----IFGVKCKHCRLKCHNKCTKEAPA-C
Consensus	H F K F C CQ G QG C C H C C

1.2.9. C1 domain and their functions

A total of thirteen typical C1 domain structures are known (Table 5). Among them ten are PKC C1 domain structures whereas rest three is for the non-PKC C1 domains. The only co-crystal structure of PKCδC1B bound to phorbol-13-O-acetate has been solved in 1995. In addition twelve atypical non-PKC C1 domain structures have been elucidated (Table 5).

Table 5: Known C1 domain structures (PKC, non-PKC, typical and atypical type)

Protein family & subtypes		UniProtKB code	# of C1 domain	Function	Known C1 structure, PDB code & structure type
Typical (binds to DAG/ Phorbol esters)					
cPKC (α, βI, βII, γ)		P17252	2	Protein kinase	PKCα C1B: 2ELI (NMR)
		P05771			PKCβ IIC1B: 3PFQ (X-ray)
		P05129			PKCγ C1A: 2E73 (NMR)
		P05129			PKCγ C1B: 1TBO/1TBN (NMR)
nPKC (δ, ε, θ, η)		Q05655	2	Protein kinase	PKCδ C1A: 2YUU (NMR)
		Q05655			PKCδ C1B: 1PTQ/1PTR (X-ray)
		Q04759			PKCθ C1A: 2ENN (NMR)
		Q04759			PKCθ C1B:2ENZ (NMR)
PKD (1, 2, 3)		O75276, Q6IVV8, O94806	2	Protein kinase	
DGK (β, γ)		Q9Y6T7, P49619	2	Lipid kinase	
Chimaerin (α1, α2, β1, β2)		P15882, B4DV19, A4D1A2,	1	Rac-GAP	Chimaerin α1C1: 3CXL (X-ray)
		B3VCF1, B3VCF3, P52757			Chimaerin βII C1: 1XA6 (X-ray)
Munc-13 (1, 2, 3)		Q9UPW8, O14795, Q8NB66, Q70J99	1	Scaffold	Munc-13-1: 1Y8F (NMR)
RasGRP (1, 4)		O95267, Q8TDF6	1	Ras-GEF	
RasGRP-3		D6W583	1	Ras/Rap-GEF	
Atypical (does not bind to DAG/Phorbol esters)					
aPKC (ζ , ι/λ)		Q05513, P41743	1	Protein kinase	
RasGRP-2		Q2YDB1	1	Ras/Rap-GEF	
DGK (α, δ, η, ε, ζ , ι)		P23743, Q16760, Q86XP1, P52429, Q13574, O75912	2	Lipid kinase	DGKδ C1B: 1R79 (NMR)
DGKθ		P52824	3	Lipid kinase	
Vav (1, 2, 3)		Q96D37, P52735, B7ZLR1	1	Rac/Rho-GEF	VAV1 C1 human: 3KY9 (X-ray)
		P27870			VAV1 C1 Mouse: 2VRW (X-ray)
Raf-1		P04049	1	Protein kinase	Raf-1 C1: 1FAQ/1FAR (NMR)
KSR (1,2)		Q8IVT5, Q6VAB6	1	Scaffold	KSR-1 C1: 1KBE/1KBF (NMR)
Dbl Lfc		Q26422	1	Rho-GEF	
ROCK (1, 2)		Q13464, O75116	1	Protein kinase	ROCK2 C1: 2ROW(NMR)
MRCK (α, β, γ)		Q3UU96, Q9Y5S2, Q6DT37	1	Protein kinase	
Citron	Citron-N	O14578	1	Rho effector	
	Citron-K	O88527	1	Protein kinase	
Miscellaneous C1 domain containing proteins					
AKAP13		Q12802	1	Rho guanyl-nucleotide exchange factor	
ARH	ARHGAP29	Q5PQJ5	1	RhoGTPase activator	
	ARHGEF2	Q92974	1	Rho guanine nucleotide exchange factor	
GMIP		Q9P107	1	a novel Rho GTPase-activator	
HMHA1		Q92619	1	GTPase activator	
MYO	MYO9A	Q9UNJ2	2	GTPase activator	
	MYO9B	Q13459	1	Rho GTPase activator	
	cMYBP-C	PMID:21148481	1	Cardiac muscle fiber effector	cMyBP-C C1: 2V6H (X-ray)
PDZD8		Q8NEN9	1	Intracellular signal transductor	
RACGAP1		Q9H0H5	1	Rac GTPase effector	
RAS	RASSF1	Q9NS23	1	Potential tumor suppressor, role in death receptor-dependent apoptosis	
	RASSF5	Q8WWW0	1	Potential tumor suppressor, role in lymphocyte adhesion	RASSF5 C1: 1RFH/2FNF (NMR)
STAC	STAC1	Q99469	1	Probably involved in a neuron-specific signal transduction	
	STAC2	Q6ZMT1	1	Intracellular signal transductor	
	STAC3	Q96MF2	1	Probably involved in a neuron-specific signal transduction	STAC3 C1: 2DB6 (NMR)
TENC1		Q8CGB6	1	Regulates cell motility, proliferation & probably has phosphatase activity.	

1.2.10. Structural features of the known C1 domains

Each of the C1 domains either typical or atypical, whether belongs to PKC or no-PKC proteins, there have been a huge variation among C1 pockets in terms of their physical features such as width at the pocket opening, depth of the pocket, inner pocket volume as well as their secondary structures. We compiled the features for all known C1 domain structures for comparison (Table 6).

Table 6: Comparison of activator binding sites in all known C1 domains

Name of the C1 domain with PDB code	**Pocket width(Å) between the residues at the opposite edges of the cavity**	**Depth (Å)**	**Pocket volume (Å^3)**	**Secondary structure (%) (Helix-H, strand- S, coil-C)**
PKCα C1B (2ELI)	08.85 (Gly-110, Leu-125)	16.15	22.60	H-0, S-12, C-88
PKC β II C1B (3PFQ) *	09.10 (Ser-111, Leu-125)	14.86	37.50	H-0, S-08, C-92
PKCγ C1A (2E73)	14.37 (Lys-44, Ile-59)	18.13	26.70	H-7, S-06, C-87
PKCγ C1B (1TBN)	15.48 (Tyr-108, Leu-124)	17.05	54.80	H-0, S-12, C-88
PKCδ C1A (2YUU)	11.54 (Gly-167, Leu-182)	18.58	132.70	H-7, S-14, C-79
PKCδ C1B (1PTQ)	08.07 (Met-239, Leu-254)	16.68	110.90	H-8, S-24, C-68
PKCθ C1A (2ENN)	10.55 (Pro-168, Asn-184)	17.65	99.00	H-3, S-22, C-75
PKCθ C1B (2ENZ)	08.72 (Lys-240, Leu-255)	20.75	38.70	H-0, S-15, C-85
PKCθ C1B (4FKD) *	**07.56 (Lys-240, Leu-255)**	**19.49**	**40.60**	**H-12, S-24, C-64**
Chimaerin α1C1(3CXL) *	09.36 (Arg-214, Leu-229)	16.25	41.50	H-8, S-20, C-72
Chimaerin βII C1 (1XA6)*	08.89 (Arg-223, Leu-238)	17.97	17.00	H-0, S-14, C-86
Munc-13-1C1 (1Y8F)	12.27 (Thr-575, Ile-590)	15.52	4.90	H-6, S-18, C-76
DGKδ C1B (1R79)	07.49 (Val-245, Val-259)	15.56	22.20	H-7, S-14, C-79
VAV1 C1 human (3KY9)*	06.99 (Glu-524, Thr-539)	15.58	49.30	H-0, S-20, C-80
VAV1 C1 Mouse (2VRW) *	07.54 (Glu-525, Thr-540)	15.67	52.90	H-0, S-20, C-80
Raf-1 C1 (1FAR)	09.74 (Leu-147, Asn-161)	15.85	13.30	H-5, S-21, C-74
KSR-1 C1(1KBE)	06.06 (Leu-342, Ile-354)	11.33	20.60	H-0, S-22, C-78
ROCK2 C1 (2ROW)	08.08 (His-1269, Phe-1285)	15.95	43.50	H-7, S-23, C-70
RASSF5 C1 (1RFH)	12.09 (Gly-127, Arg-141)	19.29	16.40	H-6, S-16, C-78
STAC3 C1 (2DB6)	12.61 (Lys-98, Leu-112)	19.56	11.90	H-9, S-24, C-67

* Complete/ partially complete structure is deposited in the PDB. The C1 domains have been truncated using Chimera 1. 5. 3. and SwissModel and then subjected to DSSP (Also used in PDB for the prediction of secondary structure of solved C1 structures) in the Swiss Model for secondary structure prediction.

1.2.11. Binding affinity of the activators in typical PKC C1 domains

Typical C1 domains of either PKC or non-PKC bind with the DAG and phorbol esters with variable affinity. Tandem repeat C1A and C1B domains of conventional and novel PKCs also showed differences in the binding affinities for DAG and phorbol esters [32-39]. With some exceptions, both conventional and novel PKC C1A subdomains bind to DAG with higher binding affinity than C1B, whereas the C1B subdomains of conventional and novel type binds to the phorbol esters with higher binding affinity than C1A. However this general trend did not fit for Protein kinase C theta (PKCθ). C1B subdomain of PKCθ binds to both DAG and phorbol esters with higher binding affinity than the C1A. The binding affinity of the typical C1 domains for DAG and phorbol esters has been outlined in Table 7A and 7B.

Table 7A: Binding affinity of common C1 activators with purified PKC C1 domains determined by Radioactive PDBu binding assay, ITC and SPR

Purified C1 domains	PDBu[a], (Radioactive PDBu binding assay), K_d, nM	PDBu (ITC[b]), K_d, nM	PMA[c] (SPR[d]) [g], K_d [i], nM	DiC8[e] (ITC[b]), K_d, nM	DiC18[f] (SPR[d]) [h], K_d [i], nM
PKCαC1A	>3000 [32] / 1.1 [34] / 0.4±0.11 [39]		121.0±26.2 [32]	10.2±3.1 [32]	3.6±0.5 [32]
PKCαC1B	46.7 [32] / 5.3 [34] / 7.4 [34] / 3.4±0.12 [39]	21.4±5.0 [32]	6.3±1.5 [32]		2700±710.0 [32]
PKCα	60 [34] / 0.15 [34] / 30 [40]			0.008 [41]	36±0.9 [42]
PKCβC1A	1.3 [34]				
PKCβC1B	1.3 [34]				
PKCβI/ βII	3.9 [34] / 9.5 [34] / 0.14 [40]				
PKCγC1A	65.8 [32] / 1.5 [35]	51.9±17.0 [32]	1.9±0.3 [32]	10.4±5.0 [32]	5.5±1.0 [32]
PKCγC1B	16.9 [32] / 1.2 [34]	9.3±3.8 [32]	1.7±0.5 [32]	8.9±3.1 [32]	5.2±0.6 [32]
PKCγ	18 [34] / 0.37 [34] / 2.4 [34] / 6.8 [40]				
PKCδC1A	300 [33] / 51.9 [34] / 0.34±0.08 [38] / 2.04±0.24 [39]		360±21 [33]	85±27 [33]	30±2 [33]
PKCδC1B	1.0±0.1 [33] / 0.53 [34] / 0.33±0.05 [39]	58±26 [33]	40±4 [33]		7800±1800 [33]
PKCδ	4.0 [34] / 0.71 [40]				6.6±1.0 [43]
PKCεC1A	5.6 [33]	74±10 [33]	14±3 [33]	38±5 [33]	11±1 [33]
PKCεC1B	0.81 [33] / 1.5 [34]	23±9 [33]	5.2±1 [33]	110±40 [33]	52±10 [33]
PKCε	18.0 [34] / 0.63 [40]				2.0±0.3 [33]
PKCθC1A	900 [34] / >200 [34]				1900±100 [35]
PKCθC1B	3.4 [34] / 0.72 [34]				26±3 [35]
PKCθ					20± 4 [37]
PKCηC1A	4.3 [34]				
PKCηC1B	0.91 [34] / 0.45 [34]				
PKCη	0.58 [40]				

Phorbol 12, 13-dibutyrate, b- isothermal calorimetry, c - phorbol 12-myristate 13- acetate, d- surface plasmon resonance, e- *Sn*-1, 2-dioctanoyl glycerol, f- *Sn*-1, 2-dioleoyl glycerol, g- POPC/ POPS/ PMA (69.95: 30: 0.05) vesicles, h- POPC/POPS/DiC18 (67.5: 30: 2.5) vesicles, i-K_d determined from equilibrium analysis for these measurements. K_d determined from SPR measurements is the dissociation constant not for DAG (or phorbol ester) but for DAG (or phorbol ester) containing vesicles, NM-not measured, Fmoc- method used in solid phase.

Table 7B: Binding affinity of common C1 activators with purified non-PKC C1 domains determined by Radioactive PDBu binding assay, ITC and SPR

Purified non PKC C1 domains	PDBu[a], K_d, nM	OAG[b], Ki, nM	DiC8[c], Ki, nM
Unc13.1C1 [44]	1.31±0.20	378±20	
Unc13.1			
Munc13.1C1 [45]	5.0		
α1-chimerinC1 [46]	2.0		
α1-chimerin [47]	0.17		
β2-ChimerinC1 [48]	4.49±0.09		
β2-Chimerin [49]	1.9±0.02	144±26	
Ras-GRP1C1 [50]	0.58±0.08		
Ras-GRP1 [50]	0.49±0.09		
Ras-GRP3C1 [48]	1.52±0.37		
Ras-GRP3 [51]	1.53±0.33		
MRCKαC1 [52]	10.3±2.0		2820±260
MRCKβC1 [52]	17±1.2		6960±300
PKD1C1B [53]	0.37±0.03		159±28
PKD2C1B [53]	0.32±0.09		154±11
PKD3C1B [53]	0.28±0.04		168±29
PKD3C1A [53]	1.62±0.03		44.1±8.5
hDGKβC1A [54]	14.6		
rDGKγC1A [54]	3.6	557	
rDGKγ [54]	4.4		

a- Phorbol 12, 13-dibutyrate, b- 1-oleoyl-2-acetyl-*Sn*-glycerol, c- *Sn*-1, 2-dioctanoyl glycerol

1.2.12. PKCδC1B complexed with phorbol-13-O acetate

PKCδC1B complexed with phorbol-13-O-acetate (1PTR) is the only known PKC C1 domain co-crystal structure. PKCδC1B possesses two long beta sheets (20% β-sheet) forming a V-shaped activator binding groove and a short alpha helix (4% α-helix) at the C-terminal end. Phorbol-13-O-acetate formed five hydrogen bonds in the activator binding groove (Figure 4). O4 of Phorbol-13-O-acetate formed one hydrogen bond with oxygen atom of the back bone carbonyl of glycine-23 whereas O3 formed another hydrogen bond with the nitrogen atom of the backbone amine of glycine-23. O20 formed two hydrogen bonds with nitrogen and oxygen atom of the back bone amine and carbonyl group of threonine-12 respectively and one hydrogen bond with oxygen atom of the back bone carbonyl of leucine-21. PKCδC1B consists of two zinc coordination sites. Each zinc atom (shown as gray balls) coordinates with three cysteines and one histidine (Figure 4).

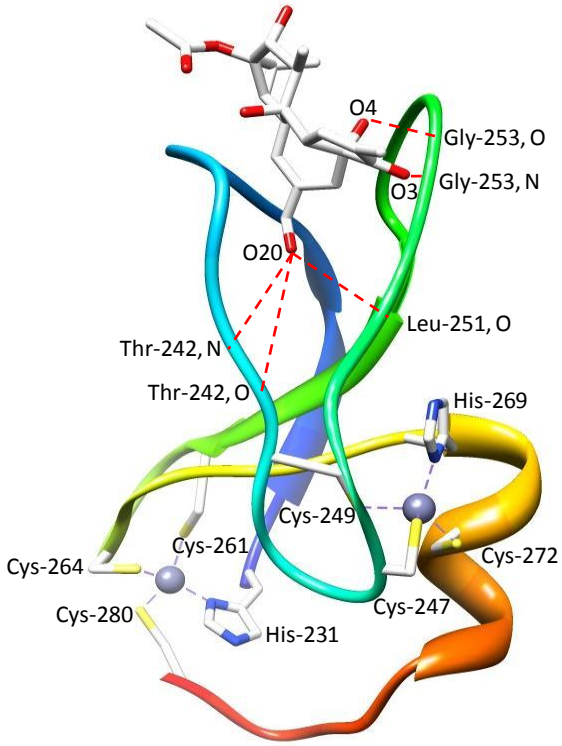

Figure 4: Crystal structure of PKCδC1B bound with Phorbol-13-O-acetate.

1.2.13. Challenges in development of PKC specific molecules

Design of PKC subtype specific modulator has been the objectives of many groups around the world. But the success story is yet unheard. The reason is all so far tried to target the catalytic region of PKCs, more specifically all the approaches were to competitively inhibit the ATP to bind into the active site of the ATP binding C3 domain. Structurally all PKCs has highly conserved C-terminal catalytic region. Therefore the C3 domain targeting was non-selective [55, 56].

The other approach has come forefront recently is to block the substrate binding pocket in the C4 domain. In the inactive state the N-terminal pseudo-substrate domain occupies the C4 substrate binding pocket. Recently pseudo-substrate peptide mimetics has been developed targeting the C4 domain [57]. However peptide mimetics has other draw backs like, formulation stability, route of delivery, expensive bioreactor design for production etc.

A suitable alternative could be the development of small molecules targeting the activator binding C1 domain. C1 domain mediates only subtype specific functions upon activation. Targeting C1 domain may stop the cross talks between the subtypes [56].

1.3. PROTEIN KINASE C THETA (PKCθ)

1.3.1. Characteristics of PKCθ

PKCθ is a serine threonine kinase (EC 2.7.11.13) [8], which in human is encoded by PRKCQ gene [58]. It is exclusively expressed in T-cells and thymocytes [58]. PKCθ plays crucial role in T-cell activation and is critically involved with immunity. PKCθ selectively translocates to the immunological synapse, which in turn activates the transcription factors such as NF-κB and AP-1 mediating the immune responses [59, 60]. PKCθ belongs to novel class of PKC and has 706 amino acid residues with a molecular mass of 81.8 kDa (human). PKCθ has a N-terminal phospholipid dependent, but Ca^{++} independent C2 domain followed by two copies of DAG/ Phorbol ester sensitive C1 domains present in PKCθ, known as C1A and C1B (Figure 3). PKCθ C1 domains are zinc fingers; each has two zinc coordinating sites consisting of three cysteines & one histidine. Membrane anchoring of activated PKCθ involves a ternary system of C1 domain, the activator and the anionic phospholipid phosphatidylserine as cofactor. Like all other kinases, PKCθ has highly conserved C-terminal catalytic region consisting of ATP binding C3 domain and substrate binding C4 domain (Figure 3).

1.3.2. Mechanism of PKCθ mediated activation of immune response

Macrophages, a type of amoeboid white blood cells as the first line of defense in the body initially respond to the invasion of the APC such as bacteria, virus, parasites, prion etc. by engulfing and digesting them, which results in subsequent generation of the

antigenic proteins from the digested APC debris. Antigenic proteins bind to the MHC present on the macrophage cell surface. In the later stage T-cells are activated by stable interaction of TCR molecules with MHC bound antigenic proteins. Activated TCR molecules upon clustered at the immunological synapses triggers the activation of PLCγ1 in the T-cell membrane, which cleaves DAG and IP_3 from PIP_2 [61]. DAG activates PKCθ, which results in the translocation of active PKCθ to the immunological synapse. Activated PKCθ in the immunological synapse mediates the activation of the downstream transcription factors associated with immune response such as NFκ-B, NFAT & AP1 and production of IL-2 [59, 60, 62] (Figure 5A and 5B).

1.3.3. Compensatory mechanism of TNF mediated activation of immune response

Tumor necrosis factor (TNF, also formerly known as TNFα) is a pro-inflammatory cytokine involved in the systemic activation of the immune response [63]. TNFα is a member of a group of cytokines, which stimulate the acute phase reaction [63]. Though TNF can be produced by other cell types as such as CD4+ lymphocytes (Helper T cells) and NK cells (Natural killer cells, cytotoxic T cells), it is produced chiefly by the activated macrophages when they encounter the exogenous proteinous fragments from the APC (Antigen presenting cells). TNF binds to the TNF receptor on the cell surface of the T-cells and activates the downstream NFκ-B, which translocate into the nucleus. Activated NFκ-B upon binding to DNA, translate the gene into mRNA, which generates the specific antibodies necessary for the immune responses [64, 65] (Figure 5C).

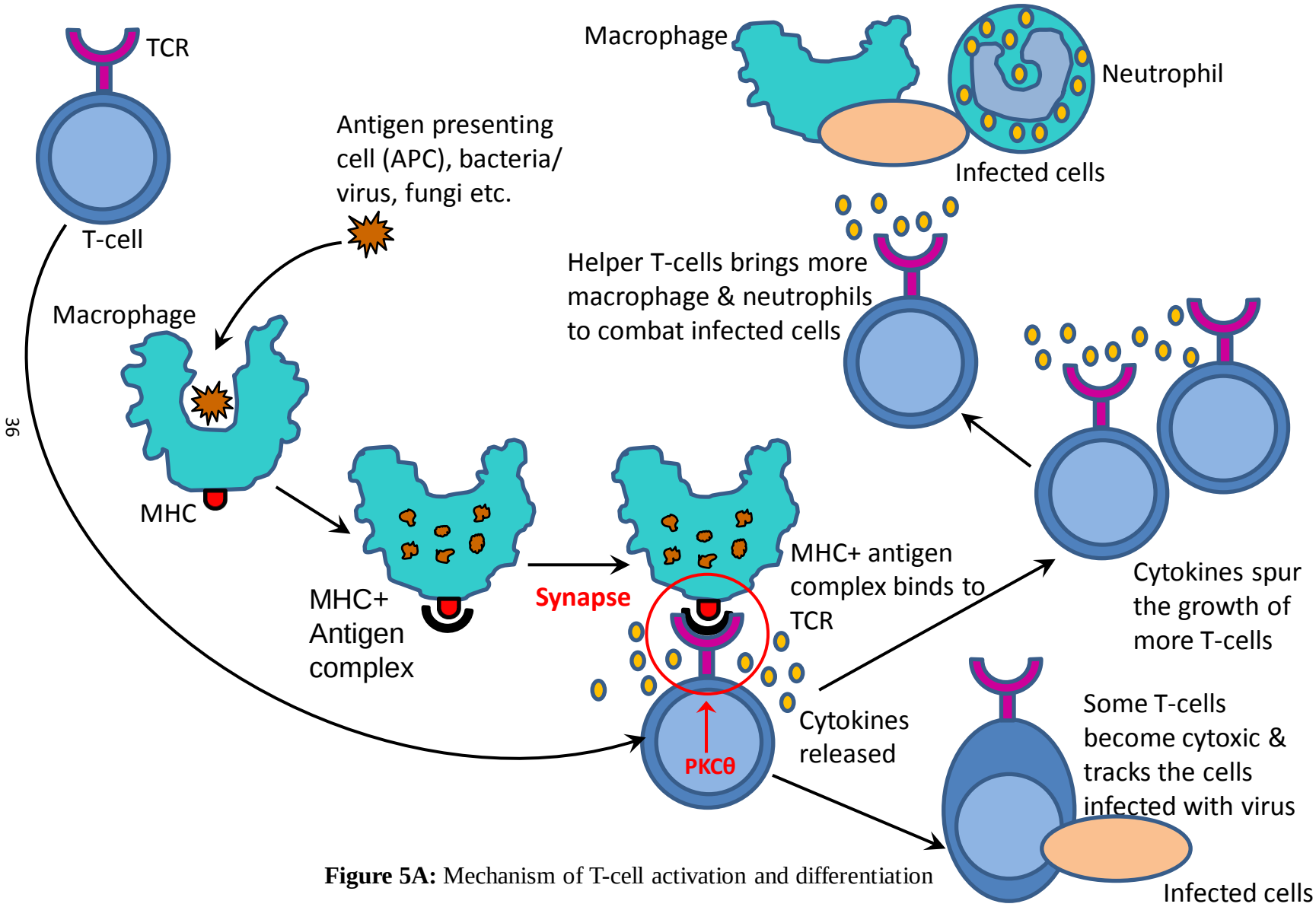

Figure 5A: Mechanism of T-cell activation and differentiation

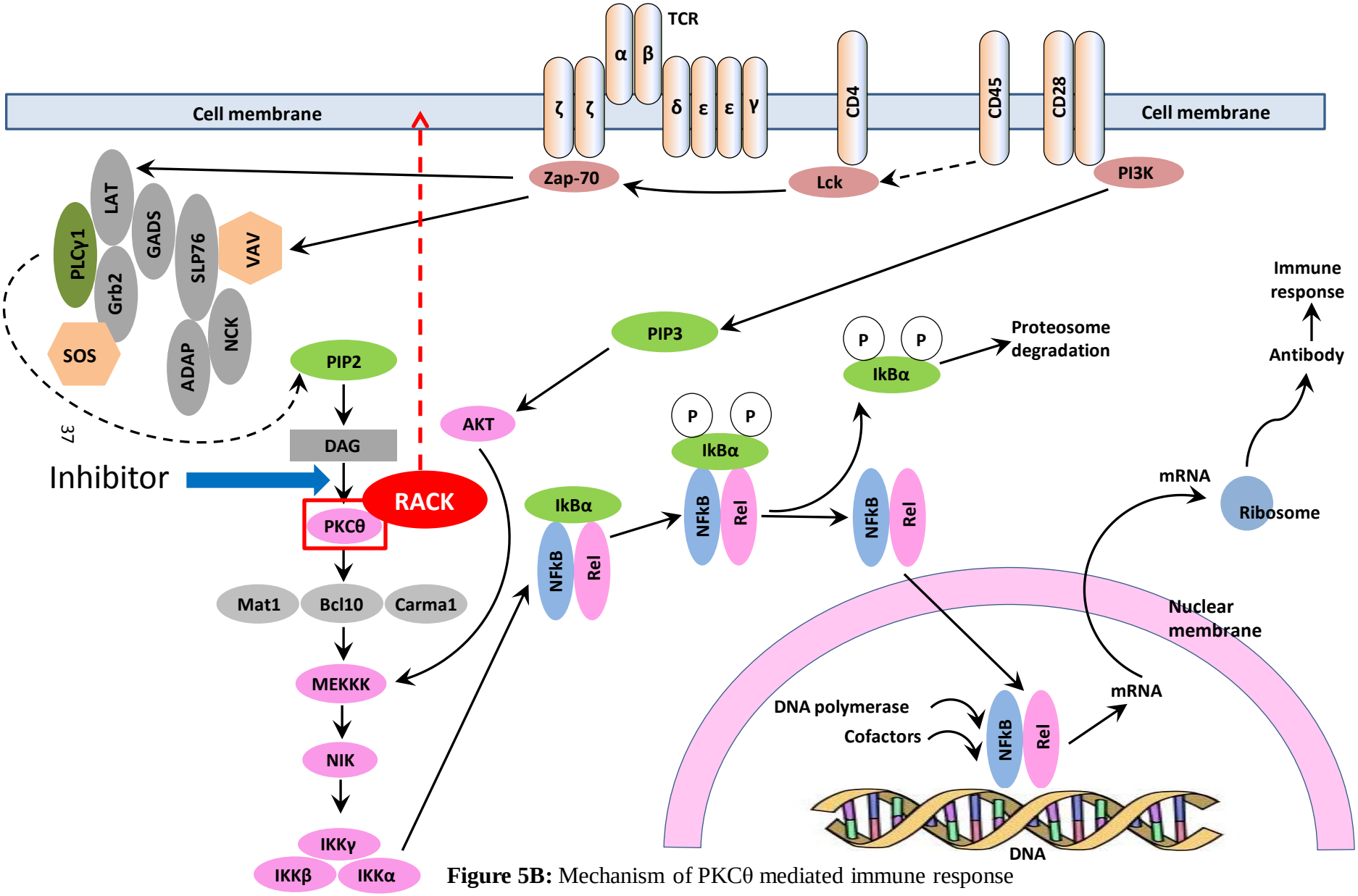

Figure 5B: Mechanism of PKCθ mediated immune response

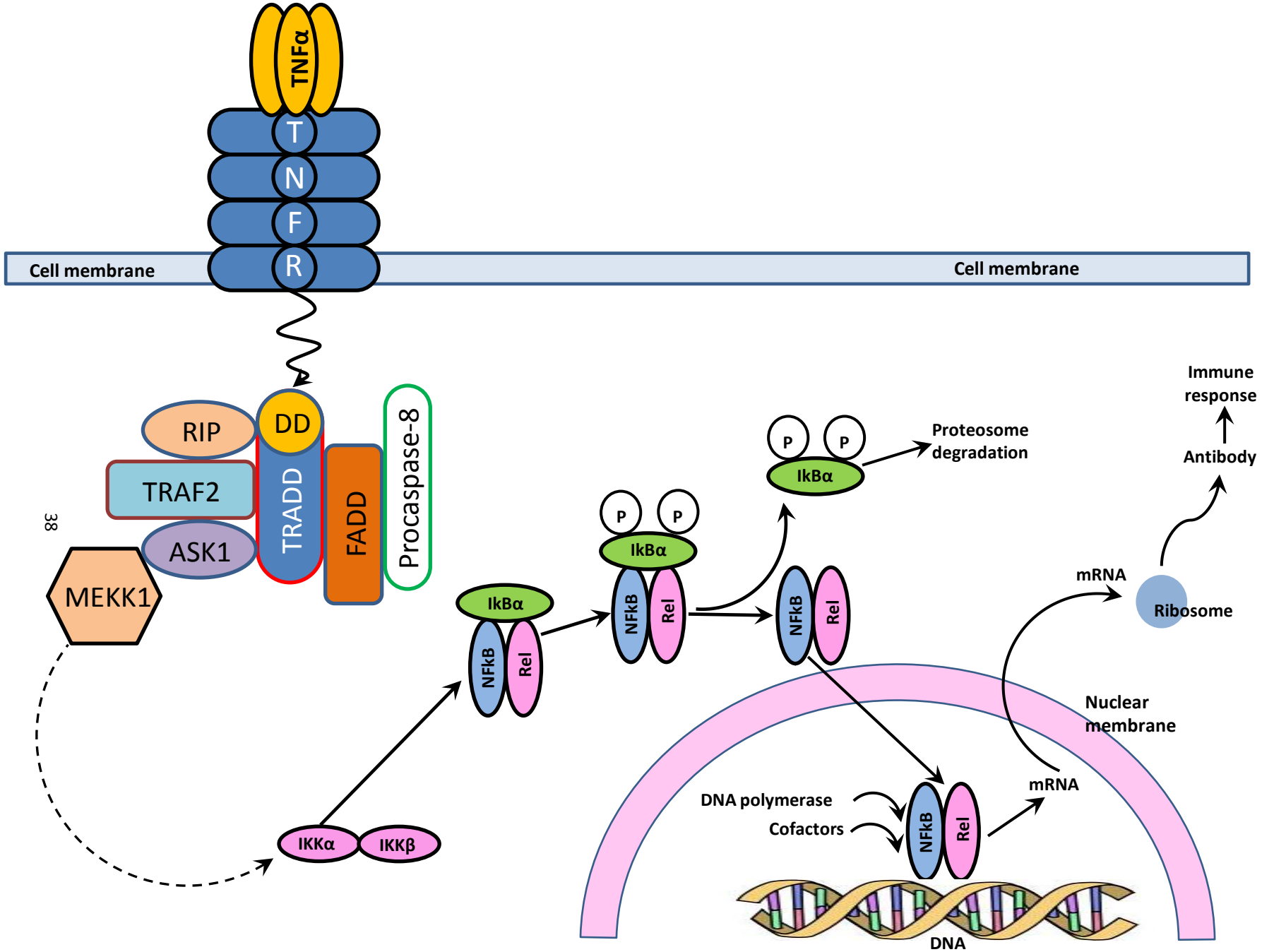

Figure 5C: Compensatory mechanism of TNFα mediated immune response.

1.3.4. Involvement of PKCθ in different T-cells

Pathogen-associated molecular pattern (PAMP), the cytokine environment, antigen load and the affinity and the presence of co-stimulatory and adhesion molecules play critical role in determining the nature of T-cell responses. Naive CD4+ T cells differentiate into different types such as IFNγ and TNFα producing Th1 cells; IL-4, IL-5, IL-10 and IL-13 producing Th2 cells; IL-17A, IL-17F and IL-22 producing Th17 cells or TGFβ and IL-10 producing regulatory Treg cells [66] to effectively counter infections by different pathogens. On the contrary majority of the CD8+ T-cells transform into a single population of CTLs producing IFNγ and TNFα. Virus and bacteria triggers the Th1 and CTL responses [67]. Contrary the allergic and parasite infections initiate the Th2 responses and are generally not associated with PAMP [68, 69]. Previous studies in PKCθ deficient mice demonstrated that T-cell proliferation and IL-2 production were significantly reduced in the absence of PKCθ *in vitro* [70-72]. But the *in vivo* studies using the PKCθ deficient mice showed that the role of PKCθ in T-cell activation and differentiation was not straight forward. Th2 immune responses against Helminthes infection or model allergens were markedly impaired, which were in agreement with the early *in vitro* studies [73, 74]. Also the PKCθ mediated T-cell activation was investigated in recently identified IL-17 induced organ-related autoimmune disorders and was found to require intact PKCθ signaling [74-77].

1.3.5. PKCθ knockout animals and autoimmune diseases

Studies showed PKCθ knockout mice were protected from allergen induced pulmonary allergic hypersensitivity responses [73]. PKCθ knockout mice models of experimental autoimmune encephalomyelitis (EAE) demonstrated reduced T-cell and macrophage infiltration and demyelination in brain in response to antigen challenge [74]. PKCθ knockout mice also demonstrated significantly diminished response in the type II collagen-induced arthritis (CIA) model [78, 79]. PKCθ is a crucial component mediating fat-induced insulin resistance; thereby selective inhibition of PKCθ can be an approach to prevent the fat-induced defects in insulin signaling and glucose transport in skeletal muscles suggesting that PKCθ is a potential therapeutic target for the treatment of type 2 diabetes [80].

1.4. PKCθ INHIBITOR

1.4.1 Rationale of targeting PKCθ

The National Institutes of Health (NIH) estimated approximately 23.5 million (as many as 8% of the U.S. population) Americans had been suffering from autoimmune disease and the prevalence is keep on rising. [81]. Collectively, autoimmune diseases are one of the most prevalent diseases in the U.S. and comprise a major clinical problem [81]. According to statistics from American Autoimmune related diseases association (AARDA), researchers have identified 80-100 different autoimmune disease and suspect that at least 40 additional diseases might have autoimmune origin [82]. Many of these diseases are chronic and can be life-threatening. Autoimmune diseases are the top 10 leading causes of death in female children and women in all age groups up to 64 years [82]. Statistics showed that a close genetic relationship exists among autoimmune disease patients of particular type, explaining common genetic trait of disease [82]. Commonly used immunosuppressant treatments for the remission of the overactive immune conditions often lead to devastating long-term side effects, of which the main problem is becoming prone to the opportunistic infections [82]. Like major clinical conditions such as type II diabetes, part of the population suffering from autoimmune disease conditions also associate with other varying degree of complications, associated morbidity and disability, and available different treatment options.

Despite the segmentation of the market of the autoimmune therapeutics, new drug developing companies found it attractive with the emergence of TNFα blockers (Figure 5C), which has now been approved for multiple indications of the autoimmune conditions including psoriasis, arthritis, rheumatoid arthritis, fibromyalgia etc. Global sales of TNFα blockers in 2009 exceeded $22 billion (www.leaddiscovery.co.uk).

Though TNFα blockers are successful for the treatment of rheumatic diseases, inflammatory bowel disease and psoriasis, this class is not completely effective in many of the autoimmune disease indications and some of the patients are even unresponsive to treatment for unknown reasons [83, 84]. Moreover there are other autoimmune disease conditions that have not been benefited from the development of TNFα blockers, have been managed by the same old therapeutics mostly anti-inflammatory steroids employed for last thirty years [85].

The area of autoimmune therapeutics overlaps with the organ transplant sector. As of April 13, 2012, according to Organ Procurement Transplant Network (OPTN), there are 51,718 people between the age of 50-64 years old on the national waiting list and 21,172 people over 65 years old on the national waiting list in U.S. for receiving an organ. Although collectively only 0.01% of the world population is transplant recipients, this field is in the lime light for the new immunosuppressant therapeutics. Earning less revenue than the TNFα blockers, transplant therapeutics however generate global annual

sales worth $2.7 billion even before the introduction of cyclosporine as an immunosuppressant for organ transplant (www.leaddiscovery.co.uk).

In this context scientists are focusing on the upstream components of PKCθ mediated cascade in the immune pathway. A selective inhibition of the PKCθ may arrest successfully the downstream propagation of the immune responses, which prevents the transfer of pro-inflammatory molecule like NFκB into the nucleus leading to generation of antibodies. However like all other class of immunosuppressant, PKCθ inhibitors may likely compromise the innate immunity against common pathogens. But the question is if the anti-PKCθ therapeutics would have a better benefit to risk profile over the others. The answer of this question lies in the future pre-clinical as well as in the Phase-1 of the clinical trials of the new anti-PKCθ therapeutics.

1.4.2. Challenges in targeting PKCθ

A possible design of PKCθ inhibitor targeting the kinase region lacks selectivity because there has been high degree of homology in kinase region among more than 500 kinases in the human genome [55, 56]. On the other hand there are fewer C1 domains (a total of 67 C1 domains and only 17 PKC C1 domains, and 14 DAG/ phorbol ester sensitive C1 domains). PKCθ C1 domains upon binding to activators translocate to the immunological synapse and mediate the subtype specific downstream immune responses.

Therefore targeting C1 domain could be more selective for the development of the PKCθ selective molecules.

1.4.3. Activator binding in novel PKC C1 domains

Though there is considerable homology among the C1A and C1B subdomains present in the PKC subtypes belonging to the conventional and novel class, yet they differ in their binding affinities for phorbol esters and DAG [25, 86]. In fact there has been an array of discrepancy in the binding affinity of DAG and phorbol esters across the novel PKC C1 domains. For PKCε, the C1B showed high binding affinity for Phorbol ester (PDBu/ PMA) and low for DAG (DiC8/ DiC18), whereas C1A binds with high affinity to DAG and showed low affinity for phorbol esters [32, 33, 35, 36] (Table 7A). Both PKCεC1A and C1B domain equally contribute to the membrane anchoring of the full length kinase [33]. In case of PKCδ, the C1B exhibits high binding affinity for phorbol esters but has a much lower binding affinity for the DAG, whereas the binding preference for C1A is opposite [32-36] (Table 7A). Mutagenesis studies showed that DAG dependant C1A domain in PKCδ plays predominant role in membrane anchoring of the full length kinases [87]. Recently the subtype specific C1B domain binding specificity for DAG has been mapped. A single conserved tryptophan residue at consensus position 22 present on the lipid binding surface of novel PKC C1Bs is responsible for the high affinity DAG binding mediating the membrane anchoring. The conserved tryptophan is replaced by a tyrosine (Tyr-123 in PKCα) in the conventional

PKCs causing the weak C1B interaction toward the membrane translocation [28]. Study also showed a tyrosine to tryptophan swapping in PKCβII C1B turns it into a DAG binding module [28].

1.4.4. Unique activator binding nature of PKCθ C1B subdomain

For all novel PKC subtypes (δ, ε and η) except PKCθ, C1B binds with higher affinity to the phorbol esters than C1A, whereas C1A binds with higher affinity to DAG than the C1B. But the binding preference is different for PKCθ; C1B binds with much higher affinity to both phorbol esters and DAG than C1A indicating that C1B is unique in terms of its structure [32-39]. Irie *et al* [88] showed that PKCθC1B binds phorbol esters with higher affinity than C1A, but DAG binding was not reported in their studies. Cho *et al* showed that C1B of theta binds DAG with higher affinity than the C1A domain and plays more prominent role in DAG-induced membrane translocation and activation [37]. However they used SPR methods using the lipid vesicles containing DiC18, which binds to C1B with higher affinity than the C1A. SPR analysis does not give the true binding affinity of an activator rather it gives the binding affinity of the lipid vesicles containing the activator like DiC18. We employed [^{3}H]PDBu (radioactive phorbol-12, 13-dibutyrate) binding assay with isolated PKCθ C1A and C1B domains to get the true binding affinity of both phorbol esters and DAG [89]. Our data confirms that C1B of PKCθ binds with both phorbol esters and DAG with high affinity.

1.4.5. Basis of targeting the PKCθ C1B subdomain

PKCθ knockout mice were found to be protected from autoimmune diseases like asthma or arthritis in response to antigen challenge, indicating the importance of PKCθ in the immune responses [73, 74, 78, 79]. A selective inhibition of PKCθ therefore can be an attractive approach in the management of overactive immune system leading to suppression of the related disorders [90]. A further reporting of the unique activator binding nature of PKCθ C1B [32-39] and its role in membrane anchoring and kinase activation makes it an ideal target to design of PKCθ specific inhibitor [37]. Besides C1 domains mediate only the downstream immune responses upon DAG induced activation [55, 91]. To design selective PKCθ inhibitor targeting the C1B subdomain requires the knowledge of the three dimensional structure of activator binding pocket and the possible activator binding residues in it.

CHAPTER 2

STATEMENT OF THE PROBLEM

It has been established that PKCθ knockout animals do not develop the autoimmune diseases upon antigen challenge, indicating clearly that PKCθ inactivation may be a therapeutic choice for the management of autoimmune conditions. Yet there no reporting of small molecule, which can selectively inhibit PKCθ. Prior attempts of targeting the ATP binding domain, was proved to be non-specific due to highly conserved catalytic region among the PKCs. Therefore our lab focuses on the C1 domain in the N-terminal regulatory region for the future design of PKCθ specific small molecule. My contribution in this long term goal is to elucidate the structure and to identify the activator binding residues of the C1 target. The goal of the present research is to determine the structure of second cysteine rich activator binding C1 domain of PKCθ and to detect the activator binding residues in it.

CENTRAL HYPOTHESIS

We hypothesize that the three dimensional structure of the C1B subdomain of PKCθ & its activator binding residues are different from other typical PKC C1 domains. This unique nature makes PKCθ to bind with the common activators with high affinity and to selectively translocate to the immunological synapse.

AIMS

Our objective of this research is to establish our hypothesis through the following three aims.

***Aim1*:** To determine the crystal structure of the activator binding pocket of C1B subdomain of PKCθ.

***Aim2*:** To identify the activator binding residues in isolated PKCθC1B subdomain and to study their role in the activator binding.

***Aim3*:** To study the role of the same C1B residues in the full length protein on the kinase activity.

WORKING HYPOTHESIS

For the ease of investigation we made the following working hypothesis for each of the aims to be achieved.

Aim1

Working hypothesis: We hypothesize that the X-ray crystal structure of PKCθC1B subdomain will be essentially different from other typical PKC C1 domains.

Aim2

Working hypothesis: We hypothesize that the activator binding residues in isolated PKCθC1B subdomain can be identified by the structure and sequence alignment with PKCδC1B (1PTQ), followed by the docking of a library of phorbol esters and DAG into PKCθC1B crystal structure as receptor. Study of the mutational effect of these residues on the binding affinity of common activators will reveal their role in activator binding.

Aim3

Working hypothesis: We hypothesize that the study of the mutational effect of the C1B residues in full length kinase, on phorbol ester and DAG induced membrane translocation will reveal their role in kinase activity.

CHAPTER 3

3. METHODS

3.1 Expression vector construction

Bacterial expression vector of PKCθC1B with N-terminal GST tag was generated by subcloning the domain sequence (232-281) from mouse PKCθ cDNA into the pGEX2TK vector (GE Healthcare Biosciences, Little Chalfont, United Kingdom) between the restriction sites *BamHI* and *EcoRI* [92]. GST fused protein consists of a thrombin cleavage site between GST and C1B subdomain. Mammalian expression vector of mouse PKCθ with an enhanced green fluorescence protein (EGFP) tag at the C-terminal was generated by subcloning the corresponding genes with the spacer sequence GGNSGG into the pEGFPN1 vector (Addgene, Cambridge, MA) between the restriction sites *BamHI* and *XhoI* as described earlier [93]. Dr. Amnon Altman (La Jolla Institute for Allergy and Immunology, La Jolla CA) kindly provided with the original PKCθ full length vector.

3.2 Generation of PKCθC1B and PKCθ mutants

The single point mutations (Y239A, T243A, W253G, L255G and Q258G) in the isolated PKCθC1B subdomain and in the full length PKCθ were introduced by polymerase chain reaction (PCR) using the Quikchange Site-Directed Mutagenesis Kit (Stratagene, Santa Clara, CA) [94-96]. Oligonucleotide primers were custom synthesized

at Seqwright, Houston, TX. The mutations were checked for their correct sequences using the sequencing facility at Seqwright. The gene sequencing chromatograms were analyzed using *GeneRunner 3.05* (Hastings Software Inc.) and *FinchTV 1.4.0* (Geospiza, Inc., Seattle, WA)

3.3 Competent cells

In our studies we used two types of competent cells. We used *E. coli* strain BL21 Gold DE3 (Stratagene, Santa Clara, CA) for the protein expression, whereas the *E. coli* strain DH5α (Invitrogen, Grand Island, NY) was used for the plasmid preparation.

3.4 Transformation of BL21 Gold DE3 competent cells

E. coli strain BL21 Gold DE3 was thawed on ice. Three 1.5 mL Eppendorf microcentrifuge tubes for each plasmid were pre-chilled on ice. The water bath was set at 42 ^{o}C for the thermal shock. 50 µL of BL21 Gold DE3 cells was transferred into each of the microcentrifuge tubes. 1 µL of plasmid DNA was added to the competent cells. Cells and plasmid were gently mixed by tapping the tubes and incubated on ice for 30 min. Three LB-ampicillin plates were pre-warmed at 37 ^{o}C. Cells in the microcentrifuge tubes were placed in the water bath for 20 seconds at 42 ^{o}C for thermal shock induction. The microcentrifuge tubes were then incubated on ice for 2 min. 0.95 mL of SOC media was added to each of the microcentrifuge tubes and incubated for 60 min at 37 ^{o}C and 225 rpm in a thermostatic shaker. After incubation 50, 100 and 150 µL of transformed

competent cells were transferred on three separate LB-ampicillin plates respectively. Cells were spreaded on the agar surface using the sterile glass beads. Inoculated plates were incubated overnight at 37 ^{o}C for the colony growth.

3.5 Preparation of stock culture and large scale bacterial culture

Under sterile conditions, 10 mL of autoclaved LB medium was transferred into three 16 mL culture tubes. 10 µL of ampicillin (100 mg/ mL) was added to the LB media before a single isolated colony of the transformed *E. coli* was transferred into each of the culture tubes. Culture tubes were incubated overnight at 37 ^{0}C and 225 rpm.

Next day 1 mL of fresh overnight stock culture was added to previously autoclaved 1 liter TB media in a 2 liter Erlenmeyer flask, followed by addition of 1 mL of ampicillin solution (100 mg/ mL). For either PKCθC1B or its mutants, we grew six liters of bacterial culture. The flasks were put into shaker at 37 ^{o}C and 225 rpm for 4 hrs. After 4 hrs a 2 mL sample was withdrawn and the absorbance was measured at 600 nm. The culture was allowed to grow until the absorbance reached to 0.8-0.9. 10 mL of un-induced culture was collected and kept in a 14 mL tube on ice. Cells were induced with 1 mL IPTG (final concentration 0.5 mM), 1 mL Ampicillin (final concentration 0.1 mg/mL), and 1 mL Zinc Sulfate (final concentration 50 µg/ mL) per flask. Cells were further incubated for another 4 hrs at temperature below 15 ^{o}C and 225 rpm. Cells were harvested when the absorbance of the culture reached to 1.8-2.0. Cells were harvested by

centrifuging the culture in 250 mL polycarbonate centrifuge tubes (Nalgene, Rochester, NY) for 6 min at 6500 rpm using SLA-1500 Sorvall rotor (Thermo Fisher Inc. USA). Harvested pellets were re-suspended in 10 mL 1X PBS containing 1 mM DTT and 1 mM PMSF and stored at -80 ^{o}C.

Previously collected 10 mL un-induced cells were divided into 10 Eppendorf microcentrifuge tubes, into each of the microcentrifuge tubes 200 µL of 50% glycerol was added and mixed well and stored at -80 ^{o}C for future use.

3.6 Protein expression and purification

PKCθC1B subdomain and its mutants fused with N-terminal GST were expressed in *E. coli* strain BL21 Gold DE3 (Stratagene, Santa Clara, CA). Expression and purification and characterization were done following the methods described earlier [33, 87, 97]. 15% SDS PAGE gel analysis of the whole cell lysate confirmed the expression of the desired proteins around 32.0 kDa. Cell pellet (approximately 80 mL) was treated with 4 mL of 20% Triton X-100 (final concentration 1.0%) and 1.6 mL of lysozyme (final concentration 1 mg/ mL) followed by cell lysis using sonication (6 min, 5 sec pulse, 50% amplitude). The lysate, upon centrifugation (40,905 g) yielded the clear supernatant. Treatment of 0.05% polyetheneimine (PEI) precipitated the nucleic acids. A further 15% SDS PAGE gel confirmed that the proteins of interest were in the soluble fraction of the lysate. The clarified supernatant was applied to a glutathione sepharose

column (Akta Prime, GE Healthcare Biosciences, Little Chalfont, United Kingdom) at a rate 1 mL/ min for binding to the matrix. The bound GST fused proteins were thoroughly washed with 1X PBS followed by overnight thrombin digestion (16 hrs at 24 ^{o}C) to cleave the GST tag. Cleaved proteins were eluted with 1X PBS. The proteins were concentrated by ammonium sulfate precipitation, and were further purified by size exclusion chromatography using a Superdex^{TM} 75 column (Akta Purifier, GE Healthcare Biosciences, Little Chalfont, United Kingdom) with the mobile phase 50 mM Tris, 150 mM NaCl, 2 mM DTT, 50 μM $ZnSO_4$, pH 7.2. Eluted dilute protein solution was concentrated using Amicon mini-centrifuge tube (Millipore Corp., GA). The concentration of the protein was measured using Bradford protein assay reagent kit (Bio-Rad, Hercules, CA). The absorbance of the blue colored solution formed upon addition of reagent to protein (400 μl reagent+ 1599 μl water+ 1 μl protein solution) was measured at 595 nm. A previously constructed standard curve of bovine serum albumin (BSA) was used to find the unknown concentration.

3.7 Characterization of the proteins

The purity of the proteins was checked by 15% SDS PAGE gel electrophoresis. The exact molecular mass of the proteins were measured by MALDI-TOF mass spectrometry (Voyager DE-STR Biospectrometry Workstation, Applied Biosystems, Foster City, CA). Proteins were further characterized by its binding to SAPD (a

fluorescent phorbol ester) using fluorescence spectroscopy (QuantaMaster™ 30, PTI Inc., Birmingham, NJ) [98].

3.7.1 SDS PAGE

Protein samples were mixed with sample loading buffer (Bio-Rad, Hercules, CA) followed by heating at 100 ^{o}C in water bath for 6 mins to denature the proteins. Protein solutions after boiling were subjected to centrifugation for 15 mins at 15000 rpm to precipitate any insoluble residue. Protein samples were then loaded in the wells of the gels and run for 60 mins at 150 volt. After separation of the proteins, gels were removed from the cast and stained with Coomasie blue for 20 mins followed by de-staining the gels for 2 hrs. Proteins were visualized as blue bands.

3.7.2 MALDI TOF mass spectral analysis

MALDI TOF mass spectra were recorded in Voyager DE-STR Biospectrometry Workstation (Applied Biosystems, Foster City, CA) using a gold coated stainless steel 100 well plate. Protein solutions of 10 pmole/ µl concentration were used. Proteins were mixed thoroughly in 1: 10 ratio with saturated solution (50:50 water/ acetonitrile with 0.1% trifluoroacetic acid final concentration) of α-cyano-4-hydroxycinnamic acid (CHCA, MW-189.04 Da, a good matrix choice for samples with MW <10,000 Da) followed by filtering using ZipTip (Millipore Corp. GA). 1 µl of the sample was

transferred on the plate in the designated well. Samples were dried under vacuum and finally subjected for run in the device.

3.7.3 Fluorescence study of Sapintoxin-D (SAPD) binding

SAPD is a fluorescent phorbol ester that binds to typical C1 domains when they are folded properly. Binding of SAPD (1 μM) (excitation λ_{max} 355 nm) to varying concentration of PKCθC1B and its mutants in buffer (50 mM Tris, 100 mM NaCl, pH 7.4) showed a characteristic blue shift of the SAPD fluorescence maxima in a concentration gradient manner.

3.7.4 Fluorescence quenching study of activator binding to PKCθC1B and its mutants

Both PKCθC1B and its mutants when excited at 288 nm, give characteristic intrinsic fluorescence peak for the single tryptophan at consensus position 22 in their sequence. The fluorescence emission maxima of the proteins upon binding with activators quenched in a sigmoidal manner with the increased molar concentration of activators added. Fluorescence quenching data collected upon activator binding were plotted and fitting into modified Hill equation to get the EC_{50} values of the activators for PKCPKCθC1B and its mutants.

3.8 Cell culture

HEK293 cell line expressing the ecdysone receptor (Invitrogen, Grand Island, NY) was used to express the full length PKCθ and its C1B subdomain mutants. The cells were cultured in plastic petridishes in DMEM supplemented with 10% fetal bovine serum (FBS) and 1% antibiotic-antimycotic at 37 °C in 5% CO_2 and 98% humidity. The confluent cells (90%) were transfected by adding 1 mL unsupplemented DMEM containing 6 μg of endotoxin-free plasmid and 9 μl of Plus reagent (Invitrogen, Grand Island, NY) and 9 μl of lipofectamine reagent (Invitrogen, Grand Island, NY) for 12 h at 37 °C. The transfection medium was removed and the cells were washed with 1X PBS followed by the addition of antibiotic-free DMEM supplemented with FBS. The protein expression was induced for 48 h from the time of transfection before the cells were ready for membrane translocation studies [37, 99]. The expression of the full length PKCθ and its mutants were detected by Western blot analysis of the cell lysate 48 h post-transfection.

3.8.1 Western blot analysis

After resolving the proteins in the SDS PAGE gel, protein bands were transferred into nitrocellulose membrane (transfer time 3 hrs at 180 ampere). Membranes with protein bands were then blocked with 1% BSA to prevent the non-specific binding of the antibodies. After blocking, the membranes were washed thoroughly (three times, 15 mins each) with TBST buffer followed by treating the membranes overnight with rabbit anti-

EGFP primary antibody (1:5000 dilution) at 4 ^{o}C. Membranes were washed another round (three times, 15 mins each) before they were treated with rabbit IgG HRP linked secondary antibody (1:5000 dilution) for one hour at room temperature for chemi-luminescence visualization.

3.9 Crystallization, data collection and refinement

Hanging drop vapor diffusion method was used to grow PKCθC1B crystals. 1 µL volume of protein solution (25 mg/mL) in buffer-E (50 mM Tris, 150 mM NaCl, 2 mM DTT, 50 µM $ZnSO_4$, pH 7.2) was mixed with equal volume of reservoir solution consisting of 0.1 M lithium acetate and 20% PEG 3350 on a siliconised glass cover slip, which was then inverted and sealed over a 0.5 mL of reservoir containing the same reservoir solution. At 20 ^{o}C protein crystals were formed after a week and half. Before data collection clean crystals were soaked for 1-2 minutes in cryo-protectant consisting of 10% glycerol in reservoir solution followed by flash freezing in liquid nitrogen [100]. Diffraction data of PKCθC1B crystal were collected at Baylor College of Medicine, Houston TX home source RIGAKU FR-E^{+} (Rigaku) X-ray diffraction facility. Diffraction data set were processed by using *HKL 2000* as implemented by the *CCP4 suite* [101]. Space group of the unliganded crystal was confirmed by *POINTLESS* [102]. *Matthew's coefficient* [103] suggested the number of molecule in the single asymmetric unit. Phase problem was solved using molecular replacement program, *PHASER* [104] in *CCP4 suite*. After automated model building from electron density and solvent addition

using *ARP/wARP* [105] the model refinement was done with *Refmac* (*CCP4*) [106]. For graphical interface, *COOT* was used [107].

3.10 Molecular docking

Three-dimensional chemical structures of DAG and phorbol ester analogs were downloaded from *PubChem* and were subjected to pre dock energy minimization using Powell method in the *Sybyl 8.0* (Tripos International, St. Louis, MO) with an iteration of 100. These analogs were incorporated together into a single activator library ready to be docked into the crystal structure of PKCθC1B. A residue-based molecular docking was done in the *SurflexDock* module of *Sybyl 8.0* using threshold-0.5, bloat-2.0 and radius-3 Å for the protomol generation. Residues Tyr-239, Lys-240, Ser-241, Pro-242, Thr-243, Phe-244, Leu-251, Leu-252, Trp-253, Gly-254, Leu-255 and Glu-258 were used to generate the protomol. These residues were selected by comparing the PKCθC1B sequence to the activator phorbol ester binding region the in PKCδC1B sequence. Ring flexibility, soft grid treatment, pre-dock and post-dock energy minimization were also applied for the docking procedure. A high total score values represent better fitting.

3.11 [^{3}H]PDBu binding assay

Binding of PDBu and DOG to PKCθC1B and its mutants was measured using the poly ethylene glycol precipitation assay method as described earlier [89]. Briefly, an assay mixture (250 µl) containing 50 mM Tris-Cl (pH 7.4), 100 µg/ mL PS, 4 mg/mL

bovine IgG, varying concentration of 2-10 nM [^{3}H]PDBu, 1 mM EGTA, and the PKCθC1B or its mutants (20 ng/ tube) were incubated for 10 minutes at 18 °C. The samples were chilled on ice for 7 min, and 200 µl of 35% poly ethylene glycol in 50 mM Tris-Cl (pH 7.4) was added and the tubes were vigorously vortexed. The tubes were incubated on ice for an additional 10 min and then centrifuged at 4 °C. A 100 µl aliquot of the supernatant was used to determine the free [^{3}H] PDBu concentration, and the pellet was carefully dried. The tip of the centrifuge tube was cut off, and the pellet was counted in a scintillation counter to determine the total bound [^{3}H] PDBu. Specific binding was calculated as the difference between the total minus the nonspecific binding. Non-specific binding was determined in the presence of 40 µM non-radioactive PDBu. For the C1B mutants with low binding affinity, the assay was modified to reduce the specific activity of the [^{3}H] PDBu by dilution with non-radioactive PDBu to permit measurement of binding activity at higher ligand concentrations. K_d were determined from the Scatchard plot obtained by fitting the data into a two component model of saturable receptor binding plus linear non-specific binding using *Prism* (Graph Pad Software, San Diego, CA) [89]. Binding affinities of DOG to PKCθC1B and its mutants were determined by competition of [^{3}H] PDBu binding using the above conditions but with a [^{3}H] PDBu, 2.5-5 times the concentration of K_d for each mutants and with a series of concentrations of DOG (1-100,000 nM). The DOG was dissolved in chloroform and added to the phospholipids; the mixture was then dried down, buffer was added, and the mixture was then sonicated and added to the assay. For analysis of the dependence on

the phospholipids composition, total phospholipids was maintained at 100 µg/ mL final concentration while the % PS was varied from 0-87.5% with the remainder as PC [89].

3.12. Membrane translocation of PKCθ

HEK 293 cells expressing full length PKCθ and its C1B mutants were treated with TPA and DOG separately for 2 h [108]. Harvested cells were then washed with cold PBS and were resuspended in lysis buffer (20 mM Tris, pH 7.4) containing protease inhibitor cocktail. Cells were lysed by pushing back and forth in a 1 mL insulin syringe with 16 gauge needle. Cell lysate was then subjected to ultracentrifugation (200000 g) for 1 h at 4 ^{o}C. The supernatant collected is designated as the cytosolic fraction. The pellet was then resuspended again in lysis buffer with protease inhibitor and 1% Triton X-100 and kept on ice for 1 h. The mixture was sonicated 3 times with 5 sec pulse. The mixture was then centrifuged at 200000 g for 1 h. This supernatant is designated as the soluble membrane fraction [109]. Western blot on the cell fractions was performed as described earlier [108]. The proteins were transferred in the nitrocellulose (0.45 µm) membrane and was immunoassayed using anti-EGFP primary antibody (1:5000 dilution) followed by a treatment of HRP linked secondary antibody (1:5000 dilution) for chemi-luminescence visualization. An enhanced chemiluminescence detection system from Thermo Scientific (Waltham, MA) was used to visualize the labeled protein bands. The relative intensity of the protein band was calculated using alphaImager from Alpha Innotech (San Leandro, CA) gel dock system [108].

3.13 Statistical analysis

Test of significance of the data obtained (for both PKCθ wild type and its C1B mutants) from activator induced membrane translocation study was analyzed using unpaired two tail T test, with 99% confidence and $P < 0.05$.

CHAPTER 4

4. RESULTS

4.1. Protein expression and purification

15% SDS-PAGE gel analysis of the whole cell lysate confirmed high level of expression of all the GST fused proteins (PKCθC1A, θC1B and the C1B mutants) in *E. coli* (BL21 Gold DE3). After purification through glutathione Sepharose column and subsequent cleavage of the GST tag, and ammonium sulphate precipitation, PKCθC1A, θC1B and its mutants were obtained in decent yield (Table 8).

Table 8: Yield of pure PKCθ C1 proteins (wild type and mutants).

PKCθC1A	PKCθC1B	PKCθC1B Y239A	PKCθC1B T243A	PKCθC1B W253G	PKCθC1B L255G	PKCθC1B Q258G
8.83 mg/ lit	9.63 mg/ lit	3.55 mg/ lit	2.41 mg/ lit	15.3 mg/ lit	4.33 mg/ lit	3.90 mg/ lit

4.2. Protein characterization

Purified proteins were thoroughly characterized by gel permeation chromatography, SDS-PAGE gel, MALDI-TOF mass spectroscopy, and phorbol ester binding.

4.2.1. Gel permeation chromatography

All the proteins showed a single symmetrical peak while eluting from the Superdex-75 column with a retention time corresponding to their stokes radii indicating the purity as well as the proper folding of the proteins. The representative single symmetrical elution peaks of PKCθC1A, PKCθC1B, and PKCθC1B L255G from the Superdex-75 column were shown (Figure 6).

4.2.2. SDS PAGE

In SDS-PAGE gel analysis all PKCθ C1 proteins showed the band around 7.0 kDa. A representative 15% SDS PAGE image of PKCθC1B and all its C1B mutant proteins is shown (Figure 7).

4.2.3. MALDI TOF mass spectroscopy

The molecular mass of the proteins were further confirmed by MALDI TOF mass spectrometry. For PKCθC1A, PKCθC1B, Y239A, T243A, W253G, L255G and Q258G, the molecular masses were found to be 7414.20, 7333.29, 7244.99, 7304.52, 7209.905, 7280.64 and 7271.53 Da respectively with an accuracy of ± 0.4%. The representative MALDI TOF spectra of the pure PKCθC1A and PKCθC1B were shown (Figure 8).

4.2.4. Fluorescence study of SAPD binding

The folding and functionality of the proteins were checked by its binding with fluorescent phorbol ester, SAPD. The fluorescence emission maximum of SAPD at 441

nm in buffer E was blue shifted in presence of fifty fold excess of proteins added to it. The observed emission maxima were 412, 418, 423, 422, 421, 417 and 435 nm for PKCθC1A, PKCθC1B, Y239A, T243A, W253G, L255G and Q258G respectively. This blue shift of the fluorescence maxima indicated that the proteins were in their active conformation therefore bound to SAPD whereas the extent of binding for the C1B mutants were different indicating the difference in their conformation compared to the PKCθC1B wild type. The representative blue shift of the fluorescence maxima for PKCθC1A and PKCθC1B are shown (Figure 9).

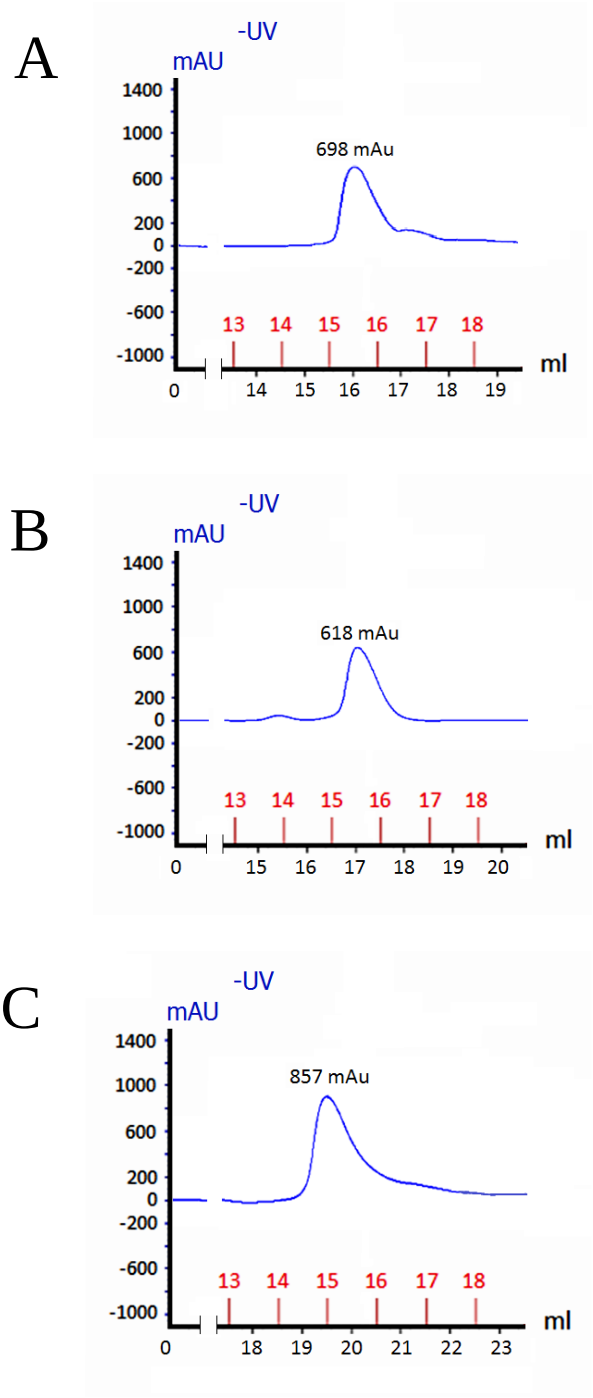

Figure 6: A single symmetrical elution peak indicates the purity and proper folding of A) PKCθC1A, B) PKCθC1B, and C) PKCθC1B L255G.

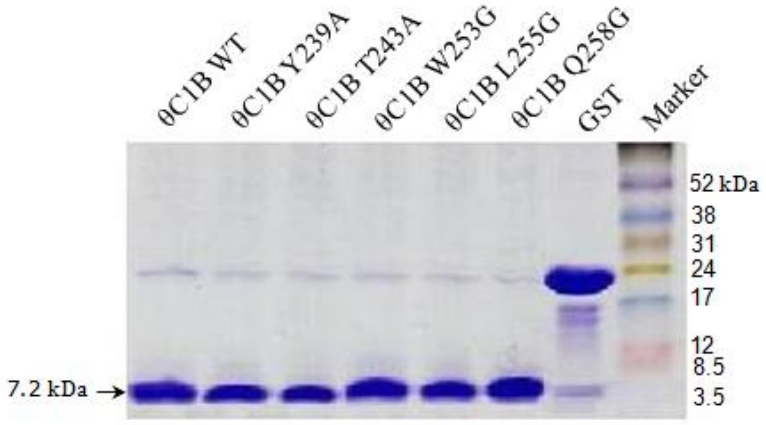

Figure 7: 15% SDS PAGE gel analysis of the GST cleaved PKCθC1B and all its C1B mutants showed the molecular mass around 7.2 kDa. Amersham (GE Healthcare Biosciences, Little Chalfont, United Kingdom) low range protein marker indicated the proteins have proper molecular masses.

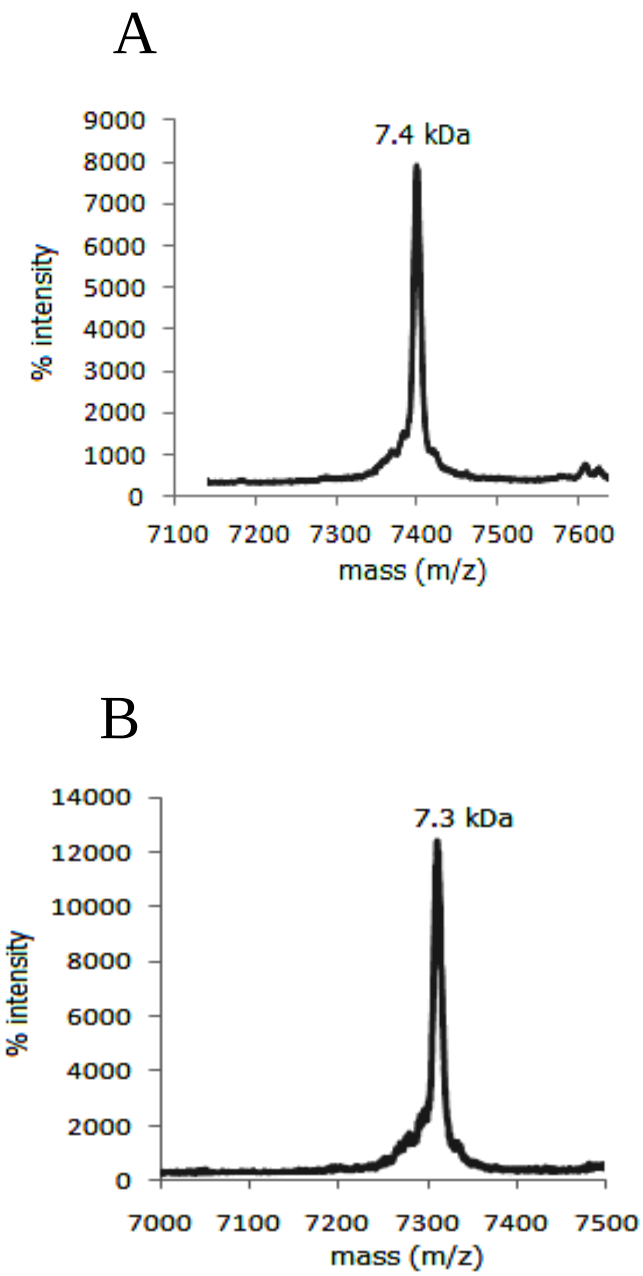

Figure 8: A sharp single peak of A) pure PKCθC1A at m/z 7.4, and B) pure PKCθC1B at m/z 7.3 in MALDI TOF mass spectra.

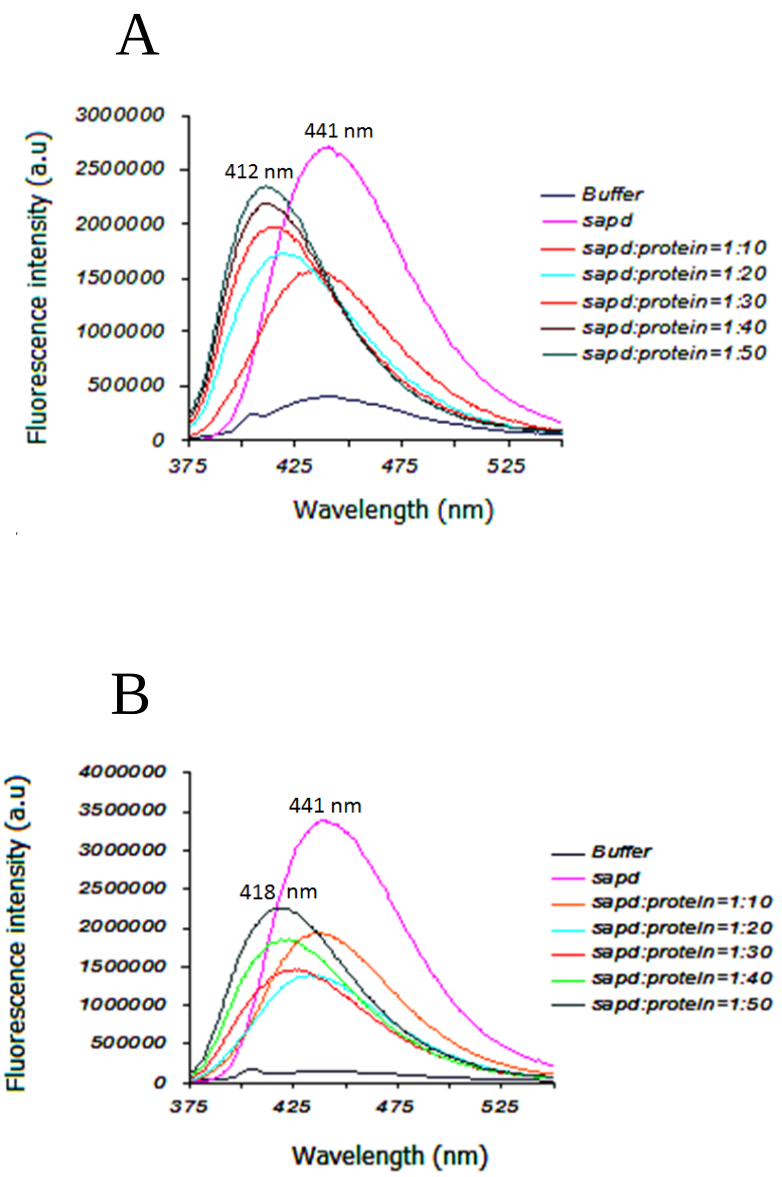

Figure 9: Blue shift of SAPD emission maxima with varying increased molar concentration of A) PKCθC1A, and B) PKCθC1B. Highest blue shift was observed at 1: 50 molar ratio of SAPD to protein.

4.3 Expression and characterization of PKCθ and its C1B subdomain mutants in HEK293 cells

Western blot analysis of the whole cell lysate of HEK293 cells transiently transfected with the corresponding PKCθ and its C1B mutants plasmids, detected a band near 100 KDa confirming the expression of the full length PKCθ and its C1B subdomain mutants (Figure 10).

Figure 10: Western blot image of whole HEK293 cell lysate expressing full length PKCθ and its C1B mutants showing the protein bands at 100 kDa.

4.4 Crystal structure of PKCθC1B

When grown in 0.2 M lithium acetate dihydrate and 20% PEG 3350, pH 7.9, diamond shaped crystals of PKCθC1B with an average dimension of 80×60×40 μm were obtained (Figure 11A). To distinguish between protein and salt crystals, crystals were soaked in Izit dye followed by washing with the mother liquor. Protein crystals retained the blue color after washing, whereas the salt crystals did not retain the blue dye (Figure 11B and C). The space group of the crystal was hexagonal $P6_1$ with a unit cell dimension of 65.71×65.71× 27.09 Å and unit angle (^{0}) α = β =90, γ =120 (Table 9). Matthew's coefficient [103] suggested one molecule in the single asymmetric unit. The structure was refined with good geometry and refinement statistics. The protein crystal was diffracted at 1.63Å resolution (Figure 12). Electron density map (σ $2F_0$-Fc) well fitted to the model (Figure 13). Refinement statistics % R_{work} and R_{free} of 16.25 and 19.97 respectively indicating that the level of disagreement between the observed structure factors and the calculated structure factors were well within the acceptable limit. The overall B factor is 21.2 (excluding all the water molecules and Zn atoms) indicating that the atoms are having less thermodynamic oscillation and hence likely positioned well within their respective electron density shell. Ramachandran plot shows that no residues were in the disallowed region (98.0% residues in favored region, 2.0% residues in allowed region) (Figure 14A and B).

A

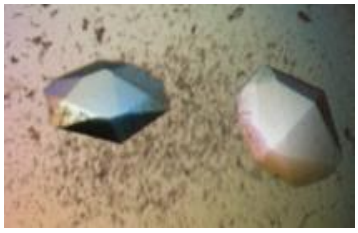

B

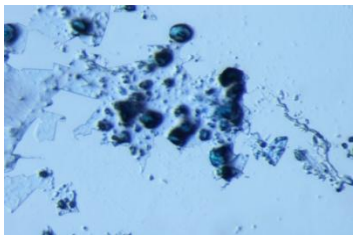

C

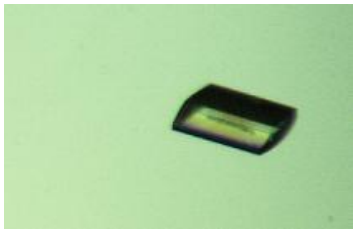

Figure 11: A) Diamond shaped crystal of PKCθC1B grown in 0.2 M lithium acetate dihydrate and 20% PEG 3350, pH 7.9, B) PKCθC1B crystal retains blue color of Izit dye upon soaking. It is a confirmatory test to distinguish the protein crystals from the salt crystals, and C) Sodium acetate crystal does not retain the blue color of the Izit dye after wash.

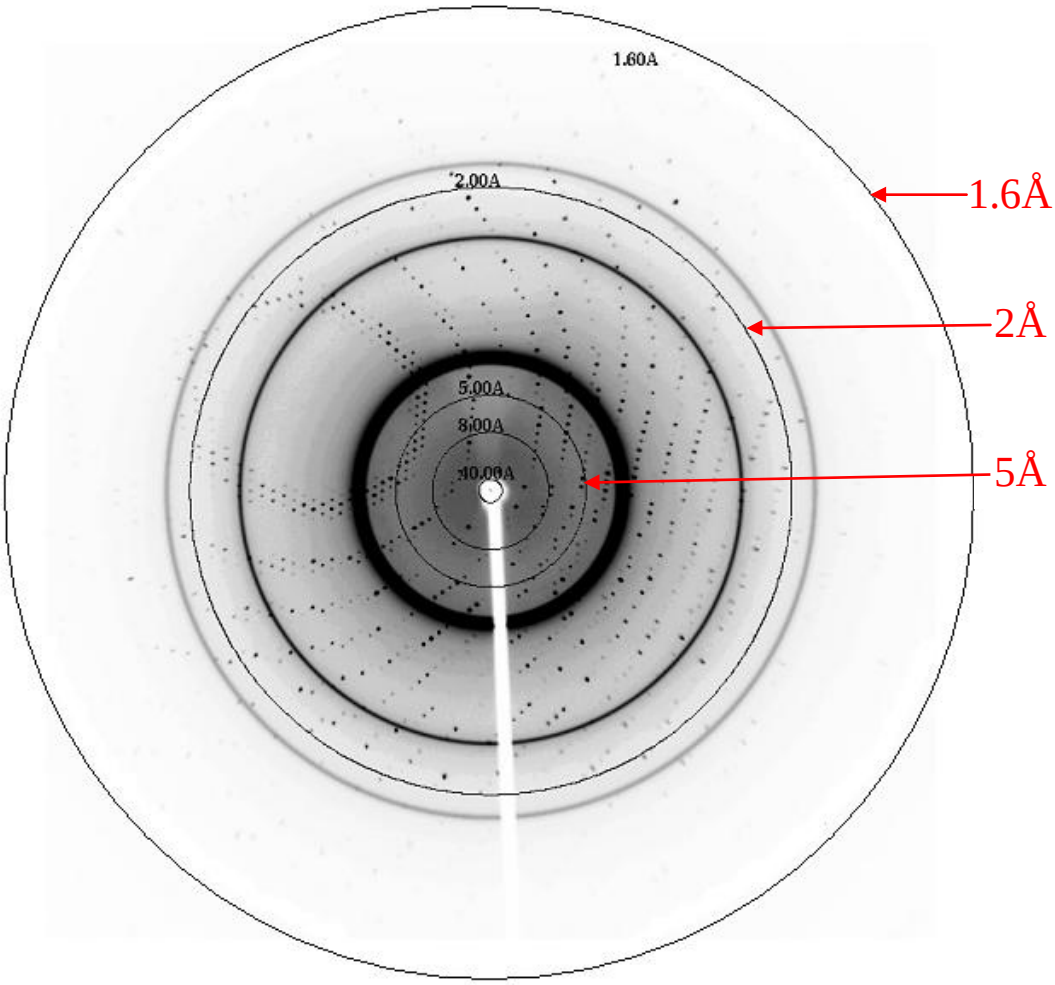

Figure 12: X-ray diffraction image of PKCθC1B showing spots at 1.60 ^{o}A resolution.

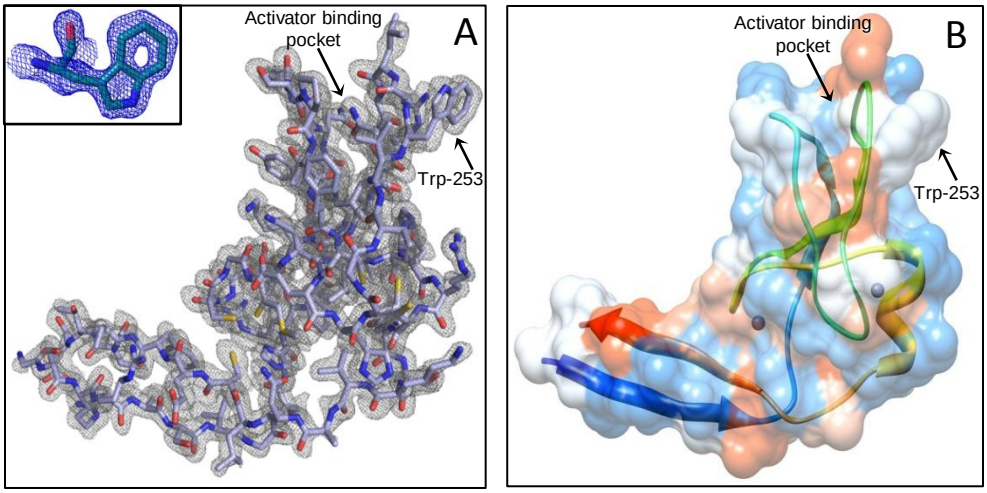

Figure 13: A) Residues are aligned to the electron density map of PKCθC1B subdomain where Trp-253 is oriented towards the membrane. Inset: A high resolution (1.68 Å) electron density map of Trp-253, B) Ribbon structure of PKCθC1B superimposed on the contour surface. Blue area on the contour surface represents the polar residues, whereas the white to orange red represents the most hydrophobic residues.

Table 9: PKCθC1B crystal data processing and refinement statistics

Crystal parameters	**Values**
Space Group	$P6_1$
Unit Cell Axis (Å)	a = b = 65.85, c = 27.12
Resolution (Å)	28.51- (1.63)
Total number of reflections	45483
Total number of unique reflections	7559
Redundancy	6.0
Completeness (%)	88.39 (98.00)
I/σ	18.6 (9.7)
R_{merge} (%)	0.044 (0.115)
R_{work}/ $R_{free\ (\%)}$	17.14/ 20.42
X-ray wavelength	1.54178 Å (copper anode)
Distance (mm)	100
Number of water molecule	130
Wilson B factor	15.2
B factor	19.93
Number of metal atom	2 Zn
Bond length (Å, rms)	0.010
Bond angle (^{0}, rms)	1.030-0.997

A

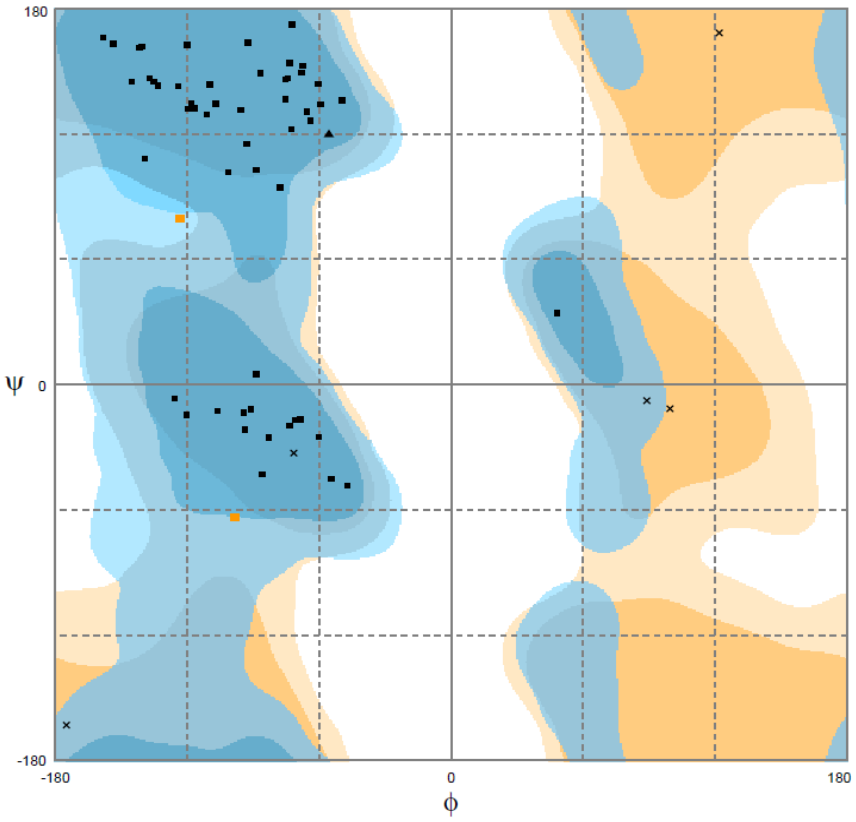

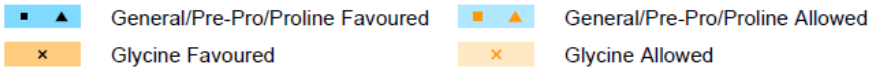

Number of residues in favoured region (~98.0% expected)	: 61 (96.8%)
Number of residues in allowed region (~2.0% expected)	: 2 (3.2%)
Number of residues in outlier region	: 0 (0.0%)

Figure 14A: Ramachandran plot of the residues in PKCθC1B crystal structure. The plot showed 98.0% residues were in favored region whereas 2.0% residues were in allowed region.

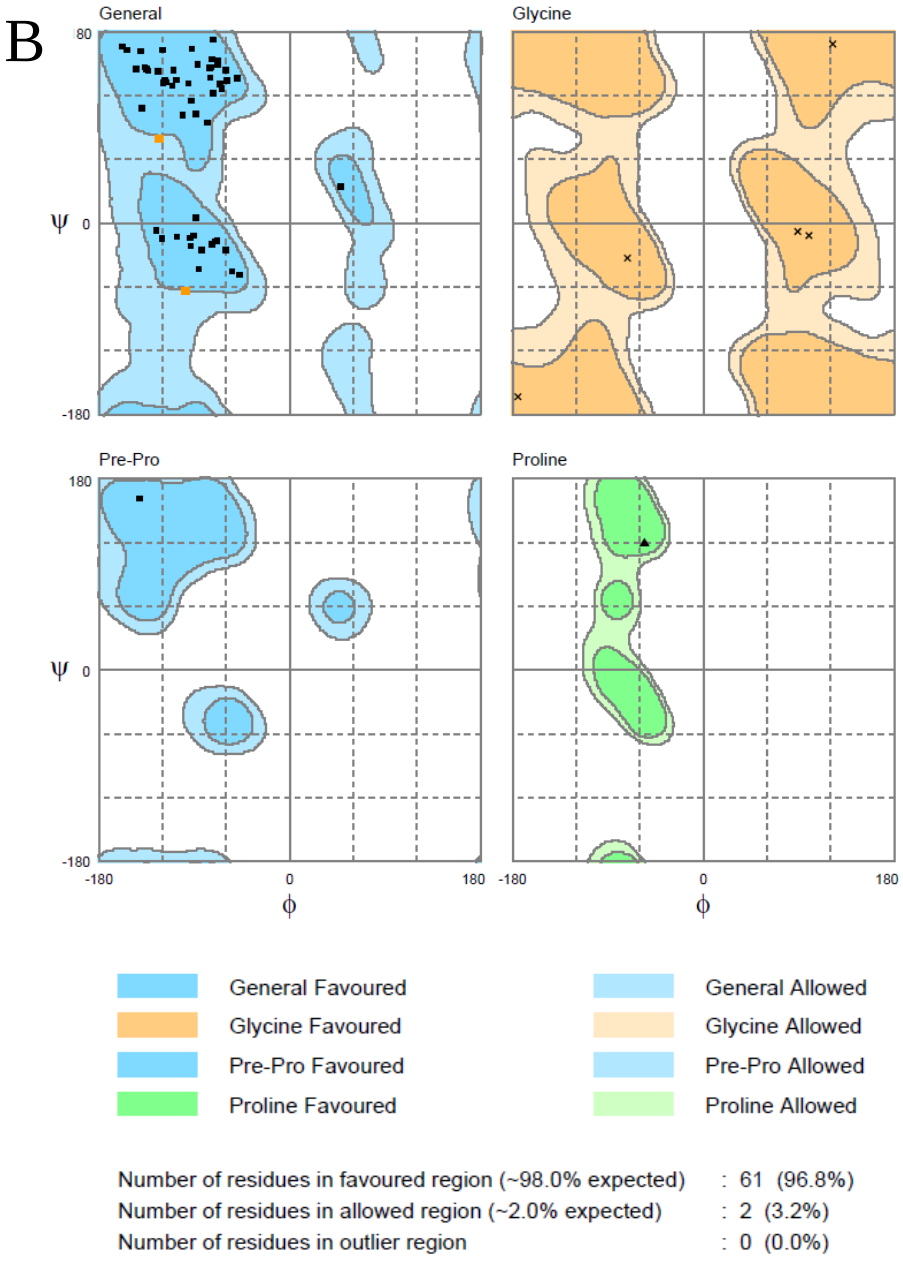

Figure 14B: Ramachandran plot of the general, glycine, pre-pro and proline residues in PKCθC1B crystal structure. The plot showed 98.0% residues were in favored region whereas 2.0% residues were in allowed region.

The overall structure consists of two beta sheets (24%) and a short alpha helix (12%) at the C terminal end identical to the crystal structure of PKCδC1B (1PTQ) [29]. The two beta sheets formed a V-shaped activator binding groove (Figure 15). Two zinc fingers were detected in the structure each of which is in coordination with three cysteines and a histidine. First zinc finger consisted of Cys-261, Cys-264, Cys-280 and His-231 whereas the second zinc finger coordinated Cys-247, Cys-244, Cys-272 and His-269 (Figure 16). A total number of 129 water molecules were present in the structure. PKCθC1B has a high sequence homology (80%) and structural similarity with the crystal structure of PKCδC1B (1PTQ) with an rmsd of 0.66 indicating that they are almost superimposable except the activator binding pocket width of PKCθC1B is slightly narrower (7.56Å) than the PKCδC1B (8.075Å). Overlaying of the crystal structures of PKCδC1B (blue) (1PTQ) to the PKCPKCθC1B (Red) showed that all the homologous residues were superimposable except the Trp-253 residue (Figure 17). In PKCθC1B the Trp-253 was oriented toward the membrane binding region of the C1B subdomain whereas the corresponding homologous Trp-252 in PKCδC1B was oriented away from the membrane binding region of the C1B subdomain (Figure 17).

We also overlaid the NMR structure of PKCθC1B (2ENZ) with PKCθC1B and δC1B (1PTQ) to get confirmed that Trp-253 was oriented towards the membrane both in NMR and crystal structure (Figure 17). The position of Trp-253 in PKCθC1B was outside the activator binding cavity and toward the membrane, therefore it might not

interact directly with the activator but it could possibly stabilize the binding of the activator through hydrophobic interactions with the membrane lipids.

Thrombin treatment cleaved the N-terminal GST tag leaving extra nine linker residues (GSRRASVGS) with the PKCθC1B. Also on the C-terminal there were another extra six (EFIVTD) residues expressed as part of the protein due to the subcloning of the PKCθC1B domain sequence in pGEX2TK vector. These extra residues form two anti-parallel beta sheets, which presumably stabilize the overall PKCθC1B structure for crystal formation (Figure 18). Zhang *et al.* reported that these extra residues were important to grow δC1B co-crystals also [29].

While an activator bound structure of PKCθC1B would be able to identify the protein residues directly involved in activator binding, attempts with several hundred precipitants and conditions did not yield the protein-ligand co-crystals. Further, soaking experiment with different activator solution was also unsuccessful due to the solubility problems of the activators in aqueous buffer.

Therefore we performed virtual molecular docking of a library of DAG (Table 10A) and phorbol esters (Table 10B) using PKCθC1B as the receptor. Docking showed the array of the possible activator binding residues capable of forming hydrogen bonds with the docked activators. Additionally the overlay of crystal structure of PKCδC1B

(1PTQ) bound to phorbol-13-O-acetate and crystal structure of PKCθC1B and the sequence alignment of PKCδC1B and PKCθC1B helped locate the possible homologous activator binding residues (Figure 19).

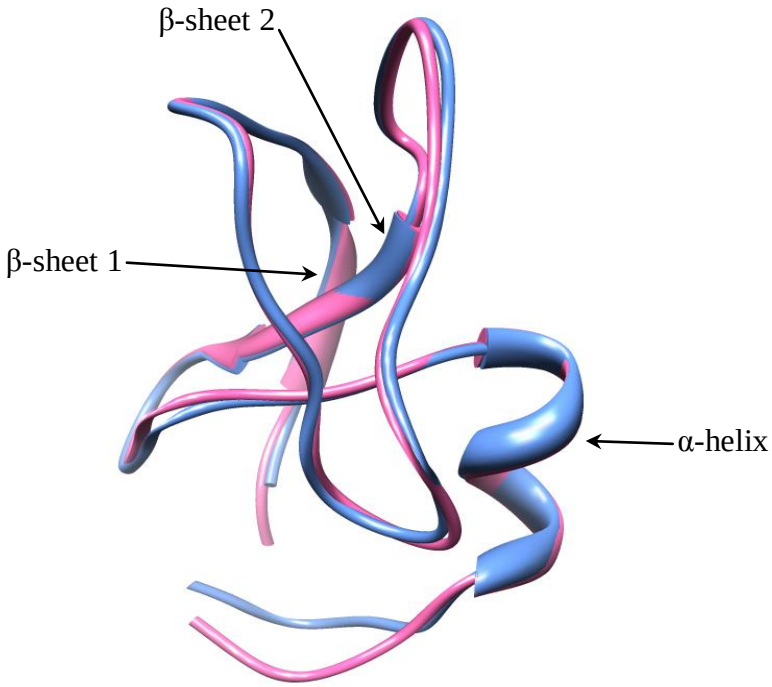

Figure 15: Overlay of the crystal structure of PKCδC1B (corn flower blue) and PKCθ C1B (hot pink). Superimposing of both C1B structures confirmed that each possessed two long beta sheets (20% β-sheet) forming a V-shaped activator binding groove and a short alpha helix (4% α-helix) at the C-terminal end. Both C1B domains share high sequence homology (80%).

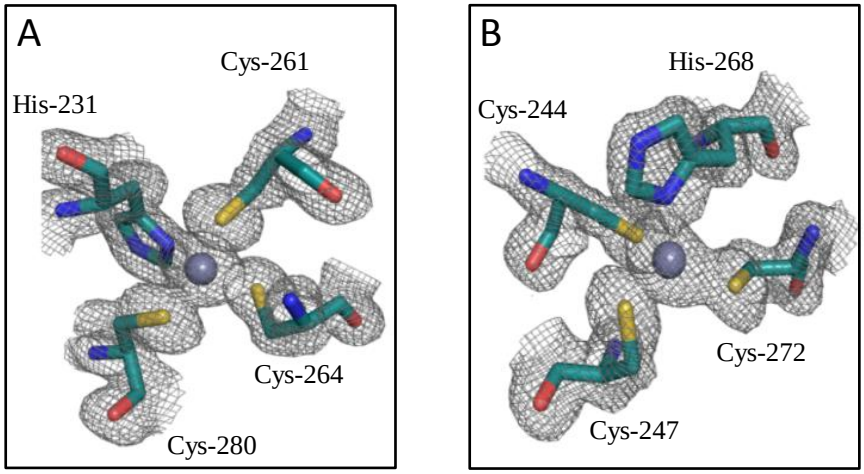

Figure 16: Electron density map of, A) first zinc coordinating site, and B) second zinc coordinating site in C1B subdomain of PKC*θ*.

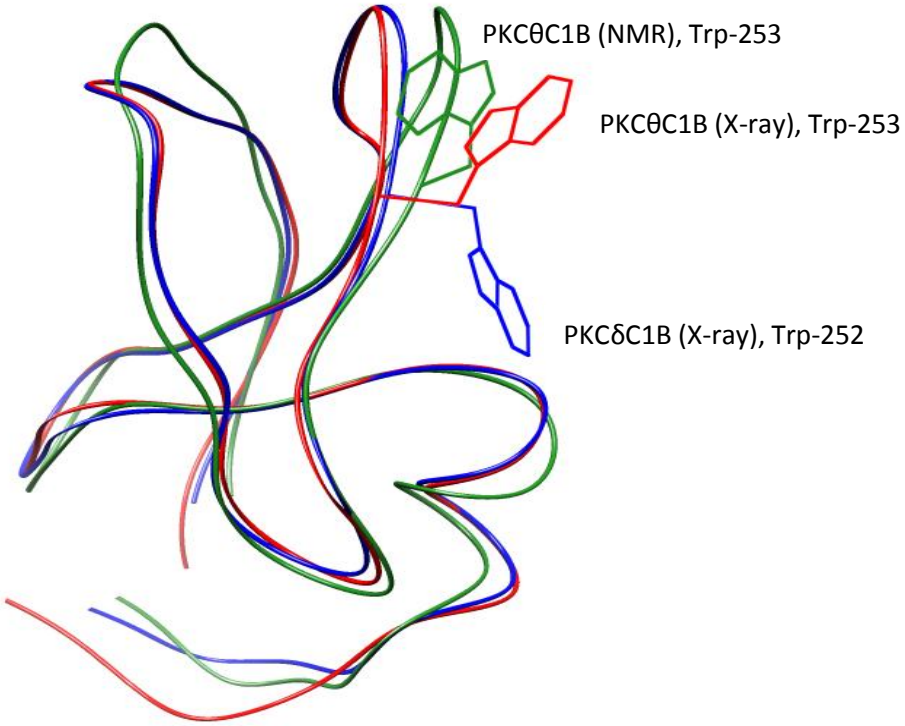

Figure 17: Overlaying structure of crystal structure of PKCθC1B (red), NMR structure of PKCθC1B (green), and crystal structure of PKCδC1B (blue) shows the relative orientation of their corresponding Trp-253 and Trp-252. Trp-253 of PKCθC1B is oriented towards the membrane whereas the Trp-252 of PKCδC1B is oriented opposite to the membrane.

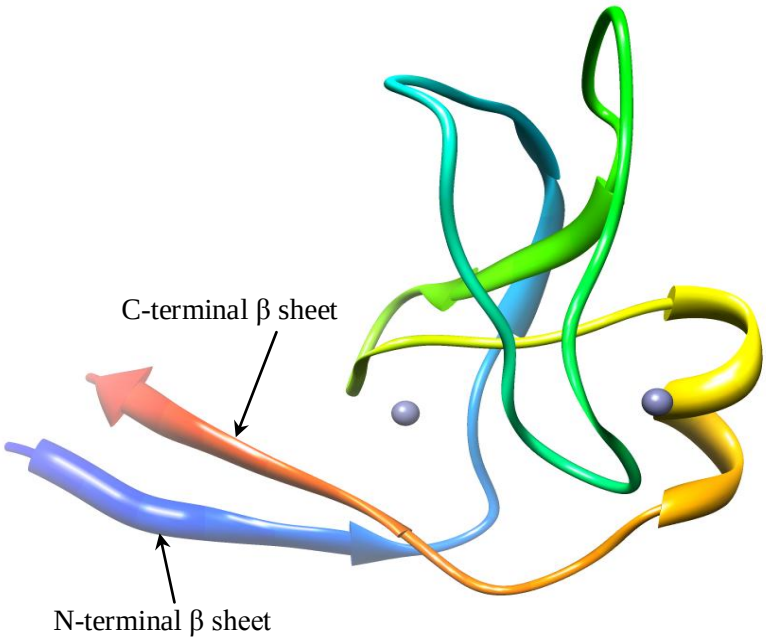

Figure 18: Extra Nine N-terminal residues (GSRRASVGS) and six C-terminal residues (EFIVTD) in PKCθC1B crystal structure formed two anti-parallel β-sheets, which stabilized the overall structure and favored the protein crystal formation.

Table 10A: List of DAG analogs docked in PKCθC1B crystal structure. The residues those forms hydrogen bond(s) with the activators are denoted with (●) symbol against them. *Sn*-1, 2 dioctanoylglycerol (DiC8) and *Sn*-1, 2 dioleoylglycerol (DiC18) are the two most common DAG analogs used for PKC activation.

PubChem ID of DAG analogs		Number of H-bonds with residues	Residues interacting						
			Y239	K240	S241	W253	G254	L255	Q258
1	M1399	1	●						
2	M151082	1			●				
3	M18920781	4					●		●
4	M18920801	1					●		
5	M5282283	0							
6	M18433649 (DiC8)	2	●				●		
7	M18920757	2					●		●
8	M1324	1		●					
9	M5316909	1		●					
10	M18920755	5	●				●		●
11	M9543716 (DiC18)	0							
12	M18920753	2			●		●		
13	M18920789	2	●				●		
14	M18920763	1					●		
15	M18920769	1	●						
16	M18920756	4					●	●	●
17	M5283470	1					●		
18	M5353266	1						●	
19	M22001195	2	●						●
20	M5283471	0							

Table 10B: List of phorbol ester analogs docked in PKCθC1B crystal structure. The residues those forms hydrogen bond(s) with the activators are denoted with (●) symbol against them. Phorbol12, 13-dibutyrate (PDBu) and Phorbol-12-myristate, 13-acetate (TPA) are the two most common phorbol ester analogs used for PKC activation.

PubChem ID of DAG analogs		Number of H-bonds with residues	Residues interacting						
			Y239	K240	S241	W253	G254	L255	Q258
1	M198501	1				●			
2	M124027	0							
3	M3035003	2		●				●	
4	M197997	0							
5	M500522	0							
6	M72292	1				●			
7	M107854	1							
8	M3036610	1		●					
9	M499957	0							
10	M336986	0							
11	M6445569	0							
12	M37783 (PDBu)	1		●					
13	M5476736	0							
14	M10282255	0							
15	M452543	0							
16	M452544	0							
17	M169936	0							
18	M122634	1						●	
19	M22833501 (TPA)	1						●	
20	M27924	1						●	

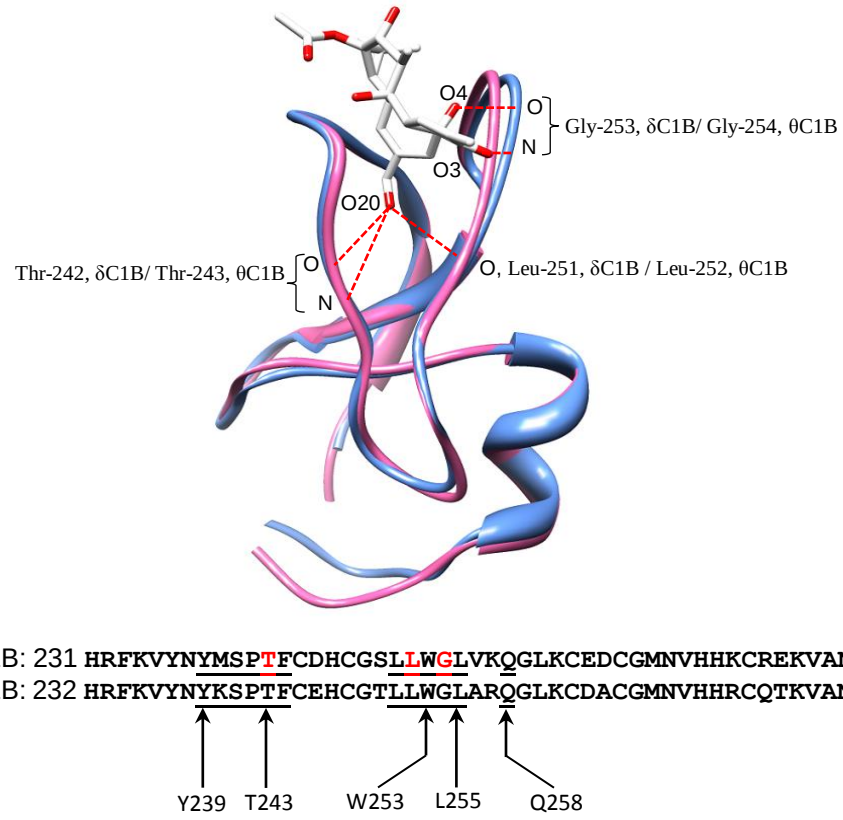

Figure 19: Overlay of the crystal structure of PKCδC1B (corn flower blue) bound with Phorbol-13-O-acetate and PKCθ C1B (hot pink) showed that they are superimposable. Phorbol-13-O-acetate formed five hydrogen bonds in the activator binding groove of PKCδC1B; two bonds with glycine-253, two bonds with threonine-242, and one bond with leucine-251 (denoted with dotted red line). PKCθC1B consists of same homologous activator binding residues indicating similar binding could be possible with Phorbol-13-O-acetate upon cocrystalization. Residues underlined in PKCδC1B sequence constitute the activator binding regions and the residues in red are the direct activator binding residues reported in the cocrystalised structure (1PTR). Residues marked with arrow in PKCθC1B were the residues mutated.

4.4.1 Intramolecular cation-π and π stack interaction

Cation–π interaction is a type of noncovalent interaction between the face of a π electron system (e.g. benzene, heterocyclic rings) and an adjacent cation (e.g. Li^+, Na^+, or quaternary ammonium nitrogen) [110]. Bonding energy of the cation-π interaction (*e.g.* lysine to phenylalanine/ tyrosine is 19 kcal/ mole) is significant and is in the same order of magnitude as hydrogen bonds (*e.g.* hydrogen bonds in water between hydrogen and oxygen is 5 kcal/mole) and salt bridges (e.g. carboxylate of aspartic acid and quaternary ammonium of lysine is 120 kcal/mole). Similar to other non-covalent bonds, cation–π interactions play important role in the biological system, particularly in protein structure, molecular recognition and enzyme catalysis [111, 112]. Early evidence of the cation–π interactions were first noticed by the crystallographers during interpreting the crystallographic data, aromatic side chains appeared in closer contact with nitrogen-containing side chains of the amino acids (which can exist as protonated, cationic species at the pH of the crystal condition) [113]. Crystallographers looking at a diverse set of protein structures found that nearly 50% of aromatic residues (Phe, Tyr, and Trp) were within 6Å of amino groups, whereas roughly about 25% of nitrogen containing side chains such as Lys, Asn, Gln, and His were within the van der Waals radii of the aromatic rings (3.5Å) [113]. About 50% of Arg were found to be in contact with multiple aromatic residues (2 on average) [113]. These all suggests that cation-π interactions exist and are important in protein structure and function.

An example of cation–π interaction in enzyme substrate binding is seen in the nAChR (nicotinic acetylcholine receptor) where endogenous acetylcholine (a positively charged molecule) binds to the active site via a cation–π interaction between its quaternary ammonium nitrogen and the π system of tryptophan in the active site of the receptor [114] (Figure 20).

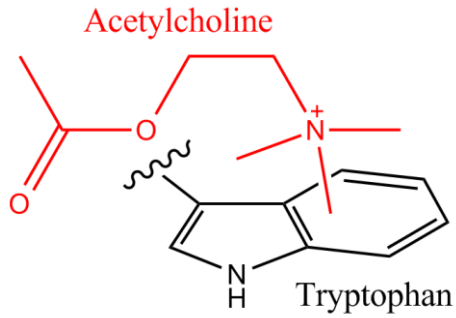

Figure 20: Cation–π interaction between acetylcholine and its receptor

The nAChR is a nicotinic neuroreceptor and a ligand gated ion channel in nature consisting of five homologous subunits of α2βγδ. The nAChR functions at the vertebrate neuromuscular junction and in the central nervous system. The regular endogenous substrate for nAChR is acetylcholine, which acts as neurotransmitter [114]. Photoaffinity labeling studies showed that there are number of aromatic residues such as tyrosine and tryptophan present in the active site for substrate binding [114]. Exogenous nicotine can compete with acetylcholine in binding to the active site of this receptor and originates the nicotine addiction [114].

Another possible cation-π interaction may be observed in the M2 protein of the influenza-A virus [115]. M2 is a transmembrane protein, which forms a tetrameric ion channel allowing protons passing across the biological membrane when the N-terminal side of the M2 protein is acidified. His-37 and Trp-41 are essential residues in the M2 transmembrane protein, which control the pH-regulated proton conductance. Knowledge from M2 ion channel model building suggests that the channel is closed by a network of hydrogen bonds formed between His-37 and Trp-41 at neutral pH among the adjacent helices, and is opened by the cation-π interaction among His-37 toTrp-41 at acidic pH [115] (Figure 21).

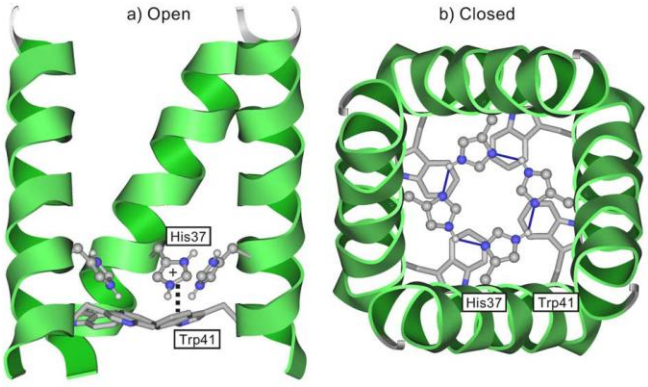

(Adapted from *FEBS Lett. 2003 Sep 18; 552(1):35-8.*)

Figure 21: pH dependant cation-π interaction in M2 proton channel in influenza-A virus

However, there is no report of the presence of cation-π interactions in the known PKC structures. In our study we proposed the possible cation-π interactions between the His-270 and Arg-272 in PKCθC1B subdomain structure (Fig. 28). We used PROPKA 3.0

(http://propka.ki.ku.dk/) to predict the pKa of the residues such as histidine capable of being protonated and how much the residue is surface exposed. The HH21 and HH22 hydrogen atoms of the Arg-272 may form two cation-π bonds with the heterocyclic aromatic system of His-270 within a distance of 3.85Å and 3.81Å respectively.

The π stacking (also called π-π interaction) is another kind of noncovalent interactions between the adjacent aromatic rings often in the parallel orientation. The π stacking interactions are also possible when the two aromatic rings are in L and T orientation [116]. The π stacking interactions are important in the base stacking of DNA nucleotides, protein folding, molecular recognition etc. There is no unified description of the factors that contribute to π stacking interactions. An example of π stacking interaction is found in the binding of FDA-approved acetylcholinesterase (AChE) inhibitor "Tacrine", which has been developed for the treatment of Alzheimer's disease to the active site of acetylcholinesterase [117] (Figure 22). Tacrine (blue) is proposed to have a π stacking interaction with the indolic ring (red) of Trp-84 present in the active site of the enzyme acetylcholinesterase, and this interaction has been exploited in the rational design of novel AChE inhibitors [117].

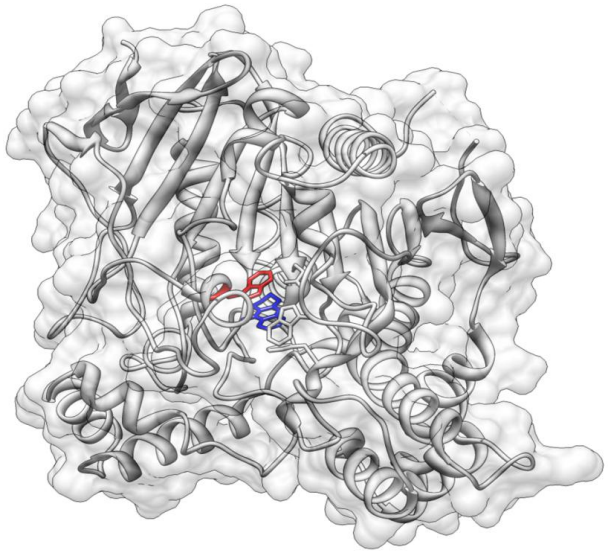

Figure 22: π stacking interaction between "Tacrine" and the acetylcholinesterase.

As of now there is no report of the π stack interactions in the known PKC structures. In our study while comparing the structures of PKCδC1B and PKCθC1B, we proposed a possible π stack interaction between Trp-252 and His-269 in PKCδC1B subdomain structure (Fig. 25A) with a distance of the face of the π rings of 4.13Å.

4.5 Molecular docking

In the phorbol-13-O-acetate bound δC1B structure (IPTQ) [29], Gly-253, Thr-242, and Leu-251 formed 2, 2 and 1 hydrogen bonds with phorbol-13-O-acetate respectively. Sequence alignment showed that PKCθC1B consists of the same set of residues at the homologous position to the activator binding residues in PKCδC1B (red) indicating that PKCθC1B could bind to phorbol-13-O-acetate in the similar fashion (Figure 19) [29]. Additionally in the activator binding region of PKCθ, there were other

residues (Tyr-239, Thr-243, Trp-253, Leu-255 and Gln-258) homologous to PKCδ, which could also play role in activator binding (Figure 19). Our docking results of phorbol ester and DAG analogs revealed that the residues we identified from sequence alignment were also capable of forming hydrogen bonds and hydrophobic interactions with the docked activators (Figure 23A and 23B).

Fig. 23A, panel A and B showed the docking interaction between DiC8 and PKCθC1B (Crystal structure PDB code: 4FKD). DiC8 formed two hydrogen bonds with the residue Thr-243 of PKCθC1B (Panel A). The glycerol moiety of DiC8 containing multiple oxygen atoms was projected deep into the activator binding cavity of the PKCθC1B subdomain (Panel B). The molecule appeared V-shaped and the lower bottom tip of the V consisted of the glycerol moiety. The hydrophobic C8 chain of the molecule on the left hand side was aligned to the hydrophobic residues Ser-241 and Pro-242 of the activator binding cleft, where as the other C8 chain of the molecule on the right hand side interacted with the hydrophobic residues Tyr-253, Gly-254 and Leu-255 in the wall of the activator binding cavity. The glycerol moiety at the bottom tip of the molecule presumably formed hydrophobic interactions with Leu-251 and Leu-252 (Panel B).

Fig. 23A, panel C and D showed the docking interaction between DAG analog M18920756 and PKCθC1B crystal structure. DAG analog M18920756 formed four hydrogen bonds respectively with the residues Leu-255, Gly-254, and Gln-256 of

PKCθC1B (Panel C). DAG analog M18920756 bound upon docking to the activator binding cleft near the mouth of the pocket seemingly wrapped around the hydrophobic residue Leu-255 (Panel D). The shorter hydrophobic chain of the molecule facing front interacted with Gly-254 and Tyr-253 in the wall of the activator binding cavity. The longer carbon chain of the molecule formed hydrophobic interaction mainly with Leu-255. Besides the molecule might have also the interactions with hydrophobic residues Ser-241 and Pro-242 on the left wall of the activator binding cleft of PKCθC1B subdomain (Panel D).

Fig. 23B, panel A and B showed the docking interaction between phorbol ester analog M72292 and PKCθC1B crystal structure. Phorbol ester analog M72292 formed a single hydrogen bond with Trp-253 of PKCθC1B (Panel A). The molecule of phorbol ester analog M72292 due to having long hydrophobic chains bound shallow into the activator binding cleft of PKCθC1B, near the mouth of the pocket (Panel B). Seemingly the molecule capped the activator binding cleft through hydrophobic interactions with Leu-255, Gly-254 and Tyr-253. Part of the hydrophobic chain was projected outward of the activator binding pocket, which did not form any interaction (Panel B).

Fig. 23B, panel C and D showed the docking interaction between phorbol ester analog TPA and PKCθC1B crystal structure. TPA formed a single hydrogen bond with Leu-255 upon docked in the activator binding cavity of PKCθC1B (Panel C). TPA

molecule due to having long hydrophobic chains bound shallow into the activator binding cleft of PKCθC1B, near the mouth of the pocket. The hydrophobic myristate chain of the molecule formed hydrophobic interactions with Ser-241 and Pro-242 and rest of the part of the chain was seemingly projected outward of the activator binding cavity. The polynuclear phorbol moiety with its acetate chain interacted with Leu-255 and Gly-254 (Panel D).

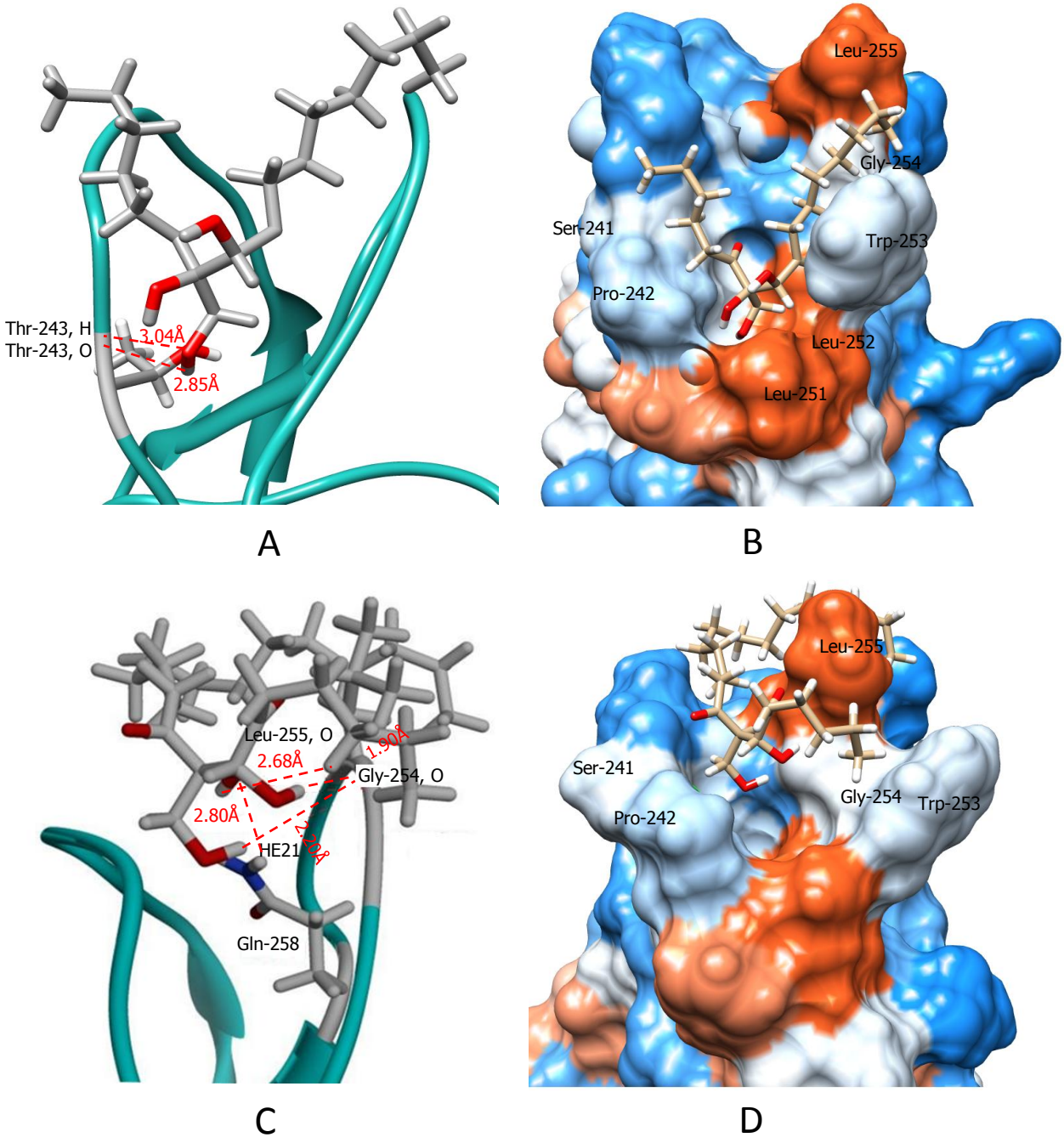

Figure 23A: A) *Sn*-1,2-dioctanoyl glycerol (DiC8, soluble DAG analog), and C) 7, 8-dihydroxy-8-(hydroxymethyl) docosane-6, 9-dione (M18920756, DAG analog) docked in the model of PKCθC1B crystal structure showing possible hydrogen bond formation with the residues. Possible hydrophobic interactions between the residues and B) DiC8 , and D) M18920756, DAG analog upon docking in PKCθC1B crystal structure. Dodger blue indicates most polar residues whereas white to orange red depicts the least to most hydrophobic residues.

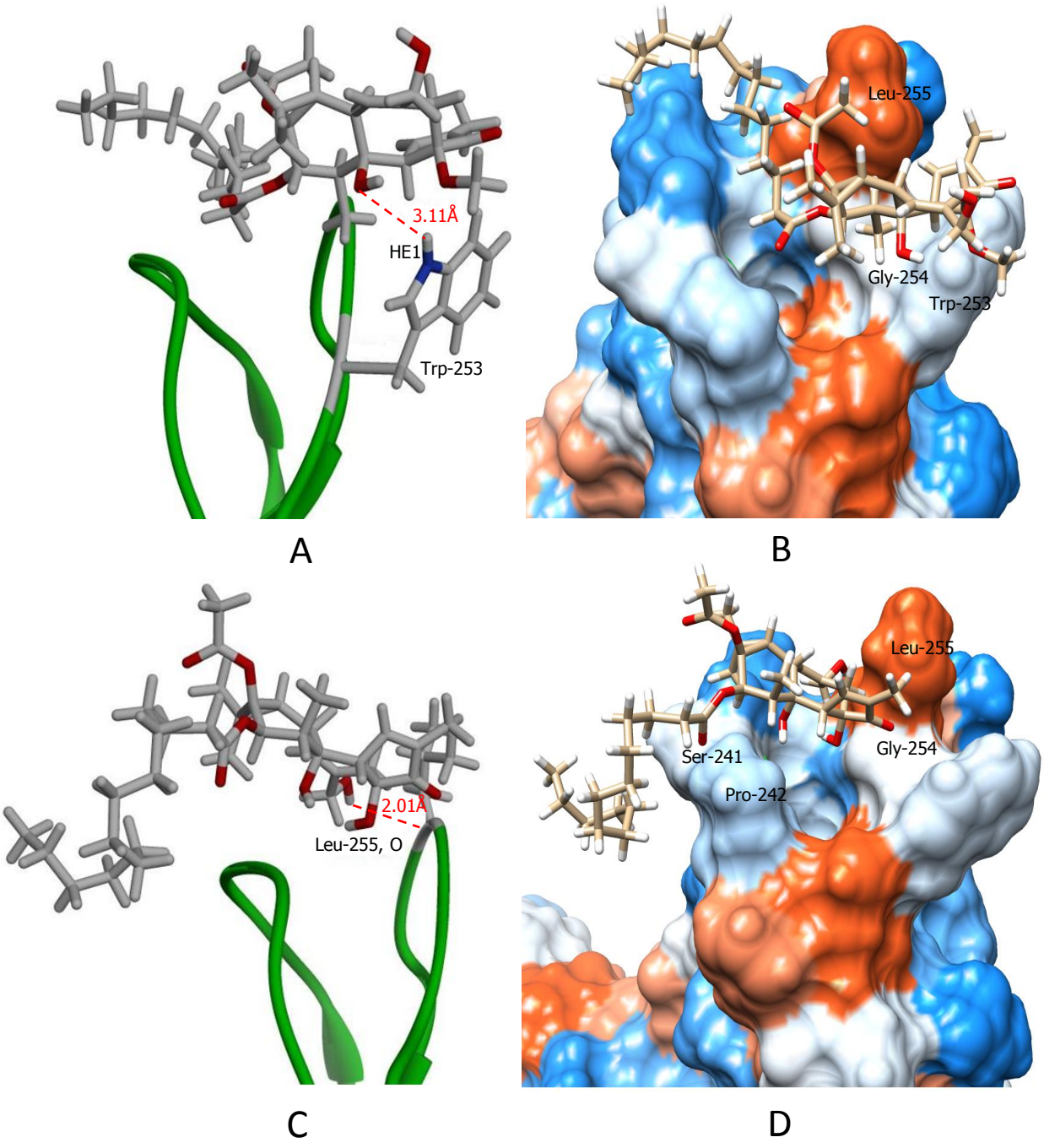

Figure 23B: A) 4-O-methyl-12-O-tetradecanoylphorbol-13-acetate (M72292, PE analog), and C) Tetradecanoyl phorbol acetate (TPA, PE analog) docked in the model of PKCθC1B crystal structure showing possible hydrogen bond formation with the residues. Possible hydrophobic interactions between the residues and B) M72292, PE analog , and D) TPA, PE analog upon docking in PKCθC1B crystal structure. Dodger blue indicates most polar residues whereas white to orange red depicts the least to most hydrophobic residues.

4.6 Phorbol esters and diacylglycerol binding of PKCθC1B and its mutants

To determine the role of these residues in activator binding Y239A, T243A, W253G, L255G and Q258G mutants were generated and their binding affinity to both PDBu (K_d) and DOG (K_i) were measured. The K_d values were in nanomolar range and the mutants showed reduced affinity as compared to the wild type PKCθC1B (Table 11). A representative plot for measuring the K_d of PDBu for its binding to PKCθC1B and L255G is shown (Figure 24). The K_d values of the PDBu binding to Y239A, T243A, W253G, L255G and Q258G showed a significant 8.51, 1.64, 7.56, 11.38 and 1717.94 fold reductions in their binding affinities respectively compared to the wild type (Figure 24, Table 11). These data indicate that Q258G has pronounced effect whereas T243A has the minimal effect on PDBu binding. When binding affinities (K_i) of DOG were measured, Y239A, T243A, W253G, L255G and Q258G showed 5.39, 1.34, 29.4, 4.74 and 114.87 fold reductions in the binding affinities respectively compared to the wild type (Table 11). A representative plot for measuring the K_i of DOG for its binding to PKCθC1B and L255G is shown (Figure 25). In this case also Q258G showed the highest reduction in binding affinities and T243A showed the lowest effect. These data indicate that glutamine is the most critical among all mutated residues tested in this study.

Table 11: Binding affinity of Phorbol-12, 13-dibutyrate (PDBu) and *Sn* 1, 2-Dioctanoylglycerol (DOG) to PKCθC1A, C1B and C1B domain mutants. Values represent the mean ± SEM of triplicate independent experiments. Comparison of the binding affinity between the wild type and the mutants are given after the K_d and K_i values within bracket indicating the times of lower binding affinity shown by the mutants.

	PKC*θ* C1B WT	PKCθ C1A WT	PKC*θ* C1B Y239A	PKC*θ* C1B T243A	PKC*θ* C1B W253G	PKC*θ* C1B L255G	PKC*θ* C1B Q258G
PDBu K_d (nM)	0.39 ± 0.2	127 ± 7.5	3.32 ± 0.34 (8.51)	0.64 ± 0.06 (1.64)	2.95 ± 0.19 (7.56)	4.44 ± 0.56 (11.38)	670 ± 150 (1717.94)
DOG K_i (nM)	28.9 ± 1.3	3000 ± 1100	156 ± 27 (5.39)	39 ± 3.0 (1.34)	850 ± 130 (29.41)	137 ± 44 (4.74)	3320 ± 580 (114.87)
K_i / K_d	74	23	47	61	287	31	5

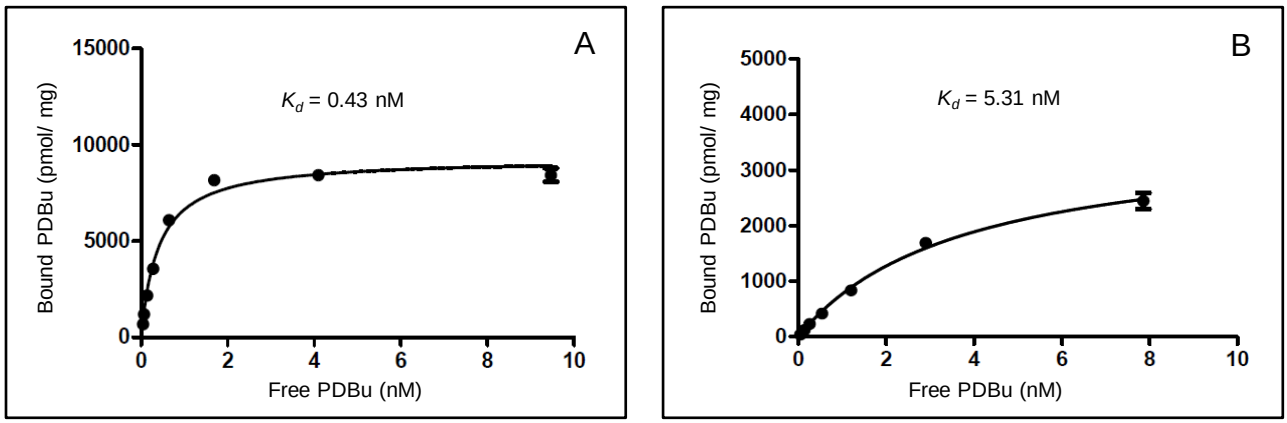

Figure 24: Determination of K_d. Saturation plots for the binding of [^{3}H]PDBu to A) PKCθC1B and B) PKCθC1B L255G. Data represent the mean ± SEM of the triplicate points in a single experiment. Where the error bars are not visible they are smaller than the symbol. The experiments illustrated are representative of the triplicate experiments performed. The mean values for K_d are presented in Table 11.

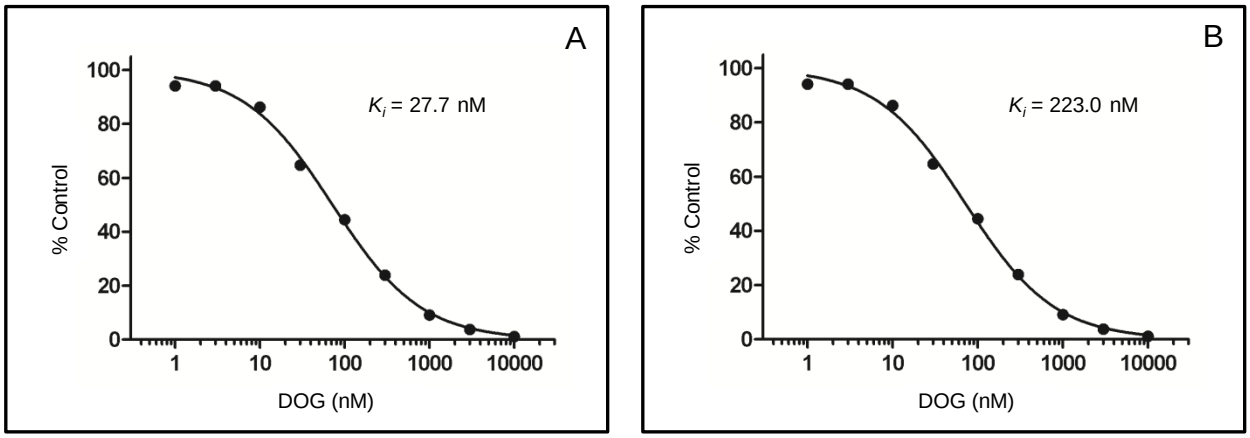

Figure 25: Determination of Ki. Plots for competitive inhibition of the binding of [3H]PDBu by *sn*-1,2-dioctanoyl glycerol to: A) PKCθC1B and B) PKCθC1B L255G. Data represent the mean ± SEM of the triplicate points in a single experiment. Where the error bars are not visible they are smaller than the symbol. The experiments illustrated are representative of the triplicate experiments performed. The mean values for *Ki* are presented in Table 11.

In addition to PKCθC1B and its mutants, we also measured the binding affinity (K_d) of PDBu and the binding affinity (K_i) of DOG for θC1A. The binding affinity of PDBu was 325 times higher for PKCθC1B (K_d = 0.39 nM) than θC1A (K_d = 127.0 nM). It has been reported earlier that the novel PKC C1B domains (δ, ε, and η) bind to phorbol esters with higher affinity than C1A. The PKC C1A domains on the other hand bind to DAG with higher affinity than C1B. In case of PKCθ, the PKCθC1B domain binds with very high affinity to both phorbol ester and DAG than θC1A [32-37]. Shindo *et al.* [34] reported radioactive PDBu binding (K_d) for PKCθ (C1A-900, C1B-3.4 nM). Our experimental data for PDBu binding is in good agreement with the reporting of Shindo *et al.* [34]

Melowic *et al.* [37] reported the DiC18 binding (K_i) by SPR method for PKCθ (C1A-1900, C1B-26.0 nM). Since determination of the binding affinity by SPR method does not give the true binding affinity of the ligand, rather it is the binding affinity of the lipid vesicles containing the ligand; we thought to measure the DOG binding affinity by radioactive method. Radioactive PDBu binding assay gives the precise binding affinity of a ligand. The true binding affinity of both PDBu and DOG were measured simultaneously for θC1A and PKCθC1B by radioactive PDBu binding assay. Interestingly, the binding affinity of DOG for PKCθC1B (K_i = 28.9 nM) was also found to be 103 times higher than θC1A (K_i = 3000.0 nM) and our DOG binding data is also in good agreement with the values reported earlier [37]. Among the 5 residues (Tyr-239,

Thr-243, Trp-253, Leu-255 and Gln-258) Melowic *et al.* [37] mutated Trp-253 and Leu-255 with glycine and measured its binding affinity for DiC18 (DAG analog) by SPR method. The binding data indicated that both W253G and L255G had less binding affinity for DiC18 than the wild type.

It is believed that PKC C1 domains anchoring to the membrane is a ternary system including C1 domains, C1 activators and the anionic phospholipids present in the membrane which binds to the positively charged residues present in the rim of the upper third of the activator binding cleft [33, 42, 87, 118, 119]. However the phospholipid dependence of the C1 membrane binding is variable depending on which tandem repeat C1 domain it is as well as the PKC isotypes [42, 118, 119]. To determine the effect of composition of anionic phosphatidylserine on activator binding we performed radioactive PDBu binding assay on PKCθC1B and its mutants in presence of varying concentration of phosphatidylserine in total lipid mixture.

4.7 Effect of the phospholipid composition on [^{3}H]PDBu binding

Among the mutants studied here for the phospholipids selectivity, PKCθC1B and W253G showed gradual increase of the PDBu binding with the increase of the concentration of PS (0-100%). For other C1B mutants similar increase in the binding affinity with PDBu was observed up to a certain percent PS, and then start decreasing with the increasing concentration of PS (Figure 26). PKCθC1B showed the highest PDBu

binding at 100% PS whereas T243A, W253G and Q258G showed maximum binding at 87.5% PS in the total lipid mixture. However, Y239A and L255G showed maximum binding at 50% and 75% PS composition respectively. This data clearly indicate that lipid composition has profound effect on the activator binding affinity in the PKCθC1B domain. At 50% PS to PC in total lipid, the variable % PDBu binding was observed both for the wild type PKCθC1B and its mutants. PKCθC1B, Y239A, T243A, W253G, L255G and Q258G showed 90.53%, 130.73%, 98.20%, 59.33%, 92.77%, and 85.73% reductions, respectively, in % PDBu binding compared to the wild type (Fig. 6).

We also determined the PS dependence of PDBu binding to PKCθC1A (Figure 26). PKCθC1A followed the same trend like C1B. The binding of PDBu to C1A increased all along with the increase of the concentration of PS in the total lipid mixture. The highest binding in C1A was observed in 100% PS. Between the PKCθC1A and C1B, the increase in PDBu binding to C1A is faster than C1B indicating that C1A probably has higher lipid dependence than C1B in membrane anchoring.

Wang *et al.* [120] earlier reported that in the absence of PS, δC1B showed a 70-fold reduction in the binding affinity of [^{3}H]PDBu. Leu-250 and Leu-255 of δC1B strongly influenced the binding of PDBu. L250D and L255D mutation completely abolished the strong binding of PDBu in the presence or absence of PS. Also, L250R and L255K mutation caused a dramatic 340 and 250 fold reductions in PDBu binding

respectively in the presence of lipid. Only a modest reduction in the PDBu binding (6.6 and 2.9 fold respectively) was observed in absence of lipid. Mutation of L250K or W252K had a 3-fold effects compared to the wild type in presence of PS whereas their

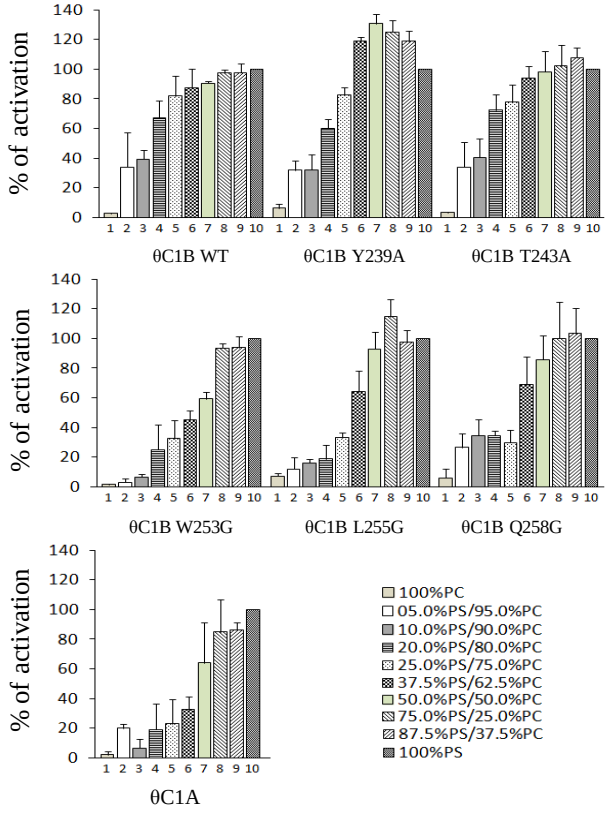

Figure 26: Dependence on phospholipid composition of [^{3}H]PDBu binding to wild type PKCθ C1B domains and the C1B mutants. Binding was measured in the presence of mixtures of phosphatidylserine (PS) to phosphatidylcholine (PC) (total amount phospholipid, 100 µg/ml). The proportions of phosphatidylserine in the various mixtures were, from left to right 0, 5, 10, 20, 25, 37.5, 50, 75, 87.5, and 100%. Values are the mean of three independent experiments and were expressed relative to the binding in the presence of 100% phosphatidylserine. Error bars, SEM. All the proteins exhibit a general trend of increase in binding affinity with increase of % PS in total PS and PC mixture. Y239A, T243A, L255G and Q258G showed increase in the binding affinity up to a certain % of PS in the total lipid mixture then they showed decrease slowly.

binding affinity remained almost the same in absence of the PS. These indicate that the activator binding is more dependent on the C1B-phospholipid interactions than the activator binding residues. Melowic *et al.* [37] reported that θC1A mutants (W181G and L183G) showed a modestly reduced binding affinity (1.7 and 1.6 fold respectively) for lipid vesicles (POPC: POPS: DiC18 = 69:30:1) containing DiC18 than the wild type. On the other hand PKCθC1B mutants (W253G and L255G) showed a significant reduction in the binding affinity (6 and 14 fold respectively) for DiC18 indicating that C1B mutants were more PS dependant in binding the DAG than C1A. These differences in PS dependence could contribute in part to the observed differences of DAG and phorbol ester binding to the θC1A and C1B domains.

After measuring the binding affinity of the phorbol esters and DAG and the dependence of PS on their binding to PKCθC1B and its mutants, we determined the effect of these mutations on the membrane translocation of full length kinase.

4.8 Effect of mutation in the C1B domain on membrane translocation

The translocation properties were measured separately in presence of 50 nM TPA and 250 nM DOG. Activator induced membrane translocation were quantified by the decrease of PKCθ and its mutants in the membrane pool (or the increase of the cytosolic pool). In presence of 50 nM TPA, Y239A, T243A, W253G, L255G and Q258G showed 17.13%, 12.54%, 14.75%, 19.41% and 21.61% reduction in membrane translocation

respectively compared to the wild type. All the mutants showed statistically significant reduction ($P < 0.05$) (Figure 27A). In the presence of 250 nM DOG, Y239A, T243A, W253G, L255G and Q258G showed 12.07%, 8.98%, 5.96%, 15.37% and 15.92% reduction in membrane translocation respectively compared to the wild type (Figure 27B). Out of these Y239A, L255G and Q258G showed significant reduction ($P < 0.05$). These results indicated that the residues mutated were important for the membrane translocation of the full length kinase. Among the residues Q258 were found to be the most important because mutation of Q258 showed significant reduction in membrane translocation in presence both TPA and DOG. However, the mutational effect depends on the activator type as evident in TPA vs DOG induced full length mutant translocation. The percent reduction of the mutant translocation is much significant in presence of TPA compared to DOG.

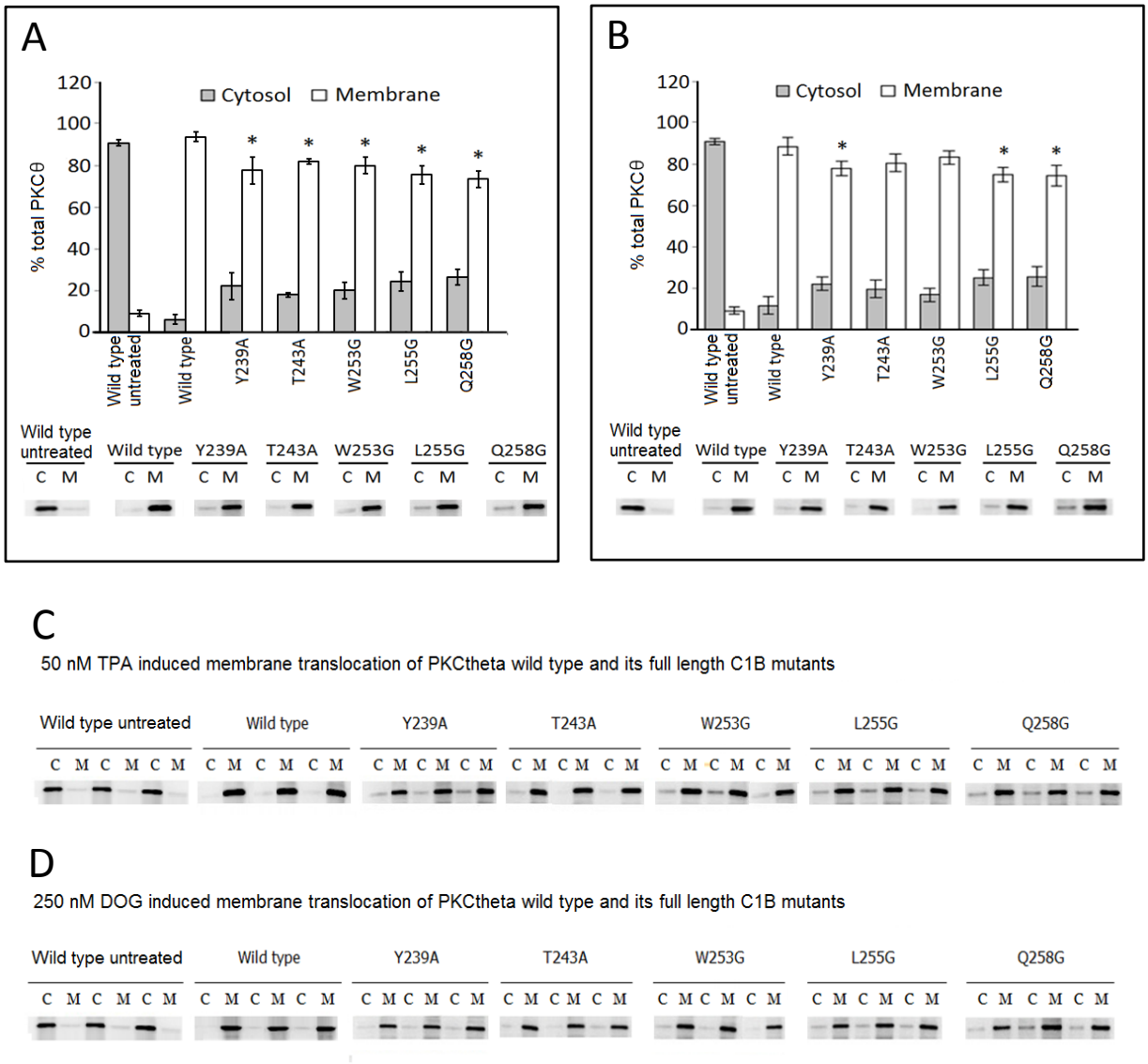

Figure 27: Plot of activator induced percent membrane translocation of PKCθ full length kinase with point mutations in the C1B subdomain and western blot images of the cytosol & membrane fractions from HEK293 cells treated with, A) 50 nM TPA, B) 250 nM DOG for 2 hrs, C) Western blot image of 50 nM TPA induced membrane translocation of PKCθ wild type and its full length C1B mutants in triplicate, and D) Western blot image of 250 nM DOG induced membrane translocation of PKCθ wild type and its full length C1B mutants in triplicate. Data points in the plot are the mean of three measurements, and the error bars indicate the standard deviation from the mean, $P<0.05$, and C, cytosolic fraction and M, membrane fraction respectively.

CHAPTER 5

5. Discussion

67 million American adults have been projected to be suffering from doctors diagnosed arthritis by 2030 (Arthritis & Rheumatism 2006; 54(1)) [121], whereas in 2003 arthritis and rheumatic conditions alone burdened the U.S. economy $128 billion (Morbidity and Mortality Weekly Report 2007; 56(01) [2]. The above figures are alarming enough to depict the current situation on autoimmune diseases. Yet, there is no FDA approved medication, which can manage the root cause of the autoimmune conditions. Current medications provide only relief of the symptomatic manifestations of the diseases. Therefore there is scope to develop new medications for remission of the autoimmune diseases.

PKCθ is unique among all the PKCs because of its predominant expression in T cells. It is the only PKC isoform, which is uniquely translocated to the immunological synapse and involved in the T cell activation process [122, 123]. It has been reported that PKCθ knockout test animals are protected from the development of allergen induced auto-immune conditions. Therefore, designing a selective inhibitor of PKCθ can be a therapeutic choice for the remission of overactive immunity related conditions [55, 73, 74, 79, 124].

In the recent years attempts have been made to design selective PKCθ inhibitors targeting different domains. The catalytic mechanism and the co-crystal structure of phosphorylated human recombinant PKCθ kinase domain with staurosporine (PDB code: 1XJD) has been reported by Xu *et al* [125]. Zhang *et al* reported the crystal structure of δC1B complexed with phorbol-13-O-acetate (PDB code: 1PTQ) [29] and Leonard *et al* reported the two steps allosteric activation of mouse PKC βII and its full length crystal structure (PDB code: 3PFQ) [99]. Elucidation of these targetable PKC domain structures and the mode of substrate binding in them opened a new frontier in rational PKCθ inhibitor design and optimization.

The limitation of designing selective PKCθ inhibitors targeting the ATP binding C3 domain has been the high degree of homology in the catalytic region among more than 500 kinases in the human genome [55, 56]. On the contrary the advantage of targeting the C1 domain of PKCθ is that it mediates only the immune response upon activation [56, 91].

We undertook this study to identify the activator binding residues of PKCθC1B subdomain with the future goal of designing PKCθ specific inhibitors. An earlier study by Melowic *et al* [37] demonstrated a dominant role of the PKCθC1B subdomain in the membrane binding and activation process of PKCθ over C1A, the other cysteine-rich subdomain.

To identify the activator binding residues, we first determined the crystal structure of the C1B domain at 1.63Å and used this structure to dock several known phorbol ester and DAG analogs to identify the possible residue in the protein that interacts with these activators. Further, comparing the activator binding residues of PKCδC1B, for which the activator bound structure is known [29], we identified five possible residues that could affect the activator binding.

Tandem repeat novel PKC C1 domains bind differently with DAG and phorbol esters. Novel PKC C1B domains (δ, ε, η) bind to phorbol ester with higher affinity than C1A, whereas C1A binds to DAG with higher affinity than C1B. However the C1B domain of PKCθ binds to both phorbol ester and DAG with higher affinity than C1A [33, 37] indicating that the spatial structure and activator binding residues in θC1B may be different from other PKCs.

Since DAG and phorbol ester induced mechanism for the activation of PKCs could be different as indicated by several studies[29, 32, 33, 126, 127], and that the former is endogenous and latter is from the plant sources, most of the earlier studies on PKC activation mechanism have been performed either with DAG or phorbol ester. In this study we used both phorbol ester and DAG. Our data indicate that for the PKCθC1B and its mutants, phorbol ester has higher affinity than the DAG. Although with different extent, all the mutants showed reduced binding affinities for both phorbol ester and the

DAG as compared to the wild type PKCθC1B. Out of the five residues that have tested, Gln-258, a conserved residue among the PKC isoforms, showed maximum effect both in terms of its binding to the phorbol ester and DAG and in membrane translocation.

An overlay of the ribbon form of the crystal structures of PKCδC1B and PKCθC1B reveals remarkable similarity of the overall structure. PKCθC1B has a high sequence homology (80%) with PKCδC1B (1PTQ) with an rmsd of 0.66 indicating the similarity between the structures. Superimposition of the PKCθC1B structure to the PKCδC1B showed that the linear distance between the alpha carbon of the two residues at the opposite cleft of the activator binding pocket opening of θC1B is slightly narrower (7.56Å) than the δC1B (8.075Å). While the orientations for most of the residues of both the structures are almost identical, except that the orientation of the tryptophan at consensus position 22 is totally opposite in these two structures. In a representation of the structure where the activator binding pockets are positioned towards the membrane, Trp-253 in PKCθC1B is found to be oriented towards the membrane and the homologous Trp-252 of PKCδC1B is oriented downwards away from the membrane.

A possible π stack interaction may be present between Trp-252 and His-269 at a parallel planner distance of 4.13Å, and the cation-π interactions between Trp-252 and Lys-271 (distance 5.49Å) and between His-269 and Lys-271 (distance 5.12Å) in PKCδC1B (1PTQ) (Panel A, Figure 28). In PKCθC1B, due to upward flipping of the

Trp-253, no such π stack interaction is possible (Panel B, Figure 28). However there is a possibility of a pair of cation-π interactions between His-270 and Arg-272 in PKCθC1B at a distance of 3.85Å and 3.81Å respectively (Panel B, Figure 28).

Additionally, the activator pocket opening of PKCθC1B apparently is narrower than PKCδC1B due to the orientation of Trp-253 (Figure 29). Although this tryptophan side chain is not directly oriented inside the activator binding loop like the homologous Trp-588 in Munc13.1, which occludes the DAG binding site [128] (Figure 30) (Table 12), our binding data for W253G showed 8 and 29 fold reductions in the binding affinity of PDBu and DOG respectively as compared to the wild type. While binding data of the DiC18 and the purified full-length W253G showed six times reductions of binding affinity in SPR analysis in an earlier study [37], our data also showed reduced membrane translocation both for PDBu and DAG. Although the Trp-253 might not interact directly with the activator, it could possibly stabilize the binding of the activator through hydrophobic interactions with the membrane lipid. A further comparison with other known C1 domain structures, it also reveals that βII chimaerin C1 (1XA6) [129] has the homologous tryptophan in the opposite direction to that of PKCθC1B (Figure 30) (Table 12).

The positive charge of Arg-272 in PKCθC1B can be stabilized either through cation-π interaction with His-270 or water mediated hydrogen bonding. We also proposed

four water mediated hydrogen bonds in the crystal structure of PKCθC1B (Figure 31). Two surface water molecules formed hydrogen bonds with Arg-272 of PKCθC1B. Water-78 molecule formed two hydrogen bonds with NH2 and HH22 respectively, whereas water-112 formed another two hydrogen bonds with HH12 and HH22 respectively. A similar environment of the homologous Lys-271 in PKCδC1B can be predicted because no water molecules have been shown in the crystal structure of PKCδC1B (1PTQ).

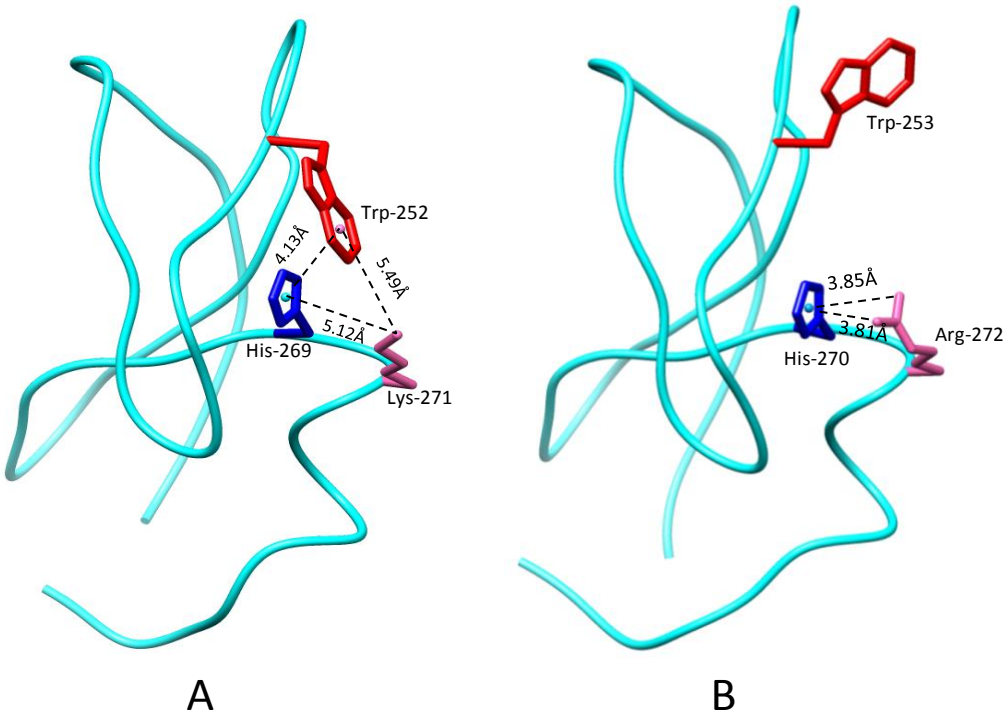

Figure 28: Relative orientation of Trp-252 in PKCδC1B and Trp-253 in PKCθC1B respectively. Trp-252 and Trp-253 both are outside the activator binding cavity. Trp-252 is oriented away from the membrane, whereas Trp-253 is oriented towards the membrane. A) A possible π stack interaction between Trp-252 and His-269 and cation-π interaction between Trp-252 and Lys-271 and between His-269 and Lys-271 in PKCδC1B (1PTQ), and B) Possible cation-π interactions between His-270 and Arg-272 in PKCθC1B

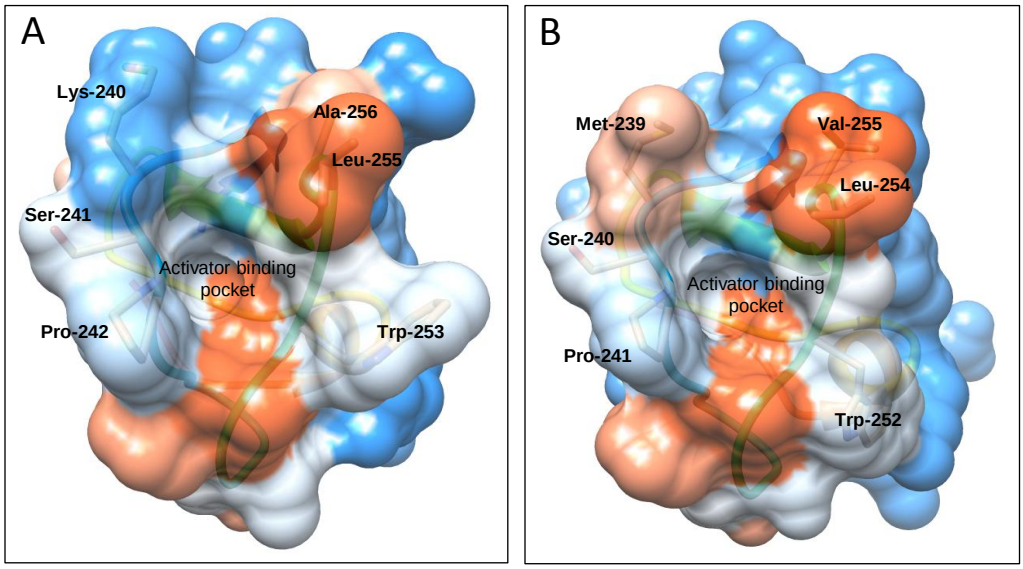

Figure 29: Activator binding pocket topology of PKCθC1B and PKCδC1B . A) Top view of the activator binding pocket topology of PKCθC1B subdomain showing electropositive Lys-240 on the lining of the left cleft and Trp-253 on the right cleft, which is oriented towards the membrane (upward) forming narrow activator pocket opening. B) Top view of the activator binding pocket topology of PKCδC1B subdomain showing hydrophobic Met-239 on the lining of the left cleft and Trp-252 on the right cleft, which is oriented away from the membrane (downward) forming wider activator pocket opening than PKCθC1B. White to orange indicates the lower to higher hydrophobicity, whereas the dodger blue indicates the polar region.

The width of the activator binding pocket opening was measured between the α carbons of the two furthest residues at the opposite end of activator binding cavity in the C1 domain.

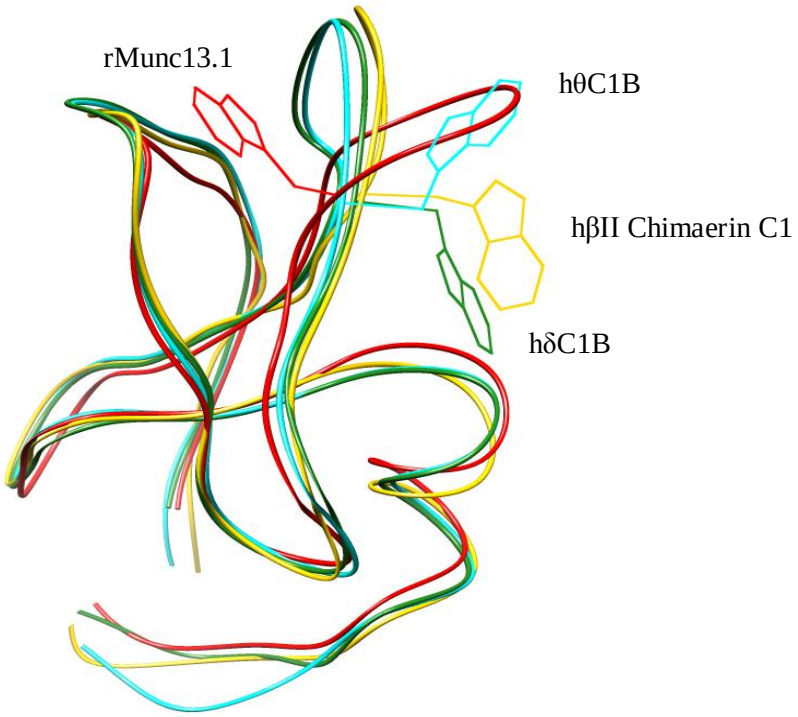

Figure 30: Relative orientation of the tryptophan in different C1 domains.

Table 12: Sequence alignment of known C1 domains structure

hθC1B	215	HNFKVHTFRGPHWCEYCANFM**W**GLIAQGVRCSDCGLNVHKQCSKHVPNDC
hδC1B	231	HRFKVHNYMSPTFCDHCGSLL**W**GLVKQGLKCEDCGMNVHHKCREKVANLC
rMunc13.1C1	567	HNFEVWTATTPTYCYECEGLL**W**GIARQGMRCTECGVKCHEKCQDLLNADC
hβIIChimerinC1	232	HRFKVYNYKSPTFCEHCGTLL**W**GLARQGLKCDACGMNVHHRCQTKVANLC

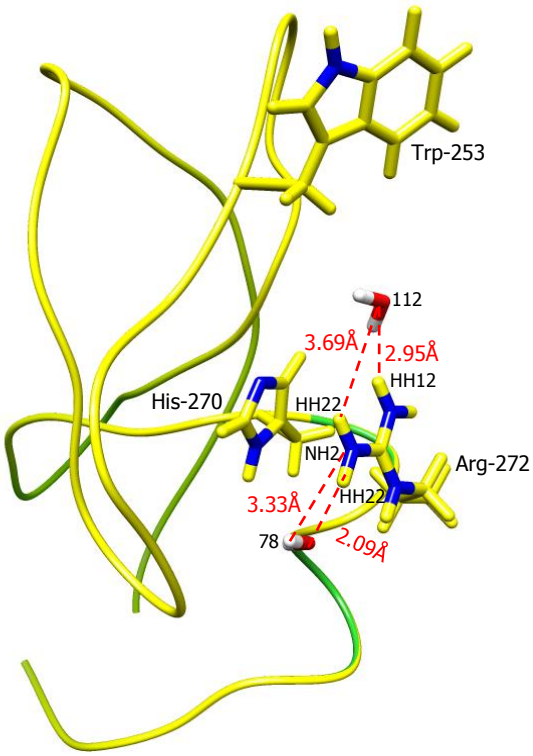

Figure 31: Possible water mediated hydrogen bond formation with Arg-272 of PKCθC1B. Water-78 molecule formed two hydrogen bonds with NH2 and HH22 respectively, whereas water-112 formed two hydrogen bonds with HH12 and HH22 respectively.

Our binding data reveals that there are differences in the binding affinity of the mutants for delta and theta, particularly for W253G and L255G. W253G and L255G in theta showed 8 and 11 fold reduction in their binding affinity for PDBu respectively as compared to the wild type. On the other hand in delta, the homologous mutants W252G and L254G showed 31 and >1000 fold reductions, respectively. For sites Q258 and T243 in theta, the mutation caused similar reductions of PDBu affinity for both delta and theta. For the Y239 in theta, the Y239A showed 8 fold reductions, homologous Y238G in delta showed 60 fold reductions in the binding affinity (Table 13).

Table 13: Comparison of the binding affinity of PDBu (K_d) for θC1B and δC1B homologous mutants. Values represent the mean ± SEM of the triplicate independent experiments.

		C1B wt	Y8A	T12A	W22G	L24G	Q27G
PKCθ	PDBu, K_d (nM)	0.39 ± 0.2	3.32 ± 0.34	0.64 ± 0.06	2.95 ± 0.19	4.44 ± 0.56	670 ± 150
	$K_{d\ mutant}$ / $K_{d\ wt}$	-	8.51	1.64	7.56	11.38	1717.94
PKCδ	PDBu, K_d (nM) [25, 130]	0.8±0.1	48±3.0*	1.7±0.3*	25±3.0	Negligible	Negligible
	$K_{d\ mutant}$ / $K_{d\ wt}$	-	60.0	2.12	31.25	>1000	>1000

* Glycine mutants, Y8G, T21G

This is not surprising since each mutation can cause change in overall lipophilicity of the domain and making each mutant having different phosphatidylserine sensitivity, which is reflected in our data describing the effect of lipid composition on the binding affinity. As the lipid selectivity of these sites for delta is not known, whether the difference for Y239 site between delta and theta is because of the difference between

alanine and glycine or it is a true reflection of the difference between delta and theta is a matter of further investigation. Our modeling and molecular dynamics studies on Y238A and Y238G however, showed that there were no significant structural changes between the two mutants and both of them form 4 hydrogen bonds with PDBu. That the same residues in the two different isoforms with similar structures show differential ligand binding affinities indicate that there may have cumulative effects including the other close by residues in determining the binding affinity.

What are the key determinants for a C1 domain to be phorbol ester/ DAG responsive? According to the prevailing concept, PKC C1 domains anchoring to the membrane is a ternary system including C1 domains, C1 activators and the anionic phospholipid phosphatidylserine present in the membrane, which binds to the positively charged residues present in the rim of the upper third of the activator binding cleft [33, 42, 87, 118, 119]. Alternation of any component in this ternary system therefore is expected to affect the ligand binding affinity. For example, in the atypical PKCζ, several arginine residues lining the activator binding pocket are responsible for its unresponsiveness towards the activator [30]. It has been suggested that these arginine residues reduce access of ligands to the binding cleft and change the electrostatic profile of the C1 domain surface, without altering the basic structure of the binding cleft. In Vav1 C1, the presence of Glu9, Glu10, Thr11, Thr24 and Tyr26 along the rim of the binding cleft reduced the overall lipophilicity of the rim impairing the membrane

association and thereby preventing the formation of the ternary complex [131]. In Munc13.1 C1, occlusion of the Trp-587 in the activator binding pocket reduces its affinity for the activators [128]. Our results emphasize that the structure and orientation of the residues are also important in determining the responsiveness of a C1 domain towards its activator.

An inhibitor targeting the C1 domain of theta should bind into the same activator binding pocket inhibiting the entry of the activator. The C1 specific molecule would have similar complementary molecular feature for binding to the cleft but it would not trigger the activation mechanism. Essentially the binding affinity of the new molecule is expected to be higher than that of the activators so it can competitively inhibit the binding of the activator.

The elucidation of the crystal structure of the θC1B activator binding cleft and its activator binding residues may be used to generate a set of geometric constraints, which can be used for virtual molecular database search for leads. Once a set of leads are identified, those can be docked in the receptor (θC1B) to know which fits best. Some scoring function categorizes the leads according to their fitting into the binding pocket. Best fit leads can then be assayed for their binding affinity or the biological efficacy relating to the receptor. Biologically prospective leads can be further chemically modified to get a successful drug candidate for further trials.

CHAPTER 6

6. Conclusion

In conclusion, our 1.63Å structure of θC1B subdomain revealed close similarity between the C1B subdomain structures of theta and delta, except the orientation of the Trp-253 residue in θC1B is toward the membrane, which contributes to apparently narrower activator pocket opening in θC1B than δC1B. Additionally Trp-253 in theta does not form intramolecular cation-π interactions with His-270 and Arg-272, allowing it to differently interact with membrane lipid during anchoring the kinase upon action.

Out of the five residues mutated, the PDBu binding to T243A and Q258G showed a minimum of 1.64 and maximum of 1717.94 fold reduction in their binding affinities respectively compared to the wild type. Similar trend was also observed for DOG binding to T243A and Q258G showed 1.34 and 114.87 fold reductions in the binding affinities respectively compared to the wild type. Molecular docking showed that the residues forming hydrogen bonds with the docked activator through their side chain heteroatoms exhibit more reductions in the binding affinity upon mutation than those interact through their backbone heteroatoms.

All the five full length C1B mutants overall showed reductions in the activator induced membrane translocation. Between the treatments of TPA and DOG, all five

mutants showed significant reductions with TPA, but for DOG only Y239A, L255G and Q258G showed the significant reduction. The extent of reductions for each of the mutants in the membrane translocation for both TPA and DOG however is not correlated to the binding data of the activators to that of the isolated C1B mutants. This discrepancy could be due to the full length mutants interact differently with the PKC subtypes specific transport scaffold proteins RACKs and to the anionic membrane phosphatidylserine.

Overall our present study showed that mutation of the Gln-258 affects both phorbol ester and DAG binding to the greater extent. Determination of the crystal structure of the C1B domain of theta revealed that Gln-258 is oriented into the activator binding cavity of the C1B domain. This finding will add to the knowledge in the future development of PKCθ specific inhibitor.

CHAPTER 7

7. Future Direction

While our studies have identified several residues that are important for activator binding, a structure of the activator-bound PKCθC1B subdomain would be able to provide much detailed atomic interactions present at the residue level. With the evidences coming in favor of the ternary complex including the protein, activator and the lipid membrane that ultimately determine the binding affinity of a ligand to a particular C1 domain, such structure would be of great importance and add to the knowledge on the mechanism by which PKCθ is specifically targeted to the immunological synapse of the T cells.

Since PKCθC1B and PKCδC1B structures are highly superimposable (rmsd-0.66), the activator binding region (239-244, 251-255, and 258) in PKCθC1B could have similarity with the PKCδC1B. We studied Tyr-239, Thr-243, Trp-253, Leu-255 and Gln-258 present in the activator binding region for their role in activator binding. The other homologous residues, namely, Ser-241, Pro-242, Phe-244, and Leu-251 can also be mutated to investigate their role in the activator binding.

The role of Trp-253 in membrane lipid interaction can further be investigated through a series of point mutations with different residues. Anionic membrane lipid

phosphatidylserine interacts with the residues in the lining of the upper third of the PKCθC1B activator binding cleft through both hydrophobic as well as electrostatic interactions. Mutational study on this site may provide valuable information on the nature of interaction tryptophan could possibly have with lipid.

In our study we found C1A subdomain of PKCθ also binds with the common activators but with lesser binding affinity. C1A can also be targeted for the theta specific molecule design. C1A consists of same residues (Phe-167, Thr-171, Trp-181, Leu-183 and Gln-186) in the homologous position to that of C1B subdomain, which can also be mutated to learn their role in activator binding.

The spatial position of the identified activator binding residues in PKCθC1B can be used to generate the 3D geometric constraints, which later can be used to search virtual molecular databases for the leads. A library of such leads upon docking in the activator binding cavity of PKCθC1B will give hits with good binding scores. In the next stage, these hits can be suitably modified as new therapeutics using both *in silico* drug design as well as conventional synthetic chemistry approach.

CHAPTER 8

8. References

1. *Hunn, M. and A.F. Quest, Cysteine-rich regions of protein kinase Cdelta are functionally non- equivalent. Differences between cysteine-rich regions of non-calcium- dependent protein kinase Cdelta and calcium-dependent protein kinase Cgamma. FEBS Lett, 1997.* ***400****(2): p. 226-32.*
2. *Hurley, J.H., et al., Taxonomy and function of C1 protein kinase C homology domains. Protein Sci, 1997.* ***6****(2): p. 477-80.*
3. *Huwiler, A., D. Fabbro, and J. Pfeilschifter, Selective ceramide binding to protein kinase C-alpha and -delta isoenzymes in renal mesangial cells. Biochemistry, 1998.* ***37****(41): p. 14556-62.*
4. *Ichikawa, S., et al., Solution structure of cysteine-rich domain of protein kinase C alpha. J Biochem, 1995.* ***117****(3): p. 566-74.*
5. *Iglesias, T., S. Matthews, and E. Rozengurt, Dissimilar phorbol ester binding properties of the individual cysteine-rich motifs of protein kinase D. FEBS Lett, 1998.* ***437****(1-2): p. 19-23.*
6. *American Lung Association. Epidemiology & Statistics Unit, Research and Program Services. Trends in Asthma Morbidity and Mortality, November 2007.*
7. *Hurley, J.H., Membrane binding domains. Biochim Biophys Acta, 2006.* ***1761****(8): p. 805-11.*
8. *Mellor, H. and P.J. Parker, The extended protein kinase C superfamily. Biochem J, 1998.* ***332 (Pt 2)****: p. 281-92.*
9. *Nishizuka, Y., Protein kinase C and lipid signaling for sustained cellular responses. FASEB J, 1995.* ***9****(7): p. 484-96.*
10. *Newton, A.C., Protein kinase C: structure, function, and regulation. J Biol Chem, 1995.* ***270****(48): p. 28495-8.*
11. *Nishizuka, Y., Studies and perspectives of protein kinase C. Science, 1986.* ***233****(4761): p. 305-12.*
12. *Takai, Y., et al., Studies on a cyclic nucleotide-independent protein kinase and its proenzyme in mammalian tissues. I. Purification and characterization of an active enzyme from bovine cerebellum. J Biol Chem, 1977.* ***252****(21): p. 7603-9.*
13. *Adams, R.A., et al., Differential spatial and temporal phosphorylation of the visual receptor, rhodopsin, at two primary phosphorylation sites in mice exposed to light. Biochem J, 2003.* ***374****(Pt 2): p. 537-43.*
14. *Koivunen, J., V. Aaltonen, and J. Peltonen, Protein kinase C (PKC) family in cancer progression. Cancer Lett, 2006.* ***235****(1): p. 1-10.*
15. *Newton, A.C., Diacylglycerol's affair with protein kinase C turns 25. Trends Pharmacol Sci, 2004.* ***25****(4): p. 175-7.*

16. *Codazzi, F., M.N. Teruel, and T. Meyer, Control of astrocyte Ca(2+) oscillations and waves by oscillating translocation and activation of protein kinase C. Curr Biol, 2001.* ***11****(14): p. 1089-97.*
17. *Yamasaki, T., et al., Phosphorylation of Activation Transcription Factor-2 at Serine 121 by Protein Kinase C Controls c-Jun-mediated Activation of Transcription. J Biol Chem, 2009.* ***284****(13): p. 8567-81.*
18. *Newton, A.C., Protein kinase C: structural and spatial regulation by phosphorylation, cofactors, and macromolecular interactions. Chem Rev, 2001.* ***101****(8): p. 2353-64.*
19. *Downward, J., et al., Stimulation of p21ras upon T-cell activation. Nature, 1990.* ***346****(6286): p. 719-23.*
20. *Gomez, D.E., et al., The role of protein kinase C and novel phorbol ester receptors in tumor cell invasion and metastasis (Review). Oncol Rep, 1999.* ***6****(6): p. 1363-70.*
21. *Ron, D. and M.G. Kazanietz, New insights into the regulation of protein kinase C and novel phorbol ester receptors. FASEB J, 1999.* ***13****(13): p. 1658-76.*
22. *Castagna, M., et al., Direct activation of calcium-activated, phospholipid-dependent protein kinase by tumor-promoting phorbol esters. J Biol Chem, 1982.* ***257****(13): p. 7847-51.*
23. *Slaga, T.J., Overview of tumor promotion in animals. Environ Health Perspect, 1983.* ***50****: p. 3-14.*
24. *Ritter, S.L. and R.A. Hall, Fine-tuning of GPCR activity by receptor-interacting proteins. Nat Rev Mol Cell Biol, 2009.* ***10****(12): p. 819-30.*
25. *Kazanietz, M.G., et al., Residues in the second cysteine-rich region of protein kinase C delta relevant to phorbol ester binding as revealed by site-directed mutagenesis. J Biol Chem, 1995.* ***270****(37): p. 21852-9.*
26. *Quest, A.F., et al., The regulatory domain of protein kinase C coordinates four atoms of zinc. J Biol Chem, 1992.* ***267****(14): p. 10193-7.*
27. *Quest, A.F., E.S. Bardes, and R.M. Bell, A phorbol ester binding domain of protein kinase C gamma. Deletion analysis of the Cys2 domain defines a minimal 43-amino acid peptide. J Biol Chem, 1994.* ***269****(4): p. 2961-70.*
28. *Dries, D.R., L.L. Gallegos, and A.C. Newton, A single residue in the C1 domain sensitizes novel protein kinase C isoforms to cellular diacylglycerol production. J Biol Chem, 2007.* ***282****(2): p. 826-30.*
29. *Zhang, G., et al., Crystal structure of the cys2 activator-binding domain of protein kinase C delta in complex with phorbol ester. Cell, 1995.* ***81****(6): p. 917-24.*
30. *Pu, Y., et al., Effects on ligand interaction and membrane translocation of the positively charged arginine residues situated along the C1 domain binding cleft in the atypical protein kinase C isoforms. J Biol Chem, 2006.* ***281****(44): p. 33773-88.*
31. *Colon-Gonzalez, F. and M.G. Kazanietz, C1 domains exposed: from diacylglycerol binding to protein-protein interactions. Biochim Biophys Acta, 2006.* ***1761****(8): p. 827-37.*
32. *Ananthanarayanan, B., et al., Activation mechanisms of conventional protein kinase C isoforms are determined by the ligand affinity and conformational flexibility of their C1 domains. J Biol Chem, 2003.* ***278****(47): p. 46886-94.*

33. *Stahelin, R.V., et al., Diacylglycerol-induced membrane targeting and activation of protein kinase Cepsilon: mechanistic differences between protein kinases Cdelta and Cepsilon. J Biol Chem, 2005.* ***280****(20): p. 19784-93.*
34. *Shindo, M., et al., Toward the identification of selective modulators of protein kinase C (PKC) isozymes: establishment of a binding assay for PKC isozymes using synthetic C1 peptide receptors and identification of the critical residues involved in the phorbol ester binding. Bioorg Med Chem, 2001.* ***9****(8): p. 2073-81.*
35. *Irie, K., Y. Nakagawa, and H. Ohigashi, Indolactam and benzolactam compounds as new medicinal leads with binding selectivity for C1 domains of protein kinase C isozymes. Curr Pharm Des, 2004.* ***10****(12): p. 1371-85.*
36. *Irie, K., et al., Establishment of a binding assay for protein kinase C isozymes using synthetic C1 peptides and development of new medicinal leads with protein kinase C isozyme and C1 domain selectivity. Pharmacol Ther, 2002.* ***93****(2-3): p. 271-81.*
37. *Melowic, H.R., et al., Mechanism of diacylglycerol-induced membrane targeting and activation of protein kinase Ctheta. J Biol Chem, 2007.* ***282****(29): p. 21467-76.*
38. *Ohashi, N., et al., Synthesis of protein kinase Cdelta C1b domain by native chemical ligation methodology and characterization of its folding and ligand binding. J Pept Sci, 2009.* ***15****(10): p. 642-6.*
39. *Pu, Y., et al., A novel diacylglycerol-lactone shows marked selectivity in vitro among C1 domains of protein kinase C (PKC) isoforms alpha and delta as well as selectivity for RasGRP compared with PKCalpha. J Biol Chem, 2005.* ***280****(29): p. 27329-38.*
40. *Irie, K., Oie, K., Nakahara, A., Yanai, Y., Ohigashi, H., Wender, P.A., Fukuda, H., Konishi, H., and Kikkawa, U., Molecular basis for Protein Kinase C isozyme-selective binding: the systhesis, folding, and phorbol ester binding of the cysteine-rich domains of all Protein Kinase C isozymes. Journal of the American Chemical Society, 1998.* ***120****: p. 9159-9167.*
41. *Bittova, L., R.V. Stahelin, and W. Cho, Roles of ionic residues of the C1 domain in protein kinase C-alpha activation and the origin of phosphatidylserine specificity. J Biol Chem, 2001.* ***276****(6): p. 4218-26.*
42. *Stahelin, R.V., et al., The origin of C1A-C2 interdomain interactions in protein kinase Calpha. J Biol Chem, 2005.* ***280****(43): p. 36452-63.*
43. *Stahelin, R.V., Digman, M.A., Medkova, M, Ananthanarayanan, B., Rafter, J.D., Melowic, H.R. and Cho, W., Mechanism of diacylglycerol-induced membrane targeting and activation of protein kinase Cdelta. J. Biol.Chem., 2004.* ***279****: p. 29501-29512.*
44. *Kazanietz, M.G., et al., Characterization of the cysteine-rich region of the Caenorhabditis elegans protein Unc-13 as a high affinity phorbol ester receptor. Analysis of ligand-binding interactions, lipid cofactor requirements, and inhibitor sensitivity. J Biol Chem, 1995.* ***270****(18): p. 10777-83.*
45. *Betz, A., et al., Munc13-1 is a presynaptic phorbol ester receptor that enhances neurotransmitter release. Neuron, 1998.* ***21****(1): p. 123-36.*
46. *Kazanietz, M.G., et al., Pharmacology of the receptors for the phorbol ester tumor promoters: multiple receptors with different biochemical properties. Biochem Pharmacol, 2000.* ***60****(10): p. 1417-24.*

47. *Areces, L.B., M.G. Kazanietz, and P.M. Blumberg, Close similarity of baculovirus-expressed n-chimaerin and protein kinase C alpha as phorbol ester receptors. J Biol Chem, 1994.* ***269****(30): p. 19553-8.*
48. *Irie, K., et al., Tumor promoter binding of the protein kinase C C1 homology domain peptides of RasGRPs, chimaerins, and Unc13s. Bioorg Med Chem, 2004.* ***12****(17): p. 4575-83.*
49. *Caloca, M.J., et al., Beta2-chimaerin is a high affinity receptor for the phorbol ester tumor promoters. J Biol Chem, 1997.* ***272****(42): p. 26488-96.*
50. *Lorenzo, P.S., et al., The guanine nucleotide exchange factor RasGRP is a high -affinity target for diacylglycerol and phorbol esters. Mol Pharmacol, 2000.* ***57****(5): p. 840-6.*
51. *Lorenzo, P.S., et al., Phorbol esters modulate the Ras exchange factor RasGRP3. Cancer Res, 2001.* ***61****(3): p. 943-9.*
52. *Choi, S.H., et al., Characterization of the interaction of phorbol esters with the C1 domain of MRCK (myotonic dystrophy kinase-related Cdc42 binding kinase) alpha/beta. J Biol Chem, 2008.* ***283****(16): p. 10543-9.*
53. *Chen, J., et al., Selective binding of phorbol esters and diacylglycerol by individual C1 domains of the PKD family. Biochem J, 2008.* ***411****(2): p. 333-42.*
54. *Shindo, M., et al., Synthesis and phorbol ester binding of the cysteine-rich domains of diacylglycerol kinase (DGK) isozymes. DGKgamma and DGKbeta are new targets of tumor-promoting phorbol esters. J Biol Chem, 2003.* ***278****(20): p. 18448-54.*
55. *Manning, G., et al., The protein kinase complement of the human genome. Science, 2002.* ***298****(5600): p. 1912-34.*
56. *Blumberg, P.M., et al., Wealth of opportunity - the C1 domain as a target for drug development. Curr Drug Targets, 2008.* ***9****(8): p. 641-52.*
57. *Felix Karim1, A.B., Jay Dela Cruz1, Derek Maclean2, Kanad Das2 and Stehen Harrision3, Development of PKC Theta-Specific Inhibitors to Modulate T-Cell Activation. The Journal of Immunology, 2007.* ***178****(B35).*
58. *Baier, G., et al., Molecular cloning and characterization of PKC theta, a novel member of the protein kinase C (PKC) gene family expressed predominantly in hematopoietic cells. J Biol Chem, 1993.* ***268****(7): p. 4997-5004.*
59. *Arendt, C.W., et al., Protein kinase C-theta;: signaling from the center of the T-cell synapse. Curr Opin Immunol, 2002.* ***14****(3): p. 323-30.*
60. *Isakov, N. and A. Altman, Protein kinase C(theta) in T cell activation. Annu Rev Immunol, 2002.* ***20****: p. 761-94.*
61. *Nishizuka, Y., Intracellular signaling by hydrolysis of phospholipids and activation of protein kinase C. Science, 1992.* ***258****(5082): p. 607-14.*
62. *Altman, A., N. Isakov, and G. Baier, Protein kinase Ctheta: a new essential superstar on the T-cell stage. Immunol Today, 2000.* ***21****(11): p. 567-73.*
63. *Vilcek, J. and T.H. Lee, Tumor necrosis factor. New insights into the molecular mechanisms of its multiple actions. J Biol Chem, 1991.* ***266****(12): p. 7313-6.*
64. *Wajant, H., K. Pfizenmaier, and P. Scheurich, Tumor necrosis factor signaling. Cell Death Differ, 2003.* ***10****(1): p. 45-65.*

65. *Chen, G. and D.V. Goeddel, TNF-R1 signaling: a beautiful pathway. Science, 2002.* ***296****(5573): p. 1634-5.*
66. *Steinman, L., A brief history of T(H)17, the first major revision in the T(H)1/T(H)2 hypothesis of T cell-mediated tissue damage. Nat Med, 2007.* ***13****(2): p. 139-45.*
67. *Nembrini, C., et al., Strong TCR signaling, TLR ligands, and cytokine redundancies ensure robust development of type 1 effector T cells. J Immunol, 2006.* ***176****(12): p. 7180-8.*
68. *Zheng, W. and R.A. Flavell, The transcription factor GATA-3 is necessary and sufficient for Th2 cytokine gene expression in CD4 T cells. Cell, 1997.* ***89****(4): p. 587-96.*
69. *Kopf, M., et al., Disruption of the murine IL-4 gene blocks Th2 cytokine responses. Nature, 1993.* ***362****(6417): p. 245-8.*
70. *Werlen, G., et al., Calcineurin preferentially synergizes with PKC-theta to activate JNK and IL-2 promoter in T lymphocytes. EMBO J, 1998.* ***17****(11): p. 3101-11.*
71. *Ghaffari-Tabrizi, N., et al., Protein kinase Ctheta, a selective upstream regulator of JNK/SAPK and IL-2 promoter activation in Jurkat T cells. Eur J Immunol, 1999.* ***29****(1): p. 132-42.*
72. *Sun, Z., et al., PKC-theta is required for TCR-induced NF-kappaB activation in mature but not immature T lymphocytes. Nature, 2000.* ***404****(6776): p. 402-7.*
73. *Marsland, B.J., et al., Protein kinase C theta is critical for the development of in vivo T helper (Th)2 cell but not Th1 cell responses. J Exp Med, 2004.* ***200****(2): p. 181-9.*
74. *Salek-Ardakani, S., et al., Protein kinase Ctheta controls Th1 cells in experimental autoimmune encephalomyelitis. J Immunol, 2005.* ***175****(11): p. 7635-41.*
75. *Marsland, B.J., et al., TLR ligands act directly upon T cells to restore proliferation in the absence of protein kinase C-theta signaling and promote autoimmune myocarditis. J Immunol, 2007.* ***178****(6): p. 3466-73.*
76. *Anderson, K., et al., Mice deficient in PKC theta demonstrate impaired in vivo T cell activation and protection from T cell-mediated inflammatory diseases. Autoimmunity, 2006.* ***39****(6): p. 469-78.*
77. *Tan, S.L., et al., Resistance to experimental autoimmune encephalomyelitis and impaired IL-17 production in protein kinase C theta-deficient mice. J Immunol, 2006.* ***176****(5): p. 2872-9.*
78. *Giannoni, F., et al., Protein kinase C theta is not essential for T-cell-mediated clearance of murine gammaherpesvirus 68. J Virol, 2005.* ***79****(11): p. 6808-13.*
79. *Healy, A.M., et al., PKC-theta-deficient mice are protected from Th1-dependent antigen-induced arthritis. J Immunol, 2006.* ***177****(3): p. 1886-93.*
80. *Kim, J.K., et al., PKC-theta knockout mice are protected from fat-induced insulin resistance. J Clin Invest, 2004.* ***114****(6): p. 823-7.*
81. *Progress in Autoimmune Diseases Research, Report to Congress, National Institutes of Health, The Autoimmune Diseases Coordinating Committee,. 2005: p. pages 1, 2, 16, 17, 28, 29, 30, 32, 52.*
82. *AARDA, Autoimmune Statistics. 2012.*
83. *Tobin, A.M. and B. Kirby, TNF alpha inhibitors in the treatment of psoriasis and psoriatic arthritis. BioDrugs, 2005.* ***19****(1): p. 47-57.*

84. *Reimold, A.M., TNFalpha as therapeutic target: new drugs, more applications. Curr Drug Targets Inflamm Allergy, 2002.* ***1****(4): p. 377-92.*
85. *Loza, M.J., et al., Systemic inflammatory profile and response to anti-tumor necrosis factor therapy in chronic obstructive pulmonary disease. Respir Res, 2012.* ***13****: p. 12.*
86. *Slater, S.J., et al., Protein kinase Calpha contains two activator binding sites that bind phorbol esters and diacylglycerols with opposite affinities. J Biol Chem, 1996.* ***271****(9): p. 4627-31.*
87. *Stahelin, R.V., et al., Mechanism of diacylglycerol-induced membrane targeting and activation of protein kinase Cdelta. J Biol Chem, 2004.* ***279****(28): p. 29501-12.*
88. *Irie, K., Y. Nakagawa, and H. Ohigashi, Toward the development of new medicinal leads with selectivity for protein kinase C isozymes. Chem Rec, 2005.* ***5****(4): p. 185-95.*
89. *Lewin, N.E. and P.M. Blumberg, [3H]Phorbol 12,13-dibutyrate binding assay for protein kinase C and related proteins. Methods Mol Biol, 2003.* ***233****: p. 129-56.*
90. *Chaudhary, D. and M. Kasaian, PKCtheta: A potential therapeutic target for T-cell-mediated diseases. Curr Opin Investig Drugs, 2006.* ***7****(5): p. 432-7.*
91. *Friedl, P., A.T. den Boer, and M. Gunzer, Tuning immune responses: diversity and adaptation of the immunological synapse. Nat Rev Immunol, 2005.* ***5****(7): p. 532-45.*
92. *Kaelin, W.G., Jr., et al., Expression cloning of a cDNA encoding a retinoblastoma-binding protein with E2F-like properties. Cell, 1992.* ***70****(2): p. 351-64.*
93. *Charoenthongtrakul, S., et al., Human T cell leukemia virus type 1 Tax inhibits innate antiviral signaling via NF-kappaB-dependent induction of SOCS1. J Virol, 2011.* ***85****(14): p. 6955-62.*
94. *Kunkel, T.A., Rapid and efficient site-specific mutagenesis without phenotypic selection. Proc Natl Acad Sci U S A, 1985.* ***82****(2): p. 488-92.*
95. *Sugimoto, M., et al., A simple and efficient method for the oligonucleotide-directed mutagenesis using plasmid DNA template and phosphorothioate-modified nucleotide. Anal Biochem, 1989.* ***179****(2): p. 309-11.*
96. *Nelson, M. and M. McClelland, Use of DNA methyltransferase/endonuclease enzyme combinations for megabase mapping of chromosomes. Methods Enzymol, 1992.* ***216****: p. 279-303.*
97. *Quest, A.F., et al., Expression of protein kinase C gamma regulatory domain elements containing cysteine-rich zinc-coordinating regions as glutathione S-transferase fusion proteins. Methods Enzymol, 1995.* ***252****: p. 153-67.*
98. *Das, J., et al., PKC epsilon has an alcohol-binding site in its second cysteine-rich regulatory domain. Biochem J, 2009.* ***421****(3): p. 405-13.*
99. *Leonard, T.A., et al., Crystal structure and allosteric activation of protein kinase C betaII. Cell, 2011.* ***144****(1): p. 55-66.*
100. *Littler, D.R., et al., Structure of human protein kinase C eta (PKCeta) C2 domain and identification of phosphorylation sites. Biochem Biophys Res Commun, 2006.* ***349****(4): p. 1182-9.*
101. *The CCP4 suite: programs for protein crystallography. Acta Crystallogr D Biol Crystallogr, 1994.* ***50****(Pt 5): p. 760-3.*

102. *Evans, P., Scaling and assessment of data quality. Acta Crystallogr D Biol Crystallogr, 2006.* ***62****(Pt 1): p. 72-82.*
103. *Matthews, B.W., Solvent content of protein crystals. J Mol Biol, 1968.* ***33****(2): p. 491-7.*
104. *McCoy, A.J., et al., Phaser crystallographic software. J Appl Crystallogr, 2007.* ***40****(Pt 4): p. 658-674.*
105. *Langer, G., et al., Automated macromolecular model building for X-ray crystallography using ARP/wARP version 7. Nat Protoc, 2008.* ***3****(7): p. 1171-9.*
106. *Winn, M.D., G.N. Murshudov, and M.Z. Papiz, Macromolecular TLS refinement in REFMAC at moderate resolutions. Methods Enzymol, 2003.* ***374****: p. 300-21.*
107. *Emsley, P. and K. Cowtan, Coot: model-building tools for molecular graphics. Acta Crystallogr D Biol Crystallogr, 2004.* ***60****(Pt 12 Pt 1): p. 2126-32.*
108. *Das, J., S. Pany, and A. Majhi, Chemical modifications of resveratrol for improved protein kinase C alpha activity. Bioorg Med Chem, 2011.* ***19****(18): p. 5321-33.*
109. *Chen, N., et al., Translocation of protein kinase Cepsilon and protein kinase Cdelta to membrane is required for ultraviolet B-induced activation of mitogen-activated protein kinases and apoptosis. J Biol Chem, 1999.* ***274****(22): p. 15389-94.*
110. *Dougherty, D.A., Cation-pi interactions in chemistry and biology: a new view of benzene, Phe, Tyr, and Trp. Science, 1996.* ***271****(5246): p. 163-8.*
111. *Eric V. Anslyn, D.A.D., Modern Physical Organic Chemistry. University Science Books. 2004.*
112. *Ma, J.C. and D.A. Dougherty, The Cationminus signpi Interaction. Chem Rev, 1997.* ***97****(5): p. 1303-1324.*
113. *Burley, S.K. and G.A. Petsko, Amino-aromatic interactions in proteins. FEBS Lett, 1986.* ***203****(2): p. 139-43.*
114. *Zhong, W., et al., From ab initio quantum mechanics to molecular neurobiology: a cation-pi binding site in the nicotinic receptor. Proc Natl Acad Sci U S A, 1998.* ***95****(21): p. 12088-93.*
115. *Takeuchi, H., A. Okada, and T. Miura, Roles of the histidine and tryptophan side chains in the M2 proton channel from influenza A virus. FEBS Lett, 2003.* ***552****(1): p. 35-8.*
116. *McGaughey, G.B., M. Gagne, and A.K. Rappe, pi-Stacking interactions. Alive and well in proteins. J Biol Chem, 1998.* ***273****(25): p. 15458-63.*
117. *da Silva, C.H., et al., Molecular modeling, docking and ADMET studies applied to the design of a novel hybrid for treatment of Alzheimer's disease. J Mol Graph Model, 2006.* ***25****(2): p. 169-75.*
118. *Giorgione, J.R., et al., Increased membrane affinity of the C1 domain of protein kinase Cdelta compensates for the lack of involvement of its C2 domain in membrane recruitment. J Biol Chem, 2006.* ***281****(3): p. 1660-9.*
119. *Slater, S.J., et al., Regulation of PKC alpha activity by C1-C2 domain interactions. J Biol Chem, 2002.* ***277****(18): p. 15277-85.*
120. *Wang, Q.J., et al., Role of hydrophobic residues in the C1b domain of protein kinase C delta on ligand and phospholipid interactions. J Biol Chem, 2001.* ***276****(22): p. 19580-7.*

121. *Hurley, J.H. and T. Meyer, Subcellular targeting by membrane lipids. Curr Opin Cell Biol, 2001.* ***13****(2): p. 146-52.*
122. *Monks, C.R., et al., Selective modulation of protein kinase C-theta during T-cell activation. Nature, 1997.* ***385****(6611): p. 83-6.*
123. *Grakoui, A., et al., The immunological synapse: a molecular machine controlling T cell activation. Science, 1999.* ***285****(5425): p. 221-7.*
124. *Salek-Ardakani, S., et al., Differential regulation of Th2 and Th1 lung inflammatory responses by protein kinase C theta. J Immunol, 2004.* ***173****(10): p. 6440-7.*
125. *Cywin, C.L., et al., Discovery of potent and selective PKC-theta inhibitors. Bioorg Med Chem Lett, 2007.* ***17****(1): p. 225-30.*
126. *Bazzi, M.D. and G.L. Nelsestuen, Properties of membrane-inserted protein kinase C. Biochemistry, 1988.* ***27****(20): p. 7589-93.*
127. *Kazanietz, M.G., K.W. Krausz, and P.M. Blumberg, Differential irreversible insertion of protein kinase C into phospholipid vesicles by phorbol esters and related activators. J Biol Chem, 1992.* ***267****(29): p. 20878-86.*
128. *Shen, N., O. Guryev, and J. Rizo, Intramolecular occlusion of the diacylglycerol-binding site in the C1 domain of munc13-1. Biochemistry, 2005.* ***44****(4): p. 1089-96.*
129. *Canagarajah, B., et al., Structural mechanism for lipid activation of the Rac-specific GAP, beta2-chimaerin. Cell, 2004.* ***119****(3): p. 407-18.*
130. *Pak, Y., et al., Structural basis of binding of high-affinity ligands to protein kinase C: prediction of the binding modes through a new molecular dynamics method and evaluation by site-directed mutagenesis. J Med Chem, 2001.* ***44****(11): p. 1690-701.*
131. *Geczy, T., et al., Molecular basis for the failure of the "atypical" C1 domain of Vav1 to bind diacylglycerol/phorbol ester. J Biol Chem, 2012.*